



VCU

Virginia Commonwealth University
VCU Scholars Compass

Theses and Dissertations

Graduate School

2017

LUNG DISPOSITION MODEL-BASED ANALYSES OF CLINICAL PHARMACOKINETIC PROFILES FOR INHALED DRUGS

Anuja Raut

Follow this and additional works at: <https://scholarscompass.vcu.edu/etd>

 Part of the [Other Pharmacy and Pharmaceutical Sciences Commons](#), and the [Pharmaceutics and Drug Design Commons](#)

© The Author

Downloaded from

<https://scholarscompass.vcu.edu/etd/4788>

This Thesis is brought to you for free and open access by the Graduate School at VCU Scholars Compass. It has been accepted for inclusion in Theses and Dissertations by an authorized administrator of VCU Scholars Compass. For more information, please contact libcompass@vcu.edu.

©Anuja Raut 2017
All Rights Reserved

**LUNG DISPOSITION MODEL-BASED ANALYSES OF CLINICAL
PHARMACOKINETIC PROFILES FOR INHALED DRUGS**

A thesis submitted in partial fulfillment of the requirements for the degree of Master of Science at Virginia Commonwealth University.

By

Anuja Raut,
Bachelor of Pharmacy, University of Pune, India, 2011
Master of Science, University of Southern California, Los Angeles, CA, USA, 2014

Director: Masahiro Sakagami, Ph.D.
Associate Professor
Department of Pharmaceutics
School of Pharmacy

Virginia Commonwealth University
Richmond, Virginia
May 2017

ACKNOWLEDGEMENTS

I would like to express my sincere gratitude to my advisor Dr. Masahiro Sakagami, for giving me the opportunity to pursue M.S. under his guidance. His support and guidance have helped me acquire more skills and confidence in my research. I sincerely appreciate his time and efforts in training me. I would also like to thank my advisory committee member, Dr. Jurgen Venitz for always finding the time to explain to me key concepts as well as patiently answering all my queries. I'd also like to thank my committee member Dr. Patricia W. Slattum for her support and guidance academically, professionally as well as her mentoring in my personal growth. I want to thank Dr. Michael Hindle, Dr. Susanna Wu-Pong, Dr. Peter Byron and Sha-kim for their extensive mentoring and support during my time at VCU. I am grateful to all professors in School of Pharmacy for their help during my coursework. I am especially thankful to Dr. Aron Lichtman for his support and to Keyetta and Laura for the kind help with everything.

I would like to thank Sneha Dhapare for her honest friendship and immense support while living in Richmond, and VCU lab-mates, Tien Truong, Hua Li, Susan Boc, Mandana Azimi and Xiangyin Wei for being amazing friends as well as playing significant roles in guiding me professionally as well as giving valuable suggestions during my tenure as a graduate student and beyond. I also want to specially thank Mengyao Li, Bishoy Hanna and Neha Maharao for their wonderful support, as well as Bhushan, Tanya, Mauli, Karthik, Nhu, Karan, Mary Ann, Bonnie and Dennis. Thank you for making my time at VCU and Richmond memorable.

I want to thank my parents, brother and husband Mayur for always being there for me in difficult times and giving me the strength to keep going.

TABLE OF CONTENTS

ACKNOWLEDGEMENTS	ii
LIST OF TABLES.....	vi
LIST OF FIGURES.....	ix
LIST OF ABBREVIATIONS.....	xiii
ABSTRACT.....	xvi
CHAPTER 1 INTRODUCTION.....	1
1.1 Inhaled drug delivery.....	1
1.2 Lung deposition and disposition complexities.....	4
1.3 Methods to determine total and regional drug lung deposition.....	9
1.4 PK modeling approaches.....	11
CHAPTER 2 HYPOTHESIS AND SPECIFIC AIMS.....	16
CHAPTER 3 LUNG DISPOSITION KINETIC ANALYSIS VIA CURVE FITTING APPROACH.....	18
3.1 Introduction.....	18
3.2 Methods.....	19
3.2.1 Literature data collection.....	19
3.2.2 Estimation of systemic PK parameters.....	20
3.2.3 Curve fitting-based estimation of lung disposition kinetic parameters.....	23
3.3 Results and Discussion.....	25
3.3.1 Literature data collection.....	25

3.3.2	Tobramycin.....	25
3.3.3	Calcitonin.....	31
3.3.4	Ciprofloxacin.....	37
3.3.5	The k_a and k_{nal} values across three molecules.....	43
3.4	Conclusions.....	48
CHAPTER 4 LUNG DISPOSITION KINETIC ANALYSIS VIA MOMENT-BASED APPROACH.....		50
4.1	Introduction.....	50
4.2	Methods.....	50
4.2.1	Literature data collection.....	50
4.2.2	Moment-based analyses for IV and inhaled PK profiles.....	51
4.2.3	Moment-based determination of lung disposition kinetic parameters.....	52
4.3	Results and Discussion.....	54
4.3.1	Tobramycin.....	54
4.3.2	Calcitonin.....	55
4.3.3	Ciprofloxacin.....	57
4.4	Comparison between moment-based analysis and curve fitting-based approaches.....	58
4.5	Conclusions.....	60
CHAPTER 5 EFFECTS OF LUNG DELIVERY AND DISPOSITION KINETIC CHANGES ON SYSTEMIC PK AND LUNG EXPOSURE PROFILES VIA SIMULATION.....		62
5.1	Introduction.....	62
5.2	Methods.....	63
5.2.1	Models and reference standard conditions.....	63
5.2.2	Systemic PK profile simulation upon $\pm 20\%$ changes of the DTL, k_a and k_{nal}	65
5.2.3	Local lung exposure profile simulation upon $\pm 20\%$ changes of the DTL, k_a and k_{nal}	65
5.3	Results and Discussion.....	66
5.3.1	Systemic PK profile simulation upon $\pm 20\%$ changes of the DTL, k_a and k_{nal}	66

5.3.1.1 Tobramycin.....	66
5.3.1.2 Calcitonin.....	67
5.3.1.3 Ciprofloxacin.....	67
5.3.1.4. Systemic PK profile simulation for three molecules.....	68
5.3.2 Local lung exposure profile simulation upon ± 20 % changes of the DTL, k_a and k_{nal}	73
5.3.2.1 Tobramycin.....	73
5.3.2.2 Calcitonin.....	73
5.3.2.3 Ciprofloxacin.....	74
5.3.2.4 Local lung exposure profile simulation for three molecules.....	74
5.4 Conclusions.....	78
CHAPTER 6 OVERALL CONCLUSIONS, LIMITATIONS AND FUTURE DIRECTIONS.....	79
REFERENCES.....	82
APPENDICES.....	87
APPENDIX A METHOD OF RESIDUALS USED FOR DERIVING INITIAL PARAMETER ESTIMATES OF IV PK PROFILE.....	88
APPENDIX B ORIGINAL DATA SETS FROM CURVE FITTING APPROACH FOR TOBRAMYCIN IV AND INHALED PK PROFILES.....	92
APPENDIX C ORIGINAL DATA SETS FROM CURVE FITTING APPROACH FOR CALCITONIN IV AND INHALED PK PROFILES.....	100
APPENDIX D ORIGINAL DATA SETS FROM CURVE FITTING APPROACH FOR CIPROFLOXACIN IV AND INHALED PK PROFILES.....	107
APPENDIX E MODEL FILE FOR LOCAL LUNG EXPOSURE PROFILE SIMULATION.....	114
VITA.....	115

LIST OF TABLES

Table 3.1. Physicochemical properties and absence/presence of GI absorption of tobramycin, calcitonin and ciprofloxacin.....	20
Table 3.2 Study design and drug assay method for the studies used in the curve fitting-based lung disposition kinetic analysis for tobramycin.....	26
Table 3.3 % tobramycin deposition following inhaled DPI and NEB administration, measured by γ -scintigraphy. Data were taken from Newhouse et al. (2003).....	28
Table 3.4 Values of the initial estimates obtained by the method of residuals and the best estimates derived by the curve fitting for the two-compartment model parameters of tobramycin from the IV PK profile data.....	29
Table 3.5 The best parameter estimates for the k_a and k_{nal} values of tobramycin derived through curve-fitting of the inhaled PK profile data reported in Newhouse et al, along with the Scientist-derived goodness-of-fit parameters, COD and MSC.....	30
Table 3.6 Study design and drug assay method for the studies used in the curve fitting - based lung disposition kinetic analysis for calcitonin.....	32
Table 3.7 Calcitonin deposition (μg) following inhaled DPI and NEB administration, measured by γ -scintigraphy. Data were taken from Clark et al. (2008).....	34
Table 3.8 Values of the initial estimates obtained by the method of residuals and the best estimates derived by the curve fitting for the one-compartment model parameters of calcitonin from the IV PK profile data.....	35
Table 3.9 The best parameter estimates for the k_a and k_{nal} values of calcitonin derived through curve fitting of the inhaled PK profile data reported in Clark et al, along with the Scientist-derived goodness-of-fit parameters, COD and MSC.....	36
Table 3.10 Study design and drug assay method for the studies used in the curve fitting-based lung disposition kinetic analysis for ciprofloxacin.....	38

Table 3.11 % Ciprofloxacin deposition following DPI administration, measured by γ -scintigraphy. Data were taken from Stass et al. (2016).....	40
Table 3.12 Values of the initial estimates obtained by the method of residuals and the best estimates derived by the curve fitting for the two-compartment model parameters of ciprofloxacin from the IV PK profile data.....	41
Table 3.13 The best parameter estimates of the k_a and k_{nal} values of ciprofloxacin derived through curve fitting of PK profile data reported in Stass et al along with the Scientist-derived goodness of fit parameters, COD and MSC.....	42
Table 3.14 Physicochemical properties and the k_a and k_{nal} values derived by curve fitting for tobramycin, calcitonin and ciprofloxacin.....	48
Table 4.1 Literature used in the moment-based lung disposition kinetics analyses.....	51
Table 4.2 The IV and inhaled PK parameters for tobramycin in the moment-based analyses.....	54
Table 4.3 The lung disposition kinetic parameters for tobramycin derived through the moment-based analyses.....	54
Table 4.4 The k_a and k_{nal} values of tobramycin derived by the curve fitting- and moment-based approaches.	55
Table 4.5 The IV and inhaled PK parameters for calcitonin in the moment-based analyses.....	56
Table 4.6 The lung disposition kinetic parameters for calcitonin derived through the moment-based analyses.....	56
Table 4.7 The k_a and k_{nal} values of calcitonin derived by the curve fitting and moment-based approaches.....	56
Table 4.8 The IV and inhaled PK parameters for ciprofloxacin in the moment-based analyses.....	57
Table 4.9 The lung disposition kinetic parameters for ciprofloxacin derived by the moment-based analyses.....	58
Table 4.10 The k_a and k_{nal} values of ciprofloxacin derived by the curve fitting- and moment-based approaches.....	58
Table 4.11 Physicochemical properties and the k_a and k_{nal} values derived by the curve fitting and moment analysis approaches for tobramycin, calcitonin and ciprofloxacin.....	61
Table B.1 Tobramycin mean serum concentration vs. time profile data reported in Pleasants et al. after IV infusion.....	92
Table B.2 Macro-rate constants derived from tobramycin IV PK profile reported in Pleasants et al. by using method of residuals.....	93
Table B.3 Goodness-of-fit statistics and statistical output for tobramycin IV PK profile curve fitting.....	95

Table B.4-A Tobramycin mean (\pm SD) serum concentration vs. time profile data reported in Newhouse et al. after inhalation from DPI.....	96
Table B.4-B Tobramycin mean (\pm SD) serum concentration vs. time profile data reported in Newhouse et al. after inhalation from NEB.....	96
Table B.5-A Goodness-of-fit statistics and statistical output for tobramycin DPI PK profile curve fitting.....	98
Table B.5-B Goodness-of-fit statistics and statistical output for tobramycin NEB PK profile curve fitting.....	99
Table C.1 Calcitonin mean (\pm SD) plasma concentration vs. time profile data reported in Buclin et al. after IV infusion.....	100
Table C.2 Goodness-of-fit statistics and statistical output for calcitonin IV PK profile curve fitting.....	102
Table C.3-A Calcitonin mean (\pm SD) plasma concentration vs. time profile data reported in Clark et al. after inhalation from DPI.....	103
Table C.3-B Calcitonin mean (\pm SD) plasma concentration vs. time profile data reported in Clark et al. after inhalation from NEB.....	103
Table C.4-A Goodness-of-fit statistics and statistical output for calcitonin DPI PK profile curve fitting.....	105
Table C.4-B Goodness-of-fit statistics and statistical output for calcitonin NEB PK profile curve fitting.....	106
Table D.1 Ciprofloxacin mean (\pm SE) serum concentration vs. time profile data reported in Brunner et al. after IV infusion.....	107
Table D.2 Macro-rate constants derived from ciprofloxacin IV PK profile reported in Brunner et al. by using method of residuals.....	108
Table D.3 Goodness-of-fit statistics and statistical output for ciprofloxacin IV PK profile curve fitting.....	110
Table D.4 Ciprofloxacin mean (\pm SD) plasma concentration vs. time profile data reported in Stass et al. after inhalation from DPI.....	111
Table D.5 Goodness-of-fit statistics and statistical output for ciprofloxacin DPI PK profile curve fitting.....	113

LIST OF FIGURES

Figure 1.1 The fate of inhaled drugs after inhalation, modified from Hochhaus (2007).....	4
Figure 1.2 Fate of inhaled drugs following deposition in the lung: (1) Deposition onto and dissolution into the lung lining fluid (LLF); (2) Absorption across the pulmonary epithelium; (3) Phagocytic and mucociliary clearance of the undissolved particles; (4) Local pulmonary metabolism; and (5) Lung tissue binding. The figure is modified from Ruge et al. (2013).....	6
Figure 3.1. One-compartment open body model: k_{10} ; first-order rate constant for elimination; and V_c : apparent volume of distribution of the central compartment.....	22
Figure 3.2 Two-compartment open body model: k_{10} , k_{12} and k_{21} : the first-order rate constants for elimination from the central compartment, transfer from the central to the peripheral compartment, and transfer from the peripheral to the central compartment, respectively; and V_c : apparent volume of distribution of the central compartment.....	22
Figure 3.3 The lung deposition and disposition model incorporating absorption and non-absorptive loss, along with the systemic elimination. The lung receives dose-to-the lung (DTL) upon inhaled administration. Lung's absorption and non-absorptive loss are kinetically described with the first-order rate constants, k_a and k_{nal} , respectively. The systemic disposition follows either one- or two-compartment model described in Figure 3.1 and 3.2, respectively. Hence, the systemic disposition kinetics were controlled not only by elimination and distribution but also by lung absorption as an input function.....	24
Figure 3.4 Mean serum tobramycin concentration vs. time following 0.5 h IV infusion at a dose of 1.5 mg/kg. Data were taken from Pleasants et al., (1988).....	27
Figure 3.5 Mean (\pm SD) serum tobramycin concentration vs. time following inhaled DPI and NEB administration. Data were taken from Newhouse et al. (2003).....	27

Figure 3.6 The model-predicted profile of the serum concentration of tobramycin vs. time following IV infusion. Data were taken from Pleasants et al. The dashed line is the model-predicted profile generated using the best parameter estimates shown in Table 3.4.....	29
Figure 3.7 The model-predicted profiles of the serum concentration of tobramycin vs. time following inhaled DPI and NEB administration. Data were taken from Newhouse et al. The dashed lines are the model-predicted profiles generated using the best parameter estimates shown in Table 3.5.....	31
Figure 3.8 Mean (\pm SD) plasma calcitonin concentration vs. time following 1 h IV infusion at a dose of 10 μ g. Data were taken from Buclin et al. (2002).....	33
Figure 3.9 Mean (\pm SD) plasma calcitonin concentration vs. time following inhaled DPI and NEB administration. Data were taken from Clark et al. (2008).....	33
Figure 3.10 The model-predicted profile of the plasma concentration of calcitonin vs. time following IV infusion. Data were taken from Buclin et al. The dashed line is the model-predicted profile generated using the best parameter estimates shown in Table 3.8.....	35
Figure 3.11 The model-predicted profiles of the plasma concentration of calcitonin vs. time following inhaled DPI and NEB administration. Data were taken from Clark et al. The dashed lines are the model-predicted profiles generated using the best parameter estimates shown in Table 3.9.....	37
Figure 3.12 Mean (\pm SE) serum ciprofloxacin concentration vs. time following 0.17 h IV infusion at a dose of 200 mg. Data were taken from Brunner et al. (1999).....	39
Figure 3.13 Mean (\pm SD) plasma ciprofloxacin concentration vs. time following inhaled DPI administration. Data were taken from Stass et al. (2016).....	39
Figure 3.14 The model-predicted profile of the serum concentration of ciprofloxacin vs. time following IV infusion. Data were taken from Brunner et al. The dashed line is the model-predicted profile generated using the best parameter estimates shown in Table 3.12.....	41
Figure 3.15 The model-predicted profiles of the plasma concentration of ciprofloxacin vs. time following inhaled DPI administration. Data were taken from Stass et al. The dashed lines are the model-predicted profiles generated using the best parameter estimates shown in Table 3.13.....	43
Figure 3.16-A Correlation between k_a and $K_D/(MW)^{1/3}$ for tobramycin, calcitonin and ciprofloxacin.....	45
Figure 3.16-B Correlation between k_a and $1/(MW)^{1/3}$ for tobramycin, calcitonin and ciprofloxacin.....	46
Figure 4.1 The lung deposition and disposition model that incorporates absorption and non-absorptive loss, along with the systemic elimination. The lung receives dose-to-the lung (DTL) upon inhaled administration. Lung's absorption and non-absorptive loss are	

kinetically described with the first-order rate constants, k_a and k_{nal} , respectively. The systemic disposition kinetics were controlled not only with elimination from the systemic circulation but also by lung absorption as the first-order input rate, k_a53

Figure 4.2 Correlation between curve fitting- and moment analysis-based k_a and $1/(MW)^{1/3}$ for tobramycin, calcitonin and ciprofloxacin.....60

Figure 5.1 The kinetic models and their parameters and the DTL used as the reference standard conditions for A) tobramycin, B) calcitonin and C) ciprofloxacin. These parameters were derived in Chapter 3 as the parameter estimates to best explain each of the inhaled PK profiles of the literature.....63-64

Figure 5.2-A Effects of $\pm 20\%$ changes in the A) DTL, B) k_a and C) k_{nal} values on the serum tobramycin concentration vs. time profiles following inhaled administration in healthy subjects and % changes in the C_{max} , AUC_{∞} and T_{max} values. The profiles in blue are drawn by simulation using DTL= 27.4 mg, $k_a= 0.45\text{ h}^{-1}$ and $k_{nal}= 0.08\text{ h}^{-1}$, as derived by the curve-fitting of the profile data in the literature in Chapter 3. The profiles in orange and gray are drawn by simulation upon +20 and -20 % change in the parameter of interest, while the remainders were held consistent with the values derived through the curve-fitting.....70

Figure 5.2-B Effects of $\pm 20\%$ changes in the A) DTL, B) k_a and C) k_{nal} values on the plasma calcitonin concentration vs. time profiles following inhaled administration in healthy subjects and % changes in the C_{max} , AUC_{∞} and T_{max} values. The profiles in blue are drawn by simulation using DTL= 52.9 μg , $k_a= 0.06\text{ h}^{-1}$ and $k_{nal}= 2.32\text{ h}^{-1}$, as derived by the curve-fitting of the profile data in the literature in Chapter 3. The profiles in orange and gray are drawn by simulation upon +20 and -20 % change in the parameter of interest, while the remainders were held consistent with the values derived through the curve-fitting.....71

Figure 5.2-C Effects of $\pm 20\%$ changes in the A) DTL, B) k_a and C) k_{nal} values on the plasma ciprofloxacin concentration vs. time profiles following inhaled administration in healthy subjects and % changes in the C_{max} , AUC_{∞} and T_{max} values. The profiles in blue are drawn by simulation using DTL= 16.58 mg, $k_a= 0.98\text{ h}^{-1}$ and $k_{nal}= 0.61\text{ h}^{-1}$, as derived by the curve-fitting of the profile data in the literature in Chapter 3. The profiles in orange and gray are drawn by simulation upon +20 and -20 % change in the parameter of interest, while the remainders were held consistent with the values derived through the curve-fitting.....72

Figure 5.3-A Effects of $\pm 20\%$ changes in the A) DTL, B) k_a and C) k_{nal} values on the tobramycin drug mass remaining in the lungs vs. time profiles following inhaled administration in healthy subjects and % changes in the AUC_{lung} and $LRT_{0.5}$ values. The profiles in blue are drawn by simulation using DTL= 27.4 mg, $k_a= 0.45\text{ h}^{-1}$ and $k_{nal}= 0.08\text{ h}^{-1}$, as derived by the curve-fitting of the profile data in the literature in Chapter 3. The profiles in orange and gray are drawn by simulation upon +20 and -20 % change in the parameter of interest.....75

Figure 5.3-B Effects of $\pm 20\%$ changes in the A) DTL, B) k_a and C) k_{nal} values on the calcitonin drug mass remaining in the lungs vs. time profiles following inhaled administration in healthy subjects and % changes in the AUC_{lung} and $LRT_{0.5}$ values. The profiles in blue are drawn by simulation using $DTL = 52.9 \mu g$, $k_a = 0.06 h^{-1}$ and $k_{nal} = 2.32 h^{-1}$, as derived by the curve-fitting of the profile data in the literature in Chapter 3. The profiles in orange and gray are drawn by simulation upon $+20\%$ and -20% change in the parameter of interest.....76

Figure 5.3-C Effects of $\pm 20\%$ changes in the A) DTL, B) k_a and C) k_{nal} values on the ciprofloxacin drug mass remaining in the lungs vs. time profiles following inhaled administration in healthy subjects and % changes in the AUC_{lung} and $LRT_{0.5}$ values. The profiles in blue are drawn by simulation using $DTL = 16.58 mg$, $k_a = 0.98 h^{-1}$ and $k_{nal} = 0.61 h^{-1}$, as derived by the curve-fitting of the profile data in the literature in Chapter 3. The profiles in orange and gray are drawn by simulation upon $+20\%$ and -20% change in the parameter of interest.....77

Figure B.1 A) model file, B) Parameter file and C) Predicted profile of the Scientist® for curve-fitting the mean serum concentration vs. time profile of tobramycin following IV infusion.....94

Figure B.2 A) model file, B) Parameter file and C) Predicted profile of the Scientist® for curve-fitting the mean serum concentration vs. time profiles of tobramycin following inhalation from DPI and NEB.....97

Figure C.1 A) model file, B) Parameter file and C) Predicted profile of the Scientist® for curve-fitting the mean plasma concentration vs. time profile of calcitonin following IV infusion.....101

Figure C.2 A) model file, B) Parameter file and C) Predicted profile of the Scientist® for curve-fitting the mean plasma concentration vs. time profiles of calcitonin following inhalation from DPI and NEB.....104

Figure D.1 A) model file, B) Parameter file and C) Predicted profile of the Scientist® for curve-fitting the mean serum concentration vs. time profile of ciprofloxacin following IV infusion.....109

Figure D.2 A) model file, B) Parameter file and C) Predicted profile of the Scientist® for curve-fitting the mean plasma concentration-time profiles of ciprofloxacin following inhalation from DPI.....112

LIST OF ABBREVIATIONS

^{99m}Tc	$^{99m}\text{technetium}$
γ -scintigraphy	Gamma-scintigraphy
ACI	Anderson Cascade Impactor
A_M	Total pulmonary membrane surface area
$\text{AUC}_{0\text{-last}}$	Area under the plasma/serum vs. time curve from time 0 to t_{last}
AUC_{∞}	Area under the plasma/serum vs. time curve to time infinity
$\text{AUC}_{\text{last-}\infty}$	Extrapolated AUC after the last sampling time point to time infinity
AUC_{lung}	Area under the drug mass remaining in the lung vs. time curve
AUC_{tot}	Total area under the plasma/serum concentration vs. time curve
$\text{AUC}_{\text{tot,inh}}$	Total area under the plasma/serum vs. time curve after inhalation
$\text{AUC}_{\text{tot,iv}}$	Total area under the plasma/serum vs. time curve after IV bolus/infusion
$\text{AUMC}_{0\text{-last}}$	Area under the moment plasma/serum vs. time curve from time 0 to t_{last}
$\text{AUMC}_{\text{last-}\infty}$	Extrapolated AUMC after the last sampling time point to time infinity
AUMC_{tot}	Total area under the moment plasma/serum concentration vs. time curve
C_C	Plasma/serum concentration
C_{Clast}	Plasma/serum concentration at the last sampling time point
CF	Cystic Fibrosis

CI	Confidence interval
C_{\max}	Peak plasma/serum concentration
COD	Coefficient of determination
COPD	Chronic obstructive pulmonary disease
CYP450	Cytochrome P450 enzymes
Da	Dalton
D_M	Diffusion coefficient through lung membrane
$Dose_{iv}$	IV dose by bolus injection or infusion
DPI	Dry powder inhaler
DTL	Drug dose delivered to the lung
F	Female
F_L	DTL-based pulmonary bioavailability
FMO	Flavin-containing monooxygenase
FPF	Fine Particle Fraction
GI	Gastrointestinal
h	Thickness of pulmonary membrane
IV	Intravenous
k_0	Infusion rate
k_{10}	First-order elimination rate constant from the central compartment
k_{12}	First-order rate constant for transfer from the central to the peripheral compartment
k_{21}	First-order rate constant for transfer from the peripheral to the central compartment
k_a	First-order rate constant for absorption
K_D	Drug's distribution coefficient
k_{mcc}	First-order rate constant for the lung's mucociliary clearance from central lung
k_{mcp}	First-order rate constant for the lung's mucociliary clearance from peripheral lung
k_{nal}	First-order rate constant for non-absorptive loss
λ	Terminal-phase slope of the semi-natural logarithmic plasma/serum concentration vs. time curve after IV bolus/infusion
LLF	Lung lining fluid
LLOQ	Lower Limit of quantitation
$LRT_{0.5}$	Lung residence half-life
M	Male
MAO	Monoamine oxidase
M_c	Drug mass in the central compartment
M_L	Drug mass remaining in the lung compartment

$M_{L,0}$	Drug mass in lung at time=0
MLRT	Mean lung residence time
MMAD	Mass Median Aerodynamic Diameter
M_P	Drug mass in the peripheral compartment
MRT	Mean Residence Time
MRT_{inh}	MRT after inhalation administration
MRT_{iv}	MRT after IV bolus/infusion
MSC	Model Selection Criterion
MW	Molecular weight
N	Number of subjects
NA	Not reported
NEB	Nebulizer
NR	Not applicable
P/C ratio	Peripheral-to-central deposition ratio
PET	Positron Emission Tomography
PK	Pharmacokinetic
pMDI	Pressurized metered dose inhaler
SD	Standard Deviation
SE	Standard Error
SLC	Solute like-carrier transporter
SPECT	Single Photon Emission Computed Tomography
T_{dose}	Time required for zero-order/constant rate administration
t_{last}	Last sampling time point
T_{max}	Time at peak plasma concentration
V_{LLF}	Lung lining fluid volume
V_C	Apparent volume of distribution of the central compartment
vs.	versus

ABSTRACT

LUNG DISPOSITION MODEL-BASED ANALYSES OF CLINICAL PHARMACOKINETIC PROFILES FOR INHALED DRUGS

By: Anuja Raut, B.PHARM., M.S.

A thesis submitted in partial fulfillment of the requirements for the degree of Master of Science at Virginia Commonwealth University.

Virginia Commonwealth University, 2017

Director: Masahiro Sakagami, Ph.D.
Associate Professor, Department of Pharmaceutics, School of Pharmacy

There has been a desire to accurately interpret the inhaled pharmacokinetic (PK) profiles of drugs in humans to aid successful inhaled drug and product developments. However, challenges are layered, as 1) the drug dose delivered to the lung (DTL) from inhalers is a portion of the formulated dose but rarely determined; 2) lung delivery and regional deposition differ, depending on drug, formulation and inhaler; 3) drugs are not

only absorbed from the lung but may also be from the gastrointestinal (GI) tract; and 4) in addition to absorption into the systemic circulation, multiple non-absorptive processes also eliminate drugs from the lung, such as mucociliary clearance, metabolism, phagocytosis and tissue binding. Hence, this thesis project aims to develop new lung disposition model-based analyses to derive the meaningful kinetic descriptors for lung disposition from inhaled PK profiles in humans.

Two approaches, curve fitting- and moment-based approaches, were developed. Both approaches modeled the kinetics of lung disposition rate-controlled by absorption (k_a) and non-absorptive loss (k_{nal}), assuming no contribution of GI absorption. An exhaustive literature review found necessary data sets for three drugs, tobramycin, calcitonin and ciprofloxacin. In the curve fitting-based approach, each inhaled PK profile was fitted to the lung disposition model, while the DTL was obtained from corresponding γ -scintigraphic lung deposition and the kinetic parameters of systemic disposition were fixed by separate intravenous PK profile model analysis. In the moment analysis-based approach, the mean lung residence times (MLRT) and the DTL-based bioavailability (F_L) were estimated and used to determine the k_a and k_{nal} values in the lung disposition model, given $F_L = MLRT \cdot k_a = k_a / (k_a + k_{nal})$.

The k_a and k_{nal} values were successfully derived for all the three drugs delivered by dry powder inhalers (DPIs) and/or nebulizers (NEB) through both approaches. Their “goodness-of-fit” was reasonably satisfactory. The k_a values appeared to be primarily described by partition-based diffusion affected by the three hydrophilic drug’s molecular weight. In contrast, the k_{nal} values differed, yet appeared to become plausible, with a notion of additional non-absorptive confoundedness due to lung tissue binding

(tobramycin) and metabolism (calcitonin), in addition to mucociliary clearance. The k_a and k_{nal} values derived by the two approaches were comparable in majority of the cases.

The success of these PK modeling analyses enabled further attempts to identify most influential attributes by simulation. The systemic PK and lung exposure profiles were predicted by simulation upon $\pm 20\%$ changes in each of the DTL, k_a and k_{nal} values to examine changes in the systemic PK metrics (C_{max} , AUC and T_{max}) and local lung exposure metrics (AUC_{lung} and $LRT_{0.5}$). For all three drugs, the C_{max} and AUC changes were identical to changes in the DTL without changing the T_{max} . In contrast, impacts of the k_a and k_{nal} changes differed between drugs, depending on the relative contribution of the rate constant to their sum (k_a+k_{nal}). It appeared that the major contributor of the sum (k_a+k_{nal}) was that rate-controlling the kinetics of lung disposition.

In conclusion, this thesis project has successfully proposed two new approaches of curve fitting and moment-based analysis by accurately deriving the kinetic descriptors of lung disposition (k_a and k_{nal}) for three drugs from the inhaled PK profiles in humans. Their applications were extended to predict likely changes in the systemic PK and local lung exposure metrics by simulation. While attempts should continue with more drugs, these approaches are believed to be useful in identifying critical attributes to determine the lung disposition kinetics and thus predicting the lung kinetic behavior and systemic PK profiles of new drug entities in humans.

CHAPTER 1

INTRODUCTION

1.1 Inhaled drug delivery

Inhaled drug delivery utilizes the lung as the route of administration primarily for treating local lung diseases such as asthma, chronic obstructive pulmonary disease (COPD) and lung infection (Labiris & Dolovich 2003; Patil & Sarasija 2012). It is also used to deliver drugs to treat systemic diseases like insulin for diabetes mellitus and nicotine for smoking cessation, while being tested in clinical trials for treating migraine (Patil & Sarasija 2012; Tfelt-Hansen et al. 2000). Regardless of use for local or systemic disease treatments, an optimal amount of drug is required to reach the lung by passing through the oropharyngeal cavity to produce the therapeutic responses following inhalation (Labiris & Dolovich 2003). This is in contrast to intravenous injection and oral administration, in which the entire drug dosage is directly injected into the systemic circulation via needles and taken by the mouth to be swallowed, respectively (Verma et al. 2010). While intravenous injection is capable of producing the fastest onset of action in less than 1 min, this route has several disadvantages, which includes a greater risk of

irreversible adverse effects due to higher systemic concentrations, a higher risk of embolism, and most critically, pain with needles (Verma et al. 2010). In this context, inhaled route is needle- and pain-free, and can produce the therapeutic responses as fast as injection for certain drug molecules, exerting the onset of action in 2-3 min. It is clear that this pharmacologic rapidity is much shorter than 30-90 min required for oral administration (Verma et al. 2010).

Unlike intravenous injection and oral administration, however, inhaled drug delivery requires an appropriate choice and use of inhaler devices for successful local or systemic therapies (Patil & Sarasija 2012). Most commonly used inhaler devices are pressurized metered dose inhalers (pMDI), nebulizers (NEB) and dry powder inhalers (DPI). Each inhaler device requires a patient's inspiratory effort that potentially causes variability as to fractions of the formulation dose to reach the lung by inhalation (Ibrahim et al. 2015). In this regard, training has been shown to be essential not only for proper use by patients in therapy but also for reproducible delivery among subjects in clinical pharmacokinetic or bioequivalence studies (Ibrahim et al. 2015).

pMDIs are most commonly used for delivering drug aerosols in the treatments of asthma and COPD. pMDI is composed of a canister, a metering valve, an actuator and a mouth piece (Ibrahim et al. 2015). The canisters are made of inert materials such as plastic, stainless steel, glass and aluminum to hold a high pressure inside to maintain propellant gas in a liquid state (Newhouse 1991). pMDIs generate aerosol drug doses from the metering valve by actuation accurately and reproducibly, so that their dose emission is not influenced by inspiratory force or maneuver of patients (Newhouse 1991).

NEBs are inhaler devices suitable for use in pediatric, ventilated or unconscious patients because aerosol delivery does not require actuations and patients' inspiratory coordination (Ibrahim et al. 2015). Two types of NEBs, jet and ultrasonic NEBs, are currently in use, depending on the type of force generating drug aerosol from solutions. NEBs are bulky, cumbersome inhaler devices, while allowing delivery of large aerosol doses; however, electric power and long inhalation time are required (Newhouse 1991).

Unlike NEBs, DPIs are portable devices and require little coordination between patient inspiration and device actuation. Since DPIs formulate and deliver drugs in a dry powder, greater chemical stability can be achieved. However, the DPI performance enabling optimal aerosol generation and delivery to the lungs in patients is highly dependent on drug, formulation and inhaler device (Ibrahim et al. 2015). DPIs employ external forces like airflow shear or particle-particle and particle-device impaction to deaggregate and aerosolize the powder drugs. The type of such external forces depends on the design of DPIs. For example, Diskus, Clickhaler and Multihaler employ airflow shear, whereas Turbuhaler and Spinhaler rely on particle-particle and particle-device impaction for drug aerosol generation. Besides, a fair balance of inhaler resistance and airflow velocity is critical for the best DPI performance. For instance, a higher flow rate increases generation of aerosols suitable for deposition in the upper respiratory tract (Ibrahim et al. 2015).

1.2 Lung deposition and disposition complexities

While inhalation therapy is intended by direct delivery of drugs to the lungs, drug mass delivered to the lung, regional (peripheral vs. central) lung deposition, drug mass deposited in the ex-lungs, e.g., oropharynx, and drug mass swallowed to the gastrointestinal (GI) tract, are all dependent on choice and use of inhaler device (pMDI, NEB or DPI) in addition to drug and formulation. The GI drug absorption and the liver metabolism determine how much of the swallowed drugs eventually contribute to the systemic drug levels (Figure 1.1).

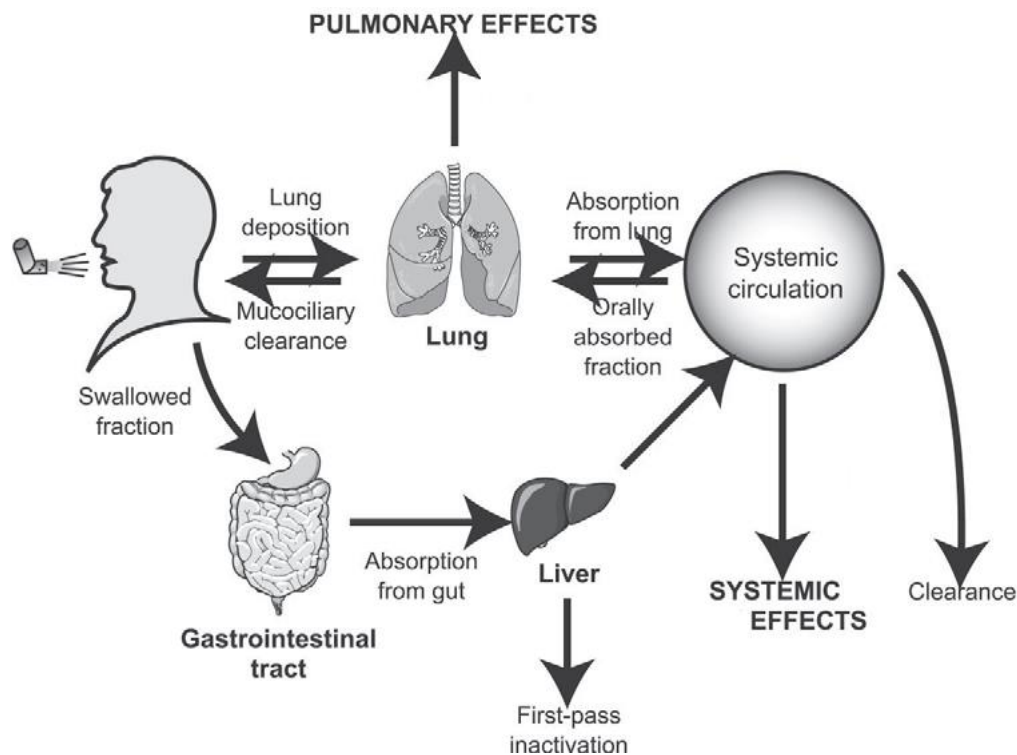


Figure 1.1 The fate of inhaled drugs after inhalation, modified from Hochhaus (2007).

Figure 1.1 shows the fate of drugs after inhalation. When a patient inhales a dose formulated in an inhaler, only a fraction is emitted, while significant fractions remain in the

inhaler. Out of the emitted drug dose, some fractions are trapped in the oropharynx or exhaled by the patient. The fraction deposited in the lung can be subjected to mucociliary clearance if its rate is faster than that of dissolution (in case of dry powder aerosol) and cellular uptake for local pulmonary effects or absorption into the systemic circulation for systemic effects. The fraction deposited in the oropharynx is swallowed into the GI tract. Depending on its GI absorption and liver metabolism, the drug could reach the systemic circulation. Hence, the fate of the drug after inhalation depends on the doses deposited not only in the lung but also in the oropharynx, the kinetics of dissolution and absorption in the lung and, GI absorption and liver metabolism (Hochhaus 2007).

As described above, regional (peripheral vs. central) deposition within the lung is also affected by drug, formulation and device characteristics, as well as patient factors, such as airway geometry, inspiratory profile, breath holding, and correct inhaler use. However, there are currently no established quantitative understanding between regional drug deposition in the lung and subsequent kinetics of lung absorption and clearance. Hence, in addition to the complexity due to inhaler delivery efficiency and patient factors, this issue of regional lung deposition needs to be taken into account for interpretation of the PK profile for inhaled drugs. However, such attempts remain theoretical to date, as described below.

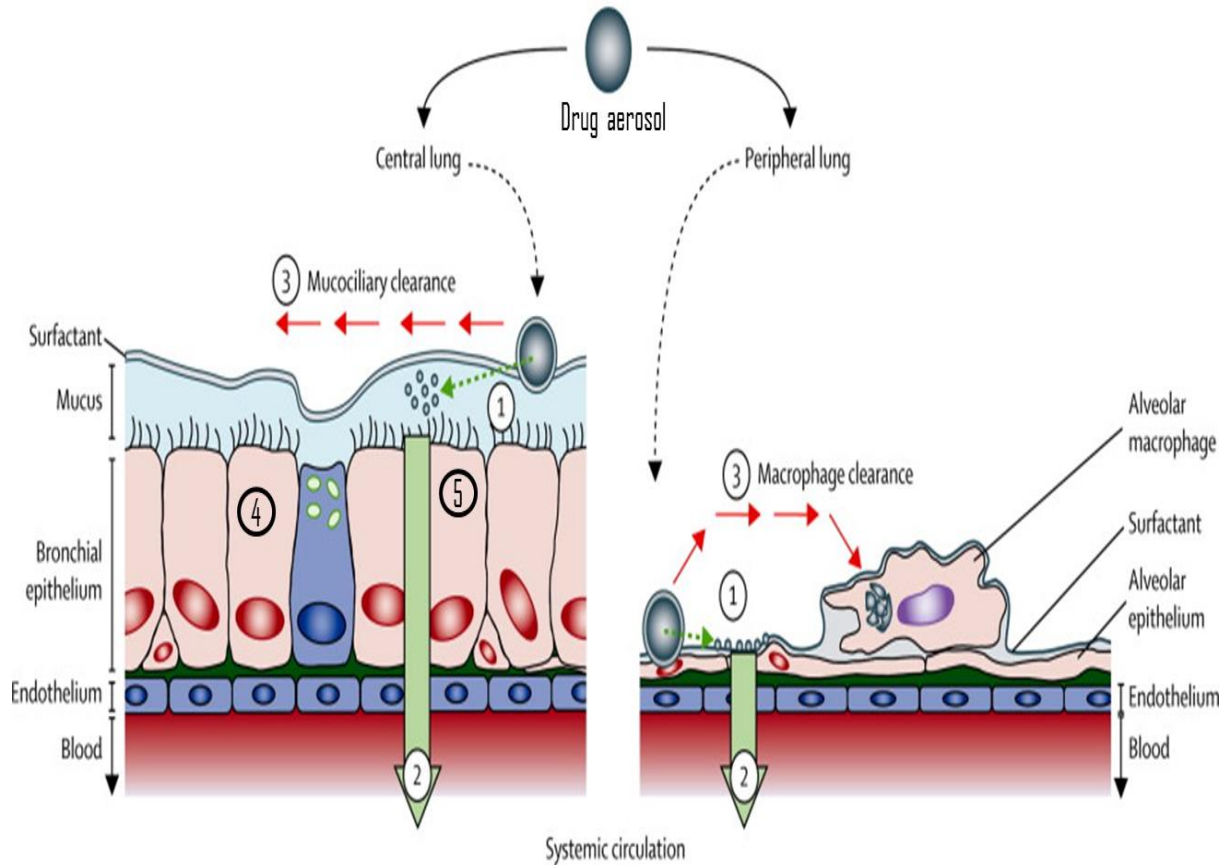


Figure 1.2 Fate of inhaled drugs following deposition in the lung: (1) Deposition onto and dissolution into the lung lining fluid (LLF); (2) Absorption across the pulmonary epithelium; (3) Phagocytic and mucociliary clearance of the undissolved particles; (4) Local pulmonary metabolism; and (5) Lung tissue binding. The figure is modified from Ruge et al. (2013).

Upon deposition in the lung as a dry powder aerosol, the drug particles must first be dissolved in the lung lining fluid (LLF) that covers the lung epithelia, and then taken by the lung cells and/or absorbed into the systemic circulation. Drug dissolution in the LLF depends on the drug's solubility as well as the LLF volume available for dissolution. Given the lung region-dependent LLF composition, volume and depth, dissolution of inhaled drugs may be different in different lung regions; however, to date, such knowledge has not been established (Olsson et al. 2011).

In general, lipophilic drugs are absorbed across the lung epithelia via passive diffusion, whereas hydrophilic drugs pass through tight junctions between epithelial cells (via paracellular route). In addition, drugs can be actively absorbed via solute-like carrier (SLC) transporter processes as well as endo/trans-cytosis. Therefore, lung absorption may be comprised of such multiple processes that simultaneously occur at different rates. Such lung absorption rates may also vary in different lung regions upon deposition. For instance, drug absorption in the peripheral lung is likely faster due to higher rate of perfusion, a greater surface area (100 m²) and a thin diffusion epithelial barrier (Borghardt et al. 2015).

In addition to dissolution and absorption, there are other kinetically competing processes, which may contribute to clearance of inhaled drugs from the lung. These include mucociliary clearance, lung metabolism, phagocytic clearance and lung tissue binding (Labiris & Dolovich 2003; Patton & Byron 2007). When drug particles deposited in the lung remain insoluble, such particles are trapped in the gel layer of the LLF, cleared toward the pharynx by an upward mucus movement by cilia beating, and eventually swallowed to the GI tract. Both the total drug mass deposited in the lung and regional lung deposition may be different among subjects. Especially in patients with asthma and COPD, their smaller airway cross-sectional areas cause more impaction in the central parts of the lung. This results in greater mucociliary clearance loss due to faster cilia movement in the central lung, compared to the peripheral lung, thereby possibly explaining a reduced systemic exposure in patients seen for some corticosteroids (Olsson et al. 2011). Thus, depending on the regional lung deposition as well as lung disease

state, mucociliary clearance may enable removal of the drugs from the lung before absorption or local pharmacologic effects.

All the drug-metabolizing enzymes found in the liver are also found throughout the conducting airways and lung alveoli, yet to a lesser extent. Cytochrome P450 (CYP450) enzymes, flavin-containing monooxygenases (FMO), monoamine oxidase (MAO), aldehyde dehydrogenase, NADPH-CYP450 reductase are all found in the lungs. Protein and peptide drugs are highly degraded by proteases that are found in the lung epithelia, alveolar macrophages and other inflammatory cells like neutrophils (Labiris & Dolovich 2003). When the drug is susceptible to degradation by such lung's metabolizing enzymes, it may contribute as non-absorptive clearance of the drug from the lung.

Drug particles deposited in the alveolar region are cleared by macrophages when the drugs are insoluble or slowly dissolved and absorbed to the systemic circulation. These alveolar macrophages phagocytose such drug particles and then translocate them into the ciliated airways for mucociliary clearance. The alveolar macrophages are also sources for lung proteases that metabolically degrade proteins and peptides, and the protease expression may differ, depending on disease states of the lungs, but is largely unknown (Labiris & Dolovich 2003).

Lipophilic or hydrophilic molecules that carry positive charge under physiological conditions, such as pentamidine, verapamil and tobramycin, are mostly basic amines, and thus may bind favorably to the lung tissue, namely via phospholipids or lysosomes (Patton & Byron 2007). Their lysosomal uptake is caused by trapping, i.e., unionized weak bases permeate and accumulate in the acidic interior of lysosomes, where the molecules get protonated and thus cannot diffuse back into the cytosol. The uptake of such basic

amines into the lysosomes depends on the lysosomal pH (Boer 2003). Thus, lung tissue binding may lead to slowing down of lung's mucociliary clearance and in turn possibly increase the duration of local effects.

1.3 Methods to determine total and regional drug lung deposition

As described previously, only a fraction of the drug dose formulated in an inhaler device is deposited in the lung after inhalation. Additionally, the regional lung deposition varies, depending on the drug, formulation and inhaler, along with a variability caused by patient factors. The drug mass deposited in the lung and regional lung deposition is therefore of interest of kinetically analyze the systemic PK profile data of inhaled drugs.

In vitro impactor-based testing methods classify inhaler device-generated aerosol particles, and “respirable” particles are generally defined as those with mass median aerodynamic diameter (MMAD) between 1 and 5 μm , i.e., “respirable fraction” or “fine particle fraction” (FPF). The particles larger than that size are “non-respirable” which are to impact on the oropharynx (after which they are swallowed and may be absorbed from the GI tract). The simplest apparatus to determine such “respirable” particle mass is the Twin Impinger, which has an angled “throat” and two collecting chambers, among which the drug particles reaching the second chamber are classified as “respirable” ones. In contrast, the Anderson cascade impactor (ACI) allows more detailed collection of inhaler device-generated aerosol particles into eight size fractionations that precede the right-angled USP induction port. Generally, while reproducible FPF data are important for quality-control, these *in vitro* impactor methods possess a number of drawbacks for prediction of lung deposition, given that the anatomy of the human respiratory tract is

complex and therefore poorly represented by these collection chambers or plates alongside their “throat” (Snell & Ganderton 1999; Chrystyn 2001). Daley-Yates et al. (2014) compared *in vitro* fine particle mass of Rotahaler and Diskus inhalers for fluticasone propionate and salmeterol against the *in vivo* performance of both the inhalers and found that the *in vitro* results had poor sensitivity and predictability of *in vivo* results. It was observed that even though the *in vitro* results were comparable for both inhalers, the *in vivo* exposure metrics area under the plasma concentration vs. time curve (AUC) was larger and time for maximum plasma concentration (T_{max}) was shorter for Rotahaler compared to Diskus. This was noted to be probably due to a larger dose delivered to lung and a greater peripheral deposition from Rotahaler due to a larger dose emission duration of 3 seconds compared to a mere 0.3 seconds from Diskus. A shorter dose emission duration may cause greater oropharyngeal and central lung deposition due to impaction with walls of these regions. However, since *in vitro* techniques do not closely mimic the complexity of the human oropharyngeal and respiratory anatomy, they were not found to be good predictors of *in vivo* performance of these inhalers.

Conventional pharmacokinetic (PK) analysis is challenging for inhaled drugs, because the systemic (plasma or serum) drug levels may be confounded by GI absorption of the swallowed fraction from the oropharyngeal deposition, in addition to lung absorption. Accordingly, co-administration of activated charcoal can be used to block GI absorption to reflect the systemic levels exclusively due to lung absorption. Note however that this becomes important only when the drug has considerable oral bioavailability. Some studies used the drug mass in urine collected in the first 30 min of inhaled administration as a quantitative measure of lung deposition and absorption. Even so, the

rate of absorption across the lung is variable and affected by depth of inspiration and breath-holding, as well as dissolution in the LLF following regional lung deposition. Therefore, such approaches best reflect whole lung drug deposition, while giving no information on lung region-dependent deposition and disposition (Chrystyn 2001).

Imaging techniques like the two dimensional γ -scintigraphy involve radiolabeling of inhaled drugs in formulations using a γ -emitting radioisotope like ^{99m}Tc technetium. The whole lung, oropharynx and stomach as well as the inhaler device and the exhalation filter are imaged using a γ -camera. The method also allows differentiation of “central” and “peripheral” lungs, thereby estimating not only total lung deposition but also regional lung deposition. While three-dimensional imaging methods like single photon emission computed tomography (SPECT) and positron emission tomography (PET) are also available, they are much more expensive, time consuming, and require highly skilled and experienced personnel to perform the imaging. As a result, two dimensional γ -scintigraphy has been most widely used to determine the total and regional lung deposition (Chrystyn 2001; Snell & Ganderton 1999).

1.4 PK modeling approaches

The total and regional deposition, aerosol drug dissolution, and absorptive and non-absorptive clearance processes in the lungs have made accurate understanding of lung disposition for inhaled drugs difficult and challenging. Successful attempts should derive and predict such complex kinetics of inhaled drugs by incorporating mucociliary clearance, absorption to the systemic circulation via the lung and the GI tract, and

dissolution in the LLF (Weber & Hochhaus 2013; Sakagami 2014). A distinction can be made in the model between central vs. peripheral lung depending on the goal of the modeling approach. While making this distinction allows accounting for disposition complexity due to inherent physiological differences in the lung, like faster absorption from peripheral lung and faster mucociliary clearance rate in the central lung; incorporating this distinction in the model makes the model more complex and necessitates making certain assumptions which may not be universally applicable. For example, when using a model which distinguishes the lung into different compartments and using that model to fit to PK data from COPD patients, the assumption that mucociliary clearance is faster from central lung may not hold true because of the impaired mucociliary clearance in such patients.

Development of a compartmental PK model to describe this complex lung disposition PK requires use of assumptions based on knowledge like different lung absorption rates due to physiological characteristics of the lung, parameters to describe different absorptive and non-absorptive routes that the drug may take after deposition, as well as formulation based assumptions, and therefore, a compromise between simplicity and realism is necessary in modeling approaches, depending on the specific goal of the modeling approach. (Borghardt et al. 2015) When the goal of the modeling approach is to understand how disposition kinetics are inhaler- and drug-dependent, it may be feasible to regard the lung as a single compartment in the model to simplify the model and decrease the number of parameters in the model that need to be derived, thereby preventing overparameterization of the model. An example of a complex PK model was published by Miller et al. (2010) which was developed with the goal to predict budesonide inhaled drug PK profile. It was observed that the model prediction of the C_{max} and T_{max} of

the budesonide inhaled PK profile were slightly deviated from the literature budesonide inhaled PK profile. This may be because the model described the lungs as a collection of up to five compartments (nose, extra-thoracic, thoracic, bronchiolar and alveolar). The lung disposition was assumed to be controlled by dissolution, absorption into pulmonary cells and eventually into systemic circulation, mucociliary clearance and metabolism with a parameter included in the model for each process; while also accounting for fractions of unbound drug in the mucus/surfactant layers and the pulmonary cells. In addition, the model also used literature values to describe human lung physiological parameters (surface area, thickness and volume for the mucus and cell) for each of the five lung compartments, pulmonary permeability and systemic PK parameters. Thus, these large number of parameters in the model could have overparameterized the model, causing some deviations in the observed budesonide PK profile and the predicted profile.

Another example of the modeling approach was published by Weber and Hochhaus (2013) where the PK parameter estimates were derived from the literature to describe the systemic PK profiles of inhaled drugs. The PK parameters that were unavailable in the literature were assigned with assumptions for characteristics of absorption rate constants and pulmonary deposition patterns. The authors also assumed the fraction of the dose deposited in the mouth-throat to be swallowed and absorbed from the GI tract to contribute to the systemic drug levels, when appropriate. Notably, the drug dose deposited in the lung was differentiated into two kinetically different absorption, by modeling different rates of absorption from two lung compartments, the central and peripheral lungs. In addition, the rate estimates for mucociliary clearance and dissolution were obtained from the literature and included in the PK model. Simulations were

performed with this PK model, which were found to be well compared with the PK results of four clinical studies. Thus, by comparing this model to the previous example published by Miller et al., it may be speculated that a simpler model with less number of parameters allowed prediction of PK profiles more consistent with the literature PK profiles. However, the impactor data was used as the total and regional lung deposited doses, which would require caution, because as described previously, such *in vitro* data may not accurately represent drug dose to lung due to poor sensitivity and predictive capability of *in vitro* data to *in vivo* performance.

Subsequently, Sakagami (2014) employed another kinetic model which incorporated a fraction of the dose deposited in the lung as well as regional lung deposition in the central and peripheral lungs, in addition to dissolution rate-controlled lung absorption and mucociliary clearance from both the central and peripheral lung to analyze clinical PK profiles from the literature for inhaled fluticasone propionate and fluticasone furoate. In the model, the systemic PK parameters and mucociliary clearance kinetics were fixed at their literature values. The model fitting was found to be successful in explaining and predicting the PK profiles for both inhaled drugs. However, the total and regional lung deposition fractions were derived from impactor data, which may not accurately predict *in vivo* deposition. This model distinguished the lung into two compartments, while assuming that the dissolution controlled-rate of absorption of fluticasone was unaltered in these two lung regions. Thus it remains to be seen how the prediction accuracy of the model would change in this case by including the lung as a single compartment in the model, thereby allowing a decrease of the number of parameters in the model.

The lung disposition kinetics is complex and confounded by many variables like lung delivery and deposition, dissolution in the LLF, absorption and several other clearance processes such as mucociliary clearance, metabolism, phagocytosis and tissue binding. However, it is desirable to minimize this complexity using a simpler lung deposition and disposition-based compartmental PK model which allows a compromise between simplicity and realism, so that accurate derivation and prediction of key parameters determining the inhaled PK profiles may become feasible. In pursuit of this goal, this thesis research describes use of a simpler lung deposition and disposition PK model to derive the lung disposition kinetic descriptors of three drug molecules using curve fitting- and moment analysis-based approaches. Simulation was then performed to assess the effects of changes in lung delivery and disposition parameters on the systemic PK and local lung exposure profiles.

CHAPTER 2

HYPOTHESIS AND SPECIFIC AIMS

This thesis project aims to apply the lung disposition model-based analysis to the inhaled pharmacokinetic (PK) profile data for three drugs in humans to derive accurate kinetic descriptors (rate constants) for lung disposition with negligible GI absorption. It is hypothesized that their lung disposition kinetics can be described with absorption (k_a) and non-absorptive loss (k_{nal}), derived from the inhaled PK profiles and corresponding γ -scintigraphic lung deposition data by using curve fitting-based and moment-based approaches. By so doing, such kinetic descriptors of lung disposition can be identified and discussed as drug-, inhaler- and lung deposition-dependent values. Moreover, inhaled PK profile prediction by simulation enables identification of the impact of change/difference/variance of each attribute. The project is designed to pursue the following five specific aims:

1. Identify drugs with available necessary data sets (i.e., inhaled PK profiles and corresponding γ -scintigraphic lung deposition data alongside intravenous PK profiles) by performing an exhaustive literature review
2. Develop a lung deposition and disposition-based compartment model for inhaled PK profile analysis using curve fitting-based and moment-based approaches

3. Derive the kinetic descriptors of lung absorption and non-absorptive loss (k_a and k_{nal} , respectively) for three drugs through curve fitting-based approach
4. Derive the kinetic descriptors of lung absorption and non-absorptive loss (k_a and k_{nal} , respectively) for three drugs through moment-based approach
5. Predict changes in the inhaled PK profiles and their parameter metrics in response to ± 20 % change/difference/variance of each attribute by simulation

In Chapter 3, upon literature selection of three drugs, i.e., tobramycin, calcitonin and ciprofloxacin, their inhaled PK profiles will be analyzed using curve fitting-based approach to derive drug-, inhaler- and/or lung deposition-dependent k_a and k_{nal} values. In Chapter 4, the identical inhaled PK and lung deposition data sets will be analyzed using moment-based approach to derive and compare the k_a and k_{nal} values. In Chapter 5, inhaled PK and lung exposure profiles will be predicted by simulation in response to ± 20 % change/difference/variance of each attribute from the reference standard condition. Finally, Chapter 6 will summarize all the findings in this thesis project and provide overall conclusions.

CHAPTER 3

LUNG DISPOSITION KINETIC ANALYSIS VIA CURVE FITTING APPROACH

3.1 Introduction

As described in Chapter 1, lung disposition kinetics of inhaled drugs is complex and thus its accurate understanding is challenging. 1) Only a portion of the formulated drugs is deposited in the lung, which is rarely determined; 2) lung-deposited drugs are absorbed from the lung, but absorption may also occur, when drugs are swallowed and reach the gastrointestinal (GI) tract; and 3) lung delivery and regional deposition depend on formulation and inhaler, which may cause different pharmacokinetic (PK) profiles (Hochhaus 2007). Even so, more accurate understanding of the inhaler- and lung deposition-dependent kinetic behavior is desired to aid successful inhaled drug and product development for local and systemic use in patients.

Nonlinear regression curve fitting can be a powerful approach to derive kinetic descriptors for such multi-complex deposition and disposition kinetics in the lungs for inhaled drugs from the PK profile data. In this chapter, the literature was searched and three drugs tested for inhalation, tobramycin, calcitonin and ciprofloxacin, were chosen, based on availability of all necessary data sets: a) dose deposited in the lung (DTL) by γ -

scintigraphy; b) intravenous injection/infusion (IV) profile data; and c) inhaled PK profile data. Hence, the lung deposition and disposition were kinetically modeled along with the systemic disposition and used for curve fitting the PK profiles to derive the lung disposition kinetic descriptors, the rate constants of absorption (k_a) and non-absorptive loss (k_{nal}) using Scientist[®] 3.0 (MicroMath, Saint Louis, MO).

3.2 Methods

3.2.1 Literature data collection

An exhaustive literature search was conducted in PubMed and Google Scholar to identify the following data sets for drugs in healthy subjects for use in this curve fitting-based lung disposition kinetic analysis: 1) PK profile and γ -scintigraphy lung deposition data following inhalation with the same inhaler device; 2) lack of GI absorption and 3) PK profile data following IV injection/infusion. The search terms used in PubMed and Google Scholar were “inhalation PK profile with lung deposition by γ -scintigraphy in healthy volunteers” for inhaled PK profiles alongside corresponding inhaler’s dose delivered to lung. Following identification of drug molecules with such available data sets for inhaled PK, the search term “IV PK profile healthy volunteers” for the corresponding drug molecule was used to identify IV PK profiles. Following identification of all necessary data sets, the study design and details, e.g., the number and demographics of healthy subjects, dose and plasma/serum concentration, sampling time interval and duration, drug assay method and validation, were also carefully inspected to be consistent or comparable across the studies. As a result, tobramycin, calcitonin and ciprofloxacin were chosen for use in this study, and their mean plasma/serum concentration vs. time profile

data for IV and inhaled administration were extracted using GetData Graph Digitizer, a program to digitize graphs and plots (<http://getdatagraphdigitizer.com>). Notably, these three drugs differ with respect to their physicochemical properties and the absence (tobramycin and calcitonin) or presence (ciprofloxacin) of GI absorption, as shown in Table 3.1.

Table 3.1. Physicochemical properties and absence/presence of GI absorption of tobramycin, calcitonin and ciprofloxacin.

Drug	Tobramycin	Calcitonin	Ciprofloxacin
MW (Da)	468	3,432	331
Log K _D	-10	-33	-2
Aqueous solubility (mg/ml)	>50	1	0.08
Oral bioavailability (%)	<1 due to low permeability	<1 due to proteolytic degradation	70
Inhaler device	DPI, NEB	DPI, NEB	DPI

K_D: Distribution coefficient, DPI: Dry powder inhaler, NEB: Nebulizer

3.2.2 Estimation of systemic PK parameters

Systemic PK parameters were estimated from the IV PK profile data first by the method of residuals, followed by nonlinear regression curve fitting using Scientist[®] 3.0 (MicroMath, Saint Louis, MO). The parameter values derived by method of residuals were used as initial estimates to derive the best estimates using curve fitting. Method of residuals employs linear regression of the α - and β -phases of the PK profiles which allows derivation of a single value as the parameter estimate. However, curve fitting employs nonlinear regression for curve fitting which derives the “best” estimate by reaching the global minimum value as the parameter estimate. Thus, nonlinear regression curve fitting was employed to more accurately derive PK parameter estimates. The one- or two-

compartment open body model shown in Figure 3.1 or 3.2, respectively, was used depending on the mono- or bi-exponential decline in the PK profiles. The PK profiles that follow the one-compartment model (Figure 3.1) were generally described by:

$$dM_C/dt = k_0 - k_{10} * M_C \quad \text{Equation 3.1}$$

where M_C is the drug mass in the central compartment; k_0 is the zero-order infusion rate for IV infusion during the infusion period and otherwise, 0 for IV bolus injection or IV infusion after the infusion period; and k_{10} is the first-order elimination rate constant from the central compartment. In contrast, the PK profiles that follow the two-compartment model (Figure 3.2) were described by:

$$dM_C/dt = k_0 + k_{21} * M_P - (k_{12} + k_{10}) * M_C \quad \text{Equation 3.2}$$

where M_P is the drug mass in the peripheral compartment; k_{12} and k_{21} : the first-order rate constants for transfer from the central to the peripheral compartment and from the peripheral to the central compartment, respectively; and k_0 is as described previously.

The IV PK profiles were first analyzed using the method of residuals as described in Gibaldi & Perrier (1982) to estimate the rate constant and V_C values for use as the initial estimates in the subsequent curve fitting. With these initial estimates, the nonlinear regression curve fitting was performed using Scientist to more accurately derive each of the rate constant and V_C values. The goodness-of-fit of the curve fitting was assessed with the 95% confidence intervals (CI) for the derived estimates, Scientist-derived coefficient of determination (COD) and model selection criterion (MSC), and visual inspection of residuals in the PK profiles.

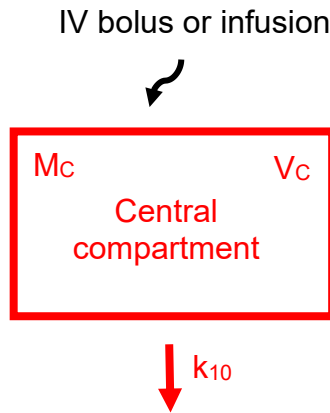


Figure 3.1. One-compartment open body model: k_{10} ; first-order rate constant for elimination; and V_c : apparent volume of distribution of the central compartment.

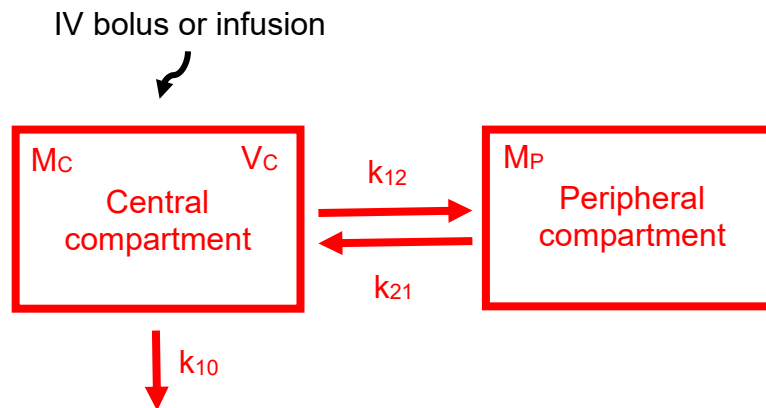


Figure 3.2 Two-compartment open body model: k_{10} , k_{12} and k_{21} : the first-order rate constants for elimination from the central compartment, transfer from the central to the peripheral compartment, and transfer from the peripheral to the central compartment, respectively; and V_c : apparent volume of distribution of the central compartment.

3.2.3 Curve fitting-based estimation of lung disposition kinetic parameters

Each of the inhaled PK profile data was then curve-fitted to the lung deposition and disposition model shown in Figure 3.3. Note that the systemic disposition model was either of the one or two-compartment model shown in Figure 3.1 or 3.2, respectively. The kinetics of lung disposition were assumed to be controlled with the first-order rate constants of absorption (k_a) and non-absorptive loss (k_{nal}), which was described by:

$$dM_L/dt = -(k_a+k_{nal}) * M_L \quad \text{Equation 3.3}$$

Upon inhaled administration ($t=0$), lung deposition, $M_{L,0}$ was equaled to DTL. Hence, the systemic compartment disposition was kinetically controlled not only by distribution and elimination but also by the input rate of $k_a * M_L$, i.e., lung absorption.

In this lung disposition PK model, the DTL was obtained from the γ -scintigraphy data for each drug dosed with the inhaler in the subjects, consistent with those used to obtain the inhaled PK profile data. The systemic disposition PK parameters were fixed at the values obtained by curve fitting the IV PK profile data described above in 3.2.2. Hence, all the parameters except k_a and k_{nal} were fixed, and the inhaled PK profile data were fitted to the model using Scientist to derive the best parameter estimates for k_a and k_{nal} . The goodness-of-fit of the curve-fitting was assessed with the 95% CIs for the derived best parameter estimates, Scientist-derived COD and MSC, and visual inspection of residuals in the PK profiles.

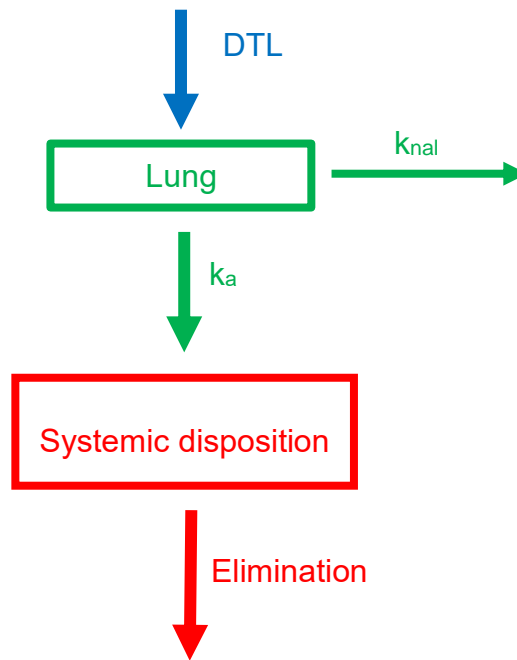


Figure 3.3 The lung deposition and disposition model incorporating absorption and non-absorptive loss, along with the systemic elimination. The lung receives dose-to-the lung (DTL) upon inhaled administration. Lung's absorption and non-absorptive loss are kinetically described with the first-order rate constants, k_a and k_{nal} , respectively. The systemic disposition follows either one- or two-compartment model described in Figure 3.1 and 3.2, respectively. Hence, the systemic disposition kinetics were controlled not only by elimination and distribution but also by lung absorption as an input function.

3.3 Results and Discussion

3.3.1 Literature data collection

By employing the search terms “inhalation PK profile with lung deposition by γ -scintigraphy in healthy volunteers” in PubMed and Google Scholar, research papers were identified for albuterol, budesonide, calcitonin, ciprofloxacin and tobramycin. After a thorough review of the five identified research papers, it was observed that inhaled PK study of albuterol (Hirst et al. 2002) reported only the γ -scintigraphy lung dose without the corresponding inhaled PK profile in healthy volunteers. In case of budesonide, the identified inhaled PK study (Thorsson et al. 1994) reported only the inhaled PK profile without GI absorption without the corresponding γ -scintigraph lung dose. On the contrary, in case of tobramycin, calcitonin and ciprofloxacin, both necessary data sets of inhaled PK profile without GI absorption and corresponding γ -scintigraphy lung deposition data following inhalation with the same inhaler device were identified. Therefore, intravenous injection/infusion (IV) PK profile literature data search was conducted only for tobramycin, calcitonin and ciprofloxacin and albuterol and budesonide were eliminated from the list of drug molecules eligible for this project on account of unavailability of all necessary data sets.

3.3.2 Tobramycin

The IV PK profile data were taken from Pleasants et al. (1988) which employed 0.5 h infusion at a dose of 1.5 mg/kg. The γ -scintigraphic DTL and inhaled PK data were taken from Newhouse et al. (2003), obtained following 0.25 h inhaled administration of spray-dried powders from Turbospin DPI (DPI) and solution aerosols from PARI LC Plus

Nebulizer (NEB). The study design and details are summarized in Table 3.2, which was considered comparable. The IV and inhaled PK profiles are shown in Figure 3.4 and 3.5, respectively, while the γ -scintigraphic data are shown in Table 3.3. Given the linear PK assumption of the lung deposition and disposition PK model, literature IV and inhaled PK data were assessed for dose proportionality. Literature reported IV dose (Pleasants et al.) and DTL (Newhouse et al.) for DPI and NEB were assessed for linearity with the corresponding literature reported area under the serum concentration vs. time curve (AUC) and it was observed that AUC showed dose linearity. Hence it was assumed that tobramycin followed linear PK at the reported IV dose and DTL for both inhalers.

Table 3.2 Study design and drug assay method for the studies used in the curve fitting-based lung disposition kinetic analysis for tobramycin.

Literature	IV PK Pleasants et al.	DTL and inhaled PK Newhouse et al.	
		DPI	NEB
Subject (N)	12	12	
Gender (M/F)	12/0	10/4	
Race	NR	NR	
Age (years)*	26 ± 3	34 ± 8	
Weight (kg)*	78.8 ± 11.4	NR	
Formulation dose	1.5 mg/kg	80 mg	300 mg
Infusion time (h)	0.5	NA	NA
Sampling points (h)	0.17, 0.33, 0.50, 0.67, 0.83, 1.00, 1.33, 1.50, 1.67, 2.00, 2.50, 3.00, 4.00, 6.00, 8.00	0, 0.25, 0.50, 1.00, 1.50, 2.00, 3.00, 4.00, 6.00, 8.00	
Assay method	Fluorescence polarization immunoassay	Fluorescence polarization immunoassay	
LLOQ ^a (mg/L)	0.18	0.05	

*Mean ± SD; ^aLower limit of quantitation; NR: Not reported; and NA: Not applicable

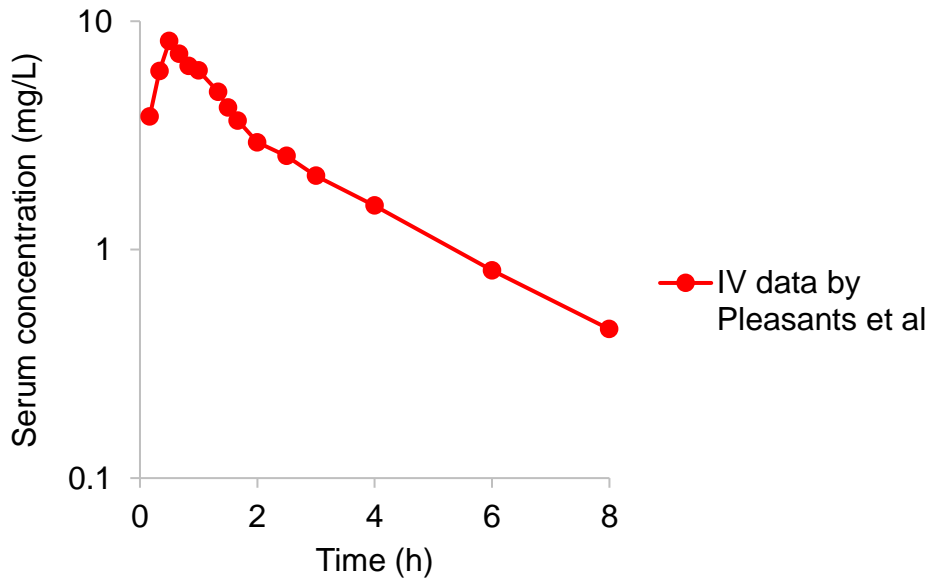


Figure 3.4 Mean serum tobramycin concentration vs. time following 0.5 h IV infusion at a dose of 1.5 mg/kg. Data were taken from Pleasants et al., (1988).

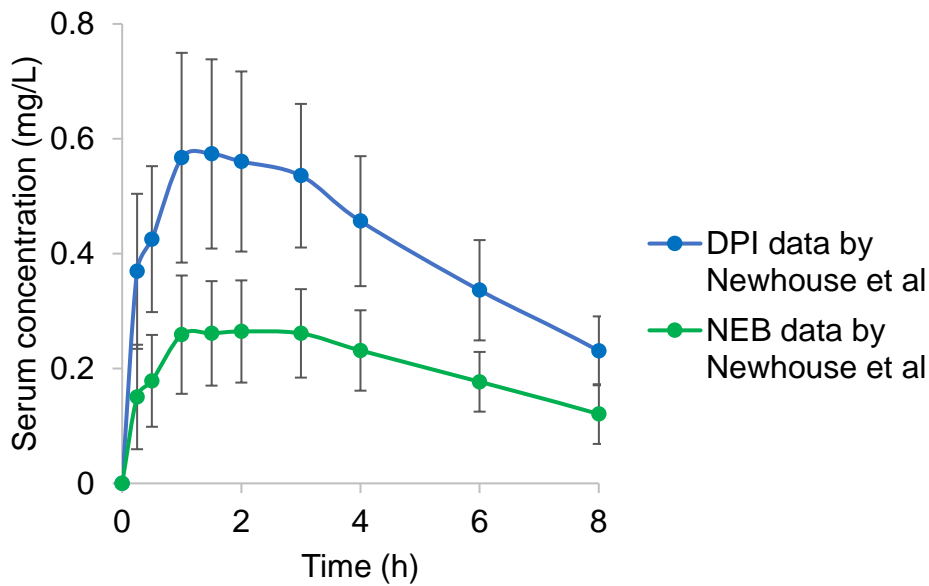


Figure 3.5 Mean (\pm SD) serum tobramycin concentration vs. time following inhaled DPI and NEB administration. Data were taken from Newhouse et al. (2003).

Table 3.3 % tobramycin deposition following inhaled DPI and NEB administration, measured by γ -scintigraphy. Data were taken from Newhouse et al. (2003).

Device	DPI	NEB
DPI capsule	13.3 \pm 4.2	NA
Turbospin inhaler	8.4 \pm 1.0	NA
Nebulizer cup	NA	55.7 \pm 5.6
Nebulizer mouthpiece and T-piece	NA	4.9 \pm 2.2
Exhalation filter	0.20 \pm 0.10	26.4 \pm 3.2
Emitted dose	78.3 \pm 10.3	39.4 \pm 5.1
Oropharynx, esophagus and stomach	43.6 \pm 8.6	8.2 \pm 3.6
DTL	34.3 \pm 5.8	5.0 \pm 2.0
P/C ratio	1.6 \pm 0.4	1.5 \pm 0.4

Data: Mean \pm SD; NA: Not applicable; P/C ratio: Peripheral-to-central deposition ratio

It should be noted that DPI and NEB employed substantially different doses (80 and 300 mg, respectively; Table 3.2), as well as differences in % emitted dose (78.3 and 39.4%; Table 3.3) and % DTL (34.3 and 5%; Table 3.3) were reported. As a result, the DTL calculated from the formulation dose and % DTL were 27.4 mg for DPI and 15.0 mg for NEB. That is, the DTL for DPI was almost twice of that for NEB in this study.

With the IV profile data shown in Figure 3.4, the initial estimates for the systemic two-compartment model disposition parameters obtained by the method of residuals are shown in Table 3.4. Curve-fitting was then performed with Scientist, which was successful, given 0.99 of COD and 4.2 of MSC as well as small residuals seen in profiles, as shown in Figure 3.6. As a result, the best parameter estimates were derived in a more accurate manner, as also shown in Table 3.4. It was observed that method of residuals derived rate constants k_{10} , k_{12} and k_{21} were bracketed by the 95% CI of those derived by curve fitting. However, method of residuals appeared to underestimate the V_c , which may have been because method of residuals does not allow accounting for the time of infusion,

which was incorporated in curve fitting based estimation of the parameters, thereby allowing an accurate estimation of the parameters.

Table 3.4 Values of the initial estimates obtained by the method of residuals and the best estimates derived by the curve fitting for the two-compartment model parameters of tobramycin from the IV PK profile data.

Systemic PK parameter	Initial estimate	Best estimate
k_{10} (h^{-1}) (95% CI)	0.63	0.53 (0.41, 0.65)
k_{12} (h^{-1}) (95% CI)	0.50	0.36 (0.14, 0.58)
k_{21} (h^{-1}) (95% CI)	0.83	0.69 (0.09, 1.48)
V_c (L) (95% CI)	8.27	11.4 (10.5, 12.3)

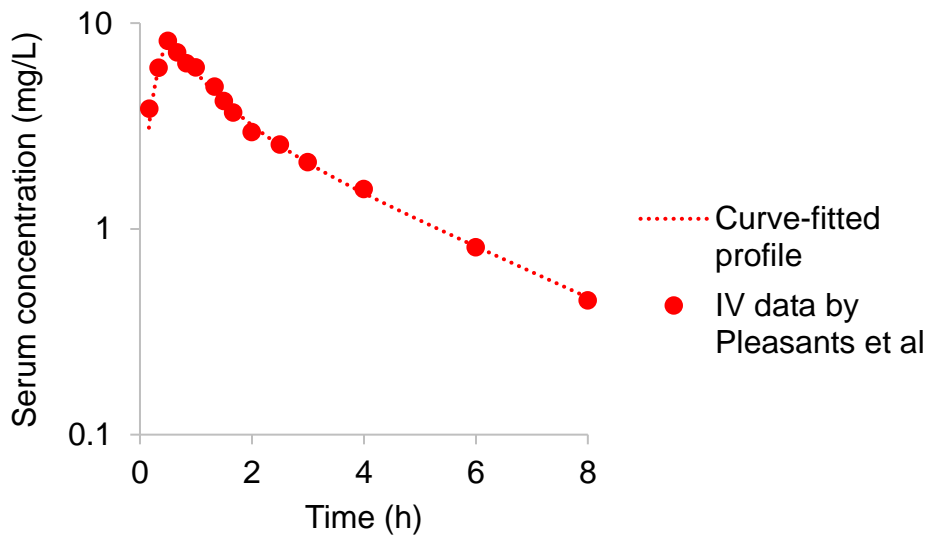


Figure 3.6 The model-predicted profile of the serum concentration of tobramycin vs. time following IV infusion. Data were taken from Pleasants et al. The dashed line is the model-predicted profile generated using the best parameter estimates shown in Table 3.4.

The inhaled PK profile data for DPI and NEB shown in Figure 3.5 were each curve-fitted to the kinetic model shown in Figure 3.3. The DTL was fixed at 27.4 mg for DPI and

15.0 mg for NEB, as estimated from the γ -scintigraphic data (i.e., the formulation dose x % DTL). The systemic disposition parameters were also fixed with the values derived from the IV PK profile data, as shown above. While these were fixed, the lung disposition kinetic parameters, k_a and k_{nal} , were floated in curve fitting with Scientist to be derived from each of the inhaled PK profiles of Newhouse et al. The derived k_a and k_{nal} values are shown in Table 3.5, along with the goodness-of-fit parameters, COD and MSC. In Figure 3.7, only small deviations are shown between the data and the prediction, demonstrating sufficient curve-fitting, despite slightly lower MSC and COD values (Table 3.5). The lower COD and MSC values may be because the number of data points before the maximum serum concentration (C_{max}) after inhalation from both DPI and NEB were only 3, with a total of 9 data points in the sampling duration of 8 h. Such limited number of data points penalizes the MSC and COD values due to overparameterization of the model, which relies on the total number of data points as well as the data points around the higher concentrations available for curve fitting to derive the k_a and k_{nal} values.

Table 3.5 The best parameter estimates for the k_a and k_{nal} values of tobramycin derived through curve-fitting of the inhaled PK profile data reported in Newhouse et al, along with the Scientist-derived goodness-of-fit parameters, COD and MSC.

Device	k_a (h^{-1}) (95% CI)	k_{nal} (h^{-1}) (95% CI)	COD*	MSC ⁺
DPI	0.45 (0.35, 0.55)	0.08 (0.02, 0.17)	0.89	1.78
NEB	0.34 (0.28, 0.40)	0.08 (0.01, 0.15)	0.92	2.15

*Coefficient of determination; ⁺Model selection criteria

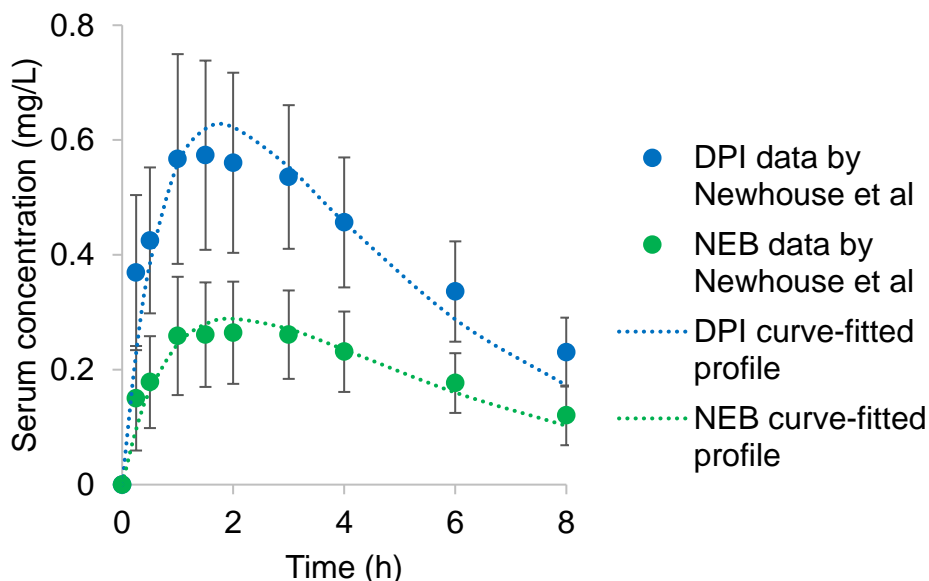


Figure 3.7 The model-predicted profiles of the serum concentration of tobramycin vs. time following inhaled DPI and NEB administration. Data were taken from Newhouse et al. The dashed lines are the model-predicted profiles generated using the best parameter estimates shown in Table 3.5.

3.3.3 Calcitonin

The IV PK profile data were taken from Buclin et al. (2002), which employed 1 h infusion at a dose of 10 μ g. The γ -scintigraphic DTL and inhaled PK data were taken from Clark et al. (2008), obtained following inhaled administration of spray-dried powders from Nektar pulmonary delivery system (DPI) and 0.04 h inhalation of solution aerosols from Salter nebulizer (NEB). The study design and details are summarized in Table 3.6, which was considered comparable. The IV and inhaled PK profiles are shown in Figure 3.8 and 3.9, respectively, while the γ -scintigraphic data are shown in Table 3.7. Both the IV and inhaled PK studies employed immunoassay based techniques to measure calcitonin concentrations after IV and inhaled administration. Given the issues of cross-reactivity based interference with immunoassay techniques, and since the inhaled PK study in

Clark et al. did not comment on the specificity of the radioimmunoassay technique used alongside possible metabolite cross-reactivity, it was assumed that the reported plasma concentrations after IV and inhaled administration were accurate, until further information on cross-reactivity is available through literature for that specific radioimmunoassay technique used in Clark et al. Given the linear PK assumption of the lung deposition and disposition PK model, literature IV and inhaled PK data were assessed for dose proportionality. Literature reported IV dose (Buclin et al.) and DTL (Clark et al.) for DPI and NEB were assessed for linearity with the corresponding literature reported area under the serum concentration vs. time curve (AUC) and it was observed that AUC showed dose linearity. Hence it was assumed that calcitonin followed linear PK at the reported IV dose and DTL for both inhalers.

Table 3.6 Study design and drug assay method for the studies used in the curve fitting -based lung disposition kinetic analysis for calcitonin.

Literature	IV PK Buclin et al.	DTL and inhaled PK Clark et al.	
		DPI	NEB
Subject (N)	8	16	
Gender (M/F)	8/0	8/8	
Race	NR	NR	
Age (years)	22-37*	32 ⁺	
Weight (kg)*	65-86	NR	
Formulation dose	10 µg	300 µg	NR
Infusion time (h)	1	NA	NA
Sampling points (h)	0, 0.25, 0.50, 0.76, 1.00, 1.50, 2.00	0, 0.08, 0.17, 0.33, 0.5, 1, 2, 4, 6	
Assay method	Chemoluminescence-based sandwich immunoassay	Radioimmunoassay	
LLOQ ^a (pg/ml)	2.5	NR	

*Range; ⁺Mean; ^aLower limit of quantitation; NR: Not reported; and NA: Not applicable

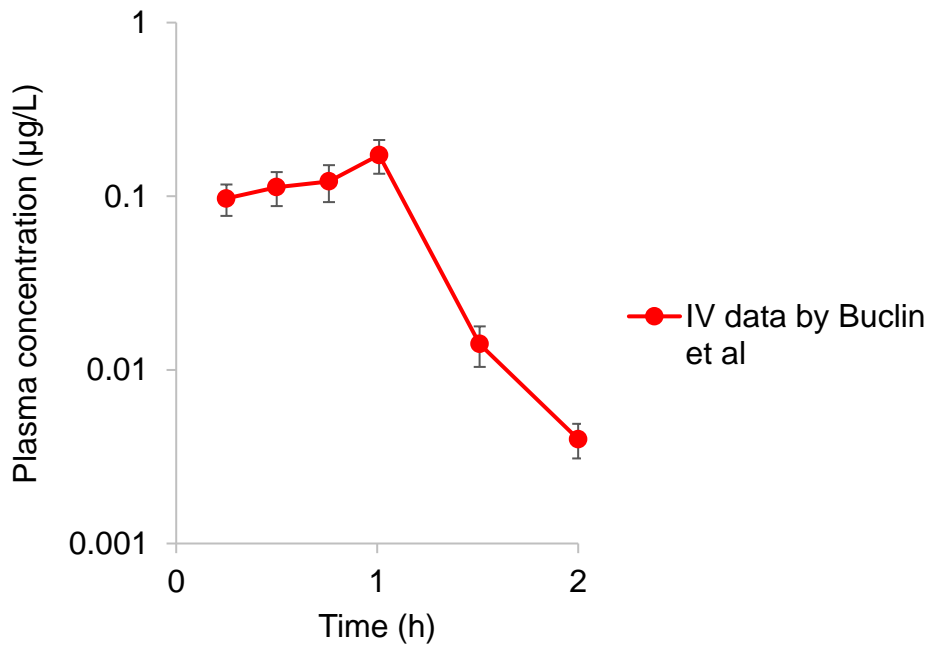


Figure 3.8 Mean (\pm SD) plasma calcitonin concentration vs. time following 1 h IV infusion at a dose of 10 μ g. Data were taken from Buclin et al. (2002).

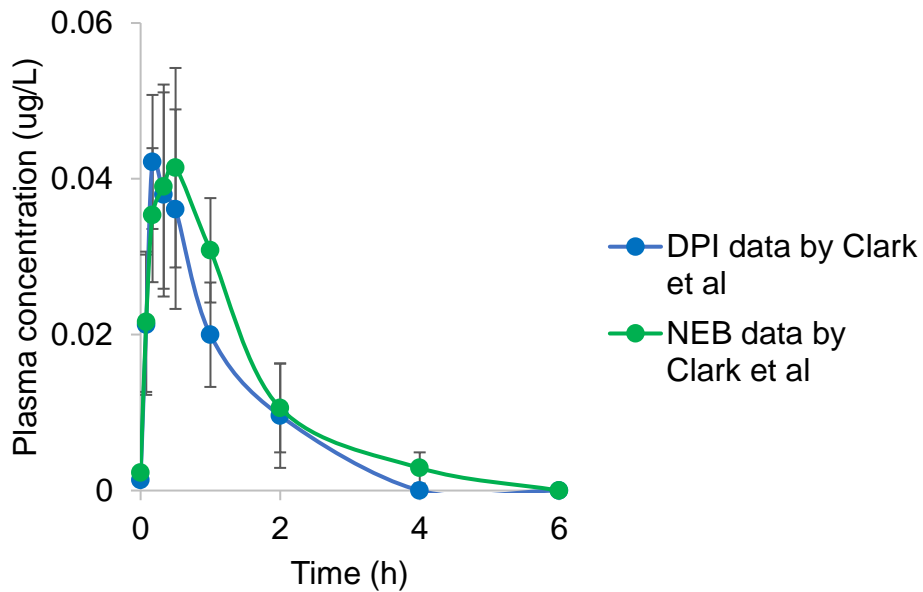


Figure 3.9 Mean (\pm SD) plasma calcitonin concentration vs. time following inhaled DPI and NEB administration. Data were taken from Clark et al. (2008).

Table 3.7 Calcitonin deposition (μg) following inhaled DPI and NEB administration, measured by γ -scintigraphy. Data were taken from Clark et al. (2008).

Device	DPI	NEB
DTL (μg)	52.9 \pm 12.8	56.9 \pm 9.00
P/C ratio	0.8 \pm 0.3	1.4 \pm 0.3

Data: Mean \pm SD; P/C ratio: Peripheral-to-central deposition ratio

It should be noted that DPI employed 300 μg of the formulation dose, while the dose formulated in NEB was not reported (Table 3.6). The DTL was reported 52.9 μg for DPI and 56.9 μg for NEB. That is, the DTL was comparable between DPI and NEB administration in this study (Table 3.7).

With the IV profile data shown in Figure 3.8, the initial estimates for the systemic one-compartment model disposition parameters were obtained, as shown in Table 3.8. Curve fitting was then performed with Scientist, yielding 0.95 of COD and 2.46 of MSC. As shown In Figure 3.10, small deviations were seen between the actual and model-predicted profiles, demonstrating sufficient curve-fitting. As a result, the best parameter estimates were derived in a more accurate manner, as shown in Table 3.8. It was observed that the k_{10} and V_C derived by method of residuals were bracketed by 95% CI of those derived by curve fitting, however it is believed that curve fitting allows a more accurate estimation of parameters because as described previously, curve fitting employs nonlinear regression which allows derivation of the “best” estimate while reaching the global minimum.

Table 3.8 Values of the initial estimates obtained by the method of residuals and the best estimates derived by the curve fitting for the one-compartment model parameters of calcitonin from the IV PK profile data.

Systemic PK parameter	Initial estimate	Best estimate
k_{10} (h^{-1}) (95% CI)	3.77	3.72 (1.24, 6.21)
V_c (L) (95% CI)	15.0	17.9 (8.24, 27.6)

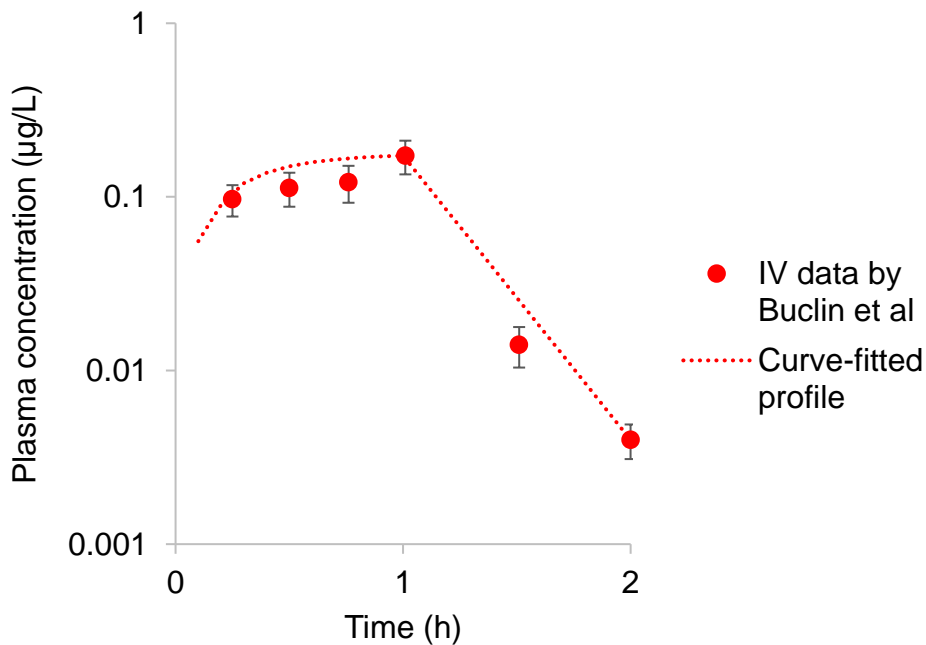


Figure 3.10 The model-predicted profile of the plasma concentration of calcitonin vs. time following IV infusion. Data were taken from Buclin et al. The dashed line is the model-predicted profile generated using the best parameter estimates shown in Table 3.8.

The inhaled PK profile data for DPI and NEB shown in Figure 3.9 were each curve-fitted to the kinetic model shown in Figure 3.3. The DTL was fixed at 52.9 μg for DPI and 56.9 μg for NEB, as reported by γ -scintigraphy. The systemic disposition parameters were also fixed with the values derived from the IV PK profile data, as shown above. While

these were fixed, the lung disposition kinetic parameters, k_a and k_{nal} , were floated in curve fitting with Scientist to be derived from each of the inhaled PK profiles of Clark et al. The derived k_a and k_{nal} values are shown in Table 3.9, along with the goodness-of-fit parameters, COD and MSC. In Figure 3.11, only small deviations are shown between the actual data and the model-predicted profiles, demonstrating sufficient curve fitting, despite slightly lower MSC and COD values (Table 3.9). The lower COD and MSC values may be because the number of data points before the maximum plasma concentration (C_{max}) after inhalation from DPI was just 1, and that after inhalation from NEB were only 3, with a total of 7 data points in the sampling duration of 6 h for both devices. Such limited number of data points penalizes the MSC and COD values due to overparameterization of the model, which relies on the total number of data points as well as the data points around the higher concentrations available for curve fitting to derive the k_a and k_{nal} values.

Table 3.9 The best parameter estimates for the k_a and k_{nal} values of calcitonin derived through curve fitting of the inhaled PK profile data reported in Clark et al, along with the Scientist-derived goodness-of-fit parameters, COD and MSC.

Device	k_a (h^{-1}) (95% CI)	k_{nal} (h^{-1}) (95% CI)	COD*	MSC ⁺
DPI	0.06 (0.04, 0.07)	2.32 (1.24, 3.40)	0.94	2.35
NEB	0.05 (0.04, 0.06)	1.22 (0.84, 1.61)	0.97	3.00

*Coefficient of determination; ⁺Model selection criteria

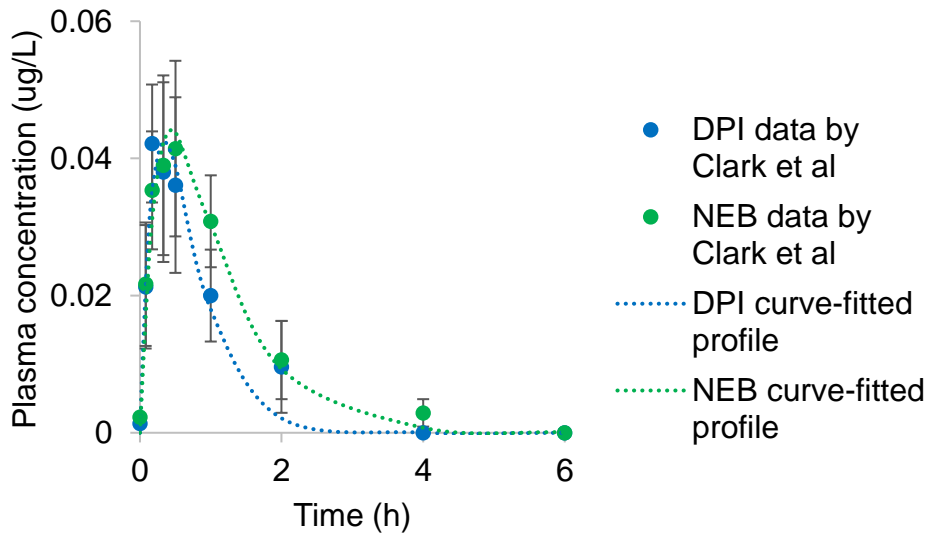


Figure 3.11 The model-predicted profiles of the plasma concentration of calcitonin vs. time following inhaled DPI and NEB administration. Data were taken from Clark et al. The dashed lines are the model-predicted profiles generated using the best parameter estimates shown in Table 3.9.

3.3.4 Ciprofloxacin

The IV PK profile data were taken from Brunner et al. (1999) which employed 0.17 h infusion at a dose of 200 mg. The γ -scintigraphic DTL and inhaled PK data were taken from Stass et al. (2016) obtained following inhaled administration of spray-dried powders from Novartis T-326 inhaler (DPI). The subjects received charcoal orally to block gastrointestinal (GI) absorption of ciprofloxacin deposited in the oropharynx and swallowed to the GI tract. The study design and details are summarized in Table 3.10, which was considered comparable. The IV and inhaled PK profiles are shown in Figure 3.12 and 3.13, respectively, while the γ -scintigraphic data are shown in Table 3.11. Given the linear PK assumption of the lung deposition and disposition PK model, literature IV and inhaled PK data were assessed for dose proportionality. Literature reported IV dose

(Brunner et al.) and DTL (Stass et al.) for DPI were assessed for linearity with the corresponding literature reported area under the serum and plasma concentration vs. time curve (AUC) and it was observed that AUC showed dose linearity. Hence it was assumed that ciprofloxacin followed linear PK at the reported IV dose and DTL for DPI.

Table 3.10 Study design and drug assay method for the studies used in the curve fitting-based lung disposition kinetic analysis for ciprofloxacin.

Literature	IV PK Brunner et al.	DTL and inhaled PK Stass et al.
		DPI
Subject (N)	8	12
Gender (M/F)	8/0	12/0
Race	NR	NR
Age (years)*	28-37	21-52
Weight (kg) ⁺	76 ± 4	NR
Formulation dose	200 mg	32.5 mg
Infusion time (h)	0.17	NA
Sampling points (h)	0.33, 0.67, 1.00, 1.33, 1.67, 2.00, 2.33, 2.67, 3.00, 3.33, 3.67, 4.00, 4.33, 4.67, 5.00, 5.33, 5.67, 6.00, 6.33, 6.67, 7.00, 7.33, 7.67, 8.00	0, 0.5, 1, 1.5, 2, 2.5, 3, 4, 6, 8
Assay method	High performance chromatography with fluorometric detection	liquid chromatography with mass spectrometry
LLOQ ^a (mg/L)	0.05	NR

*Range; ⁺Mean ± SE; ^aLower limit of quantitation; NR: Not reported; and NA: Not applicable

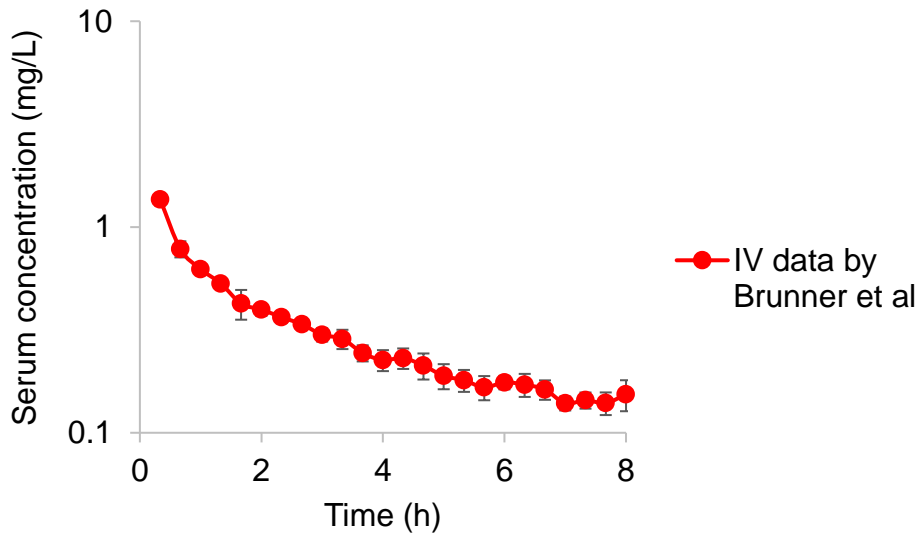


Figure 3.12 Mean (\pm SE) serum ciprofloxacin concentration vs. time following 0.17 h IV infusion at a dose of 200 mg. Data were taken from Brunner et al. (1999).

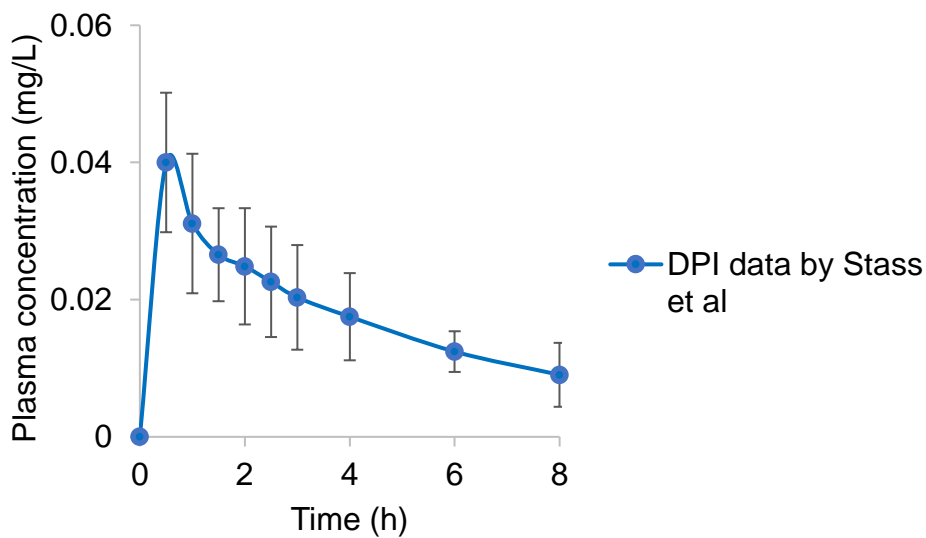


Figure 3.13 Mean (\pm SD) plasma ciprofloxacin concentration vs. time following inhaled DPI administration. Data were taken from Stass et al. (2016).

Table 3.11 % Ciprofloxacin deposition following DPI administration, measured by γ -scintigraphy. Data were taken from Stass et al. (2016).

Inhaler	4 ± 1
Exhaled	1
Extra-thoracic region	44 ± 8
DTL	51 ± 7
P/C ratio	0.6

Data: Mean ± SD; P/C ratio: Peripheral-to-central deposition ratio

Note that the DPI formulation dose was 32.5 mg (Table 3.10) and % DTL was 51% (Table 3.11), thereby estimating 16.58 mg of the DTL.

The initial estimates for the systemic disposition two-compartment model disposition parameters were estimated by the method of residuals on the IV PK profile reported in Brunner et al., as summarized in Table 3.12. The IV PK profile was then fitted to the two-compartment model with the initial estimates (Table 3.12) for a more accurate determination. The best estimates were derived as shown in Table 3.12. The fitted profile provided a good fit of the data as shown in Figure 3.14, and the COD was 0.99 and the MSC was 4.88. It was observed that k_{10} and V_C derived by method of residuals were bracketed by the 95% CI of those derived by curve fitting, whereas k_{12} and k_{21} values derived by method of residuals were smaller than the lower level of the 95% CI of those derived by curve fitting. However, curve fitting derived values of parameters were assumed to be more accurate, as described previously.

Table 3.12 Values of the initial estimates obtained by the method of residuals and the best estimates derived by the curve fitting for the two-compartment model parameters of ciprofloxacin from the IV PK profile data.

Systemic PK parameter	Initial estimate	Best estimate
k_{10} (h^{-1}) (95% CI)	0.58	0.64 (0.57, 0.72)
k_{12} (h^{-1}) (95% CI)	1.02	1.42 (1.11, 1.73)
k_{21} (h^{-1}) (95% CI)	0.64	0.86 (0.70, 1.03)
V_c (L) (95% CI)	95.4	93.2 (84.4, 100)

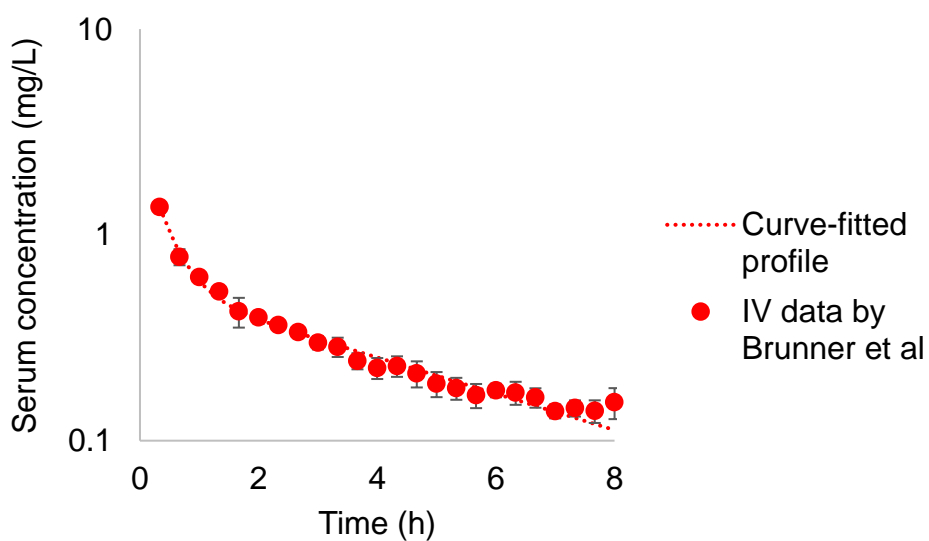


Figure 3.14 The model-predicted profile of the serum concentration of ciprofloxacin vs. time following IV infusion. Data were taken from Brunner et al. The dashed line is the model-predicted profile generated using the best parameter estimates shown in Table 3.12.

The lung disposition kinetic parameters, k_a and k_{nal} , were derived by curve fitting the inhaled PK profiles of ciprofloxacin for DPI reported in Stass et al. The PK profile data was fitted to the lung disposition PK model shown in Figure 3.3, with the systemic

disposition kinetic parameters fixed as described by the two-compartment model (Table 3.12). The γ -scintigraphic DTL was also fixed as shown in Table 3.11. The k_a and k_{nal} values derived for DPI are shown in Table 3.13 along with 95% CI and goodness of fit statistics. The curve fitting provided a good fit of the data with the lung disposition model with the systemic PK described by the two-compartment model. The COD and MSC were slightly lower, while only small deviations were seen between the data and the model-predicted profile (Figure 3.15). The lower COD and MSC values may be because there were no data points before the maximum plasma concentration after inhalation from DPI, with a total of 9 data points in the sampling duration of 8 h. Such limited number of data points penalizes the MSC and COD values due to overparameterization of the model, which relies on the total number of data points as well as the data points around the higher concentrations available for curve fitting to derive the k_a and k_{nal} values.

Table 3.13 The best parameter estimates of the k_a and k_{nal} values of ciprofloxacin derived through curve fitting of PK profile data reported in Stass et al along with the Scientist-derived goodness of fit parameters, COD and MSC.

Device	k_a (h^{-1}) (95% CI)	k_{nal} (h^{-1}) (95% CI)	COD*	MSC ⁺
DPI	0.98 (0.71, 1.25)	0.61 (0.36, 0.86)	0.94	2.45

*Coefficient of determination; ⁺Model selection criteria

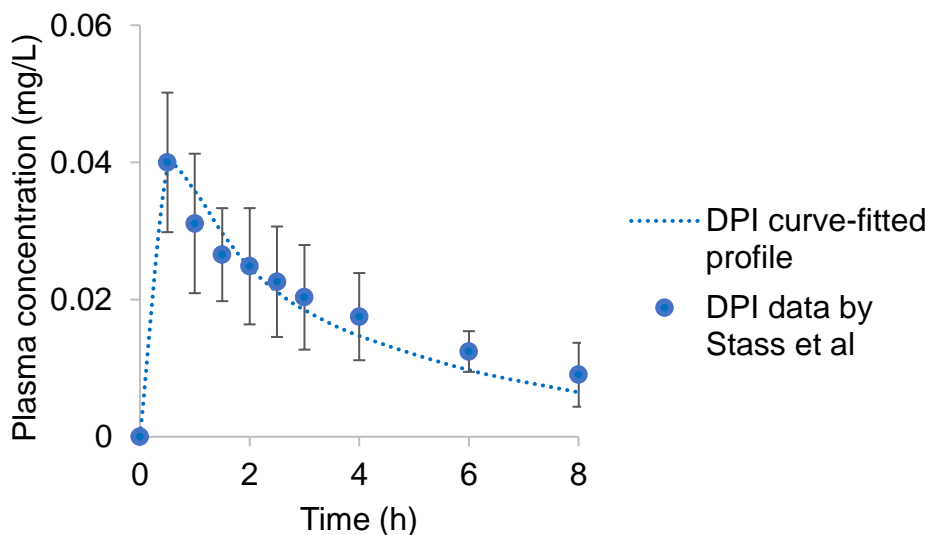


Figure 3.15 The model-predicted profiles of the plasma concentration of ciprofloxacin vs. time following inhaled DPI administration. Data were taken from Stass et al. The dashed lines are the model-predicted profiles generated using the best parameter estimates shown in Table 3.13.

3.3.5 The k_a and k_{nal} values across three molecules

Curve fitting approach was successfully used, yielding sufficient “goodness-of-fit” statistical parameters and deriving the k_a and k_{nal} values for all the three molecules with small 95% CI. The curve fitting approach employed compartment model-based differential equations for non-linear regression of the literature PK profile data for IV and inhaled administration. The DTL and systemic PK parameters were fixed and only the k_a and k_{nal} were allowed to float.

The IV PK profile of tobramycin in healthy volunteers was also found in Haughey et al. (1980) and P  ch  re et al. (1976). However, Pleasants et al. (1988) was chosen, because most frequent sampling over a sufficient length of time (8 h) was taken, and the

assay method was reliable and same as that used in Newhouse et al. (2003). Haughey et al. and P  ch  re et al. both used a microbiological assay. Besides, Haughey et al. (1980) reported the PK profile from just one volunteer. The inhaled PK profiles of tobramycin were also found in Pilcer et al. (2008), but in cystic fibrosis (CF) patients. Given the pathophysiology of CF lungs, inhaled drug disposition kinetics were likely affected by the disease condition. For calcitonin and ciprofloxacin, an exhaustive literature search could not find other IV or inhaled PK profiles in healthy volunteers or the corresponding γ -scintigraphy-based lung deposition data.

Byron and Patton (1994) proposed the following equation with an assumption that lung absorption undergoes passive diffusion via partitioning through cell membranes:

$$k_a = \frac{D_M \cdot A_M \cdot K_D}{h \cdot V_{LLF}} \quad \text{Equation 3.4}$$

where D_M is the diffusion coefficient through lung membrane, A_M is the total lung membrane surface area, K_D is the drug partition/distribution coefficient, h is the thickness of lung membrane and V_{LLF} is the lung lining fluid (LLF) volume. Assuming the physiological parameters A_M , h and V_{LLF} as constant, k_a now becomes dependent on $D_M \cdot K_D$ and given that D_M is proportional to $1/(MW)^{1/3}$ as per the Stokes-Einstein equation, k_a is now dependent on $K_D/(MW)^{1/3}$. Therefore, the derived k_a values were plotted against the respective $K_D/(MW)^{1/3}$, yielding equation $\log [k_a] = 0.05 + 0.04 \times \log [K_D/(MW)^{1/3}]$ ($R^2 = 0.99$) which found a good correlation, as shown in Figure 3.16-A. However, given the log-log plot, the equation implies that k_a is proportional to $K_D/(MW)^{1/3}$ only when it is raised to power 0.04 (slope).

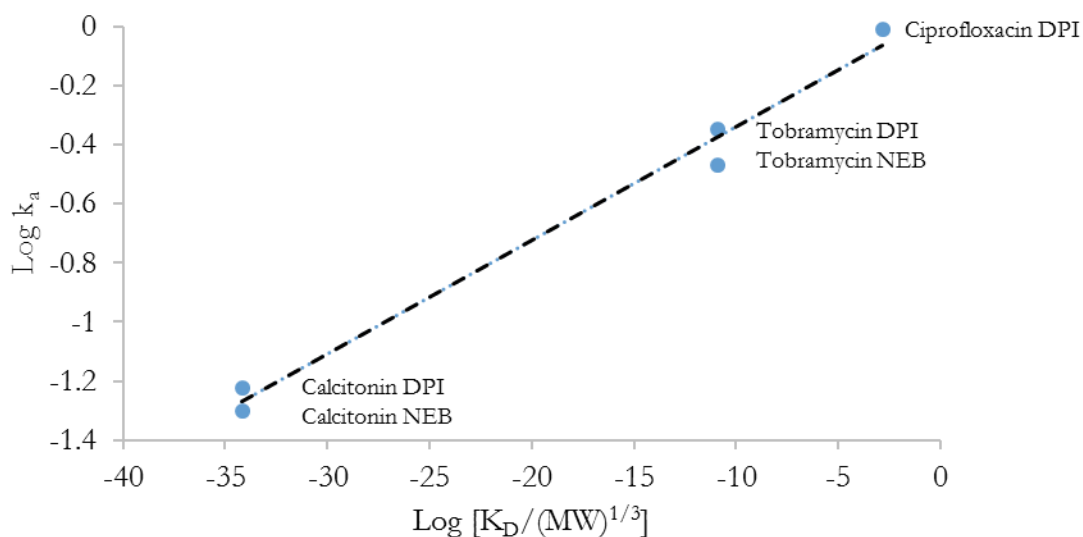


Figure 3.16-A Correlation between k_a and $K_D/(MW)^{1/3}$ for tobramycin, calcitonin and ciprofloxacin.

Figure 3.16-A implies that k_a is not proportional to $K_D/(MW)^{1/3}$ unless it was raised to a power of 0.04. It may be because all the molecules are hydrophilic in nature with negative log K_D values. Thus, assuming k_a to be independent of K_D in case of these three hydrophilic molecules, k_a was plotted against $1/(MW)^{1/3}$ only, as can be seen in Figure 3.16-B yielding equation $\log [k_a] = 2.6 + 3.0 \times \log [1/(MW)^{1/3}]$ ($R^2 = 0.96$) which also found a good correlation. However, given the log-log plot, the equation implies that k_a is proportional to $1/(MW)^{1/3}$ only when it is raised to power 3 (slope). This in turn implies that for tobramycin, calcitonin and ciprofloxacin, k_a is proportional to $1/(MW)$, indicating that their molecular weight appears to primarily control their absorption kinetics from the lung. That is, for large hydrophilic calcitonin, the k_a value was the smallest, followed by small hydrophilic tobramycin, and finally, smaller hydrophilic ciprofloxacin. Ciprofloxacin is a substrate for active transport through bronchial epithelium by OCTs and OATP2B1 (Ong

et al. 2013), and so even though Figure 3.16-B implies ciprofloxacin absorption kinetics being primarily controlled by its MW, the derived high k_a value may also be confounded by its active uptake through the central lung, which is consistent with its low P/C ratio of 0.6 indicating its deposition primarily in the central lung.

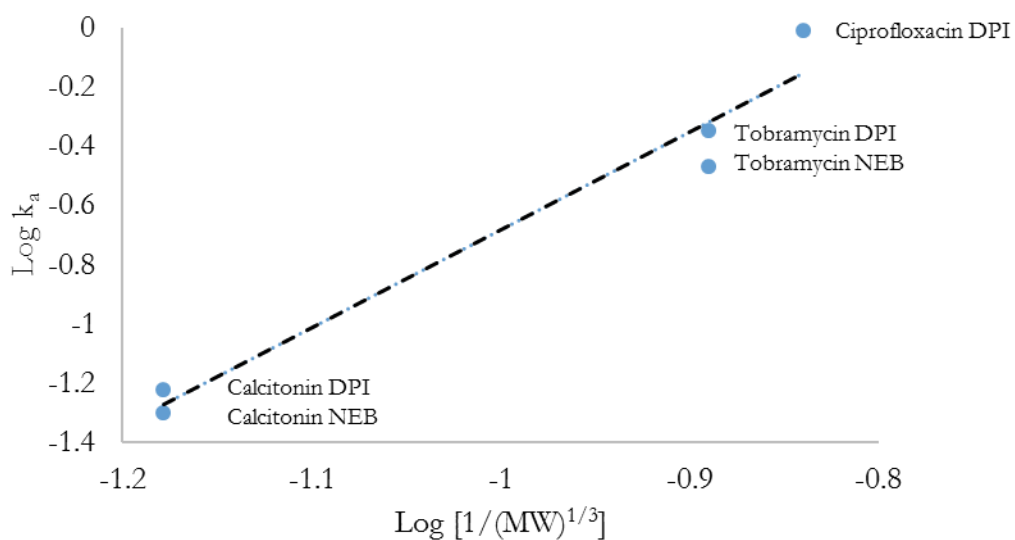


Figure 3.16-B Correlation between k_a and $1/(\text{MW})^{1/3}$ for tobramycin, calcitonin and ciprofloxacin.

The drug's solubility may also play an important role in its absorption rate, and if so, their lung absorption kinetics could be dissolution controlled, especially for small lipophilic molecules like fluticasone propionate (Sakagami 2014). However, the aqueous solubility values for tobramycin, calcitonin and ciprofloxacin (Table 3.1) are adequately high and therefore, it is unlikely that their absorption was rate-limited by solubility/dissolution.

The k_a values also seemed to be dependent on inhaler device as seen for tobramycin. Different inhalers resulted in different regional lung deposition and accordingly, different k_a values presumably due to different regional lung deposition. It can be seen that a higher P/C ratio, which indicates a greater fractional deposition in the peripheral (deeper) lung, produced a greater k_a value, in line with our conventional belief that absorption is faster from the peripheral (deeper) lung by virtue of greater perfusion and thinner pulmonary membranes.

The k_{nal} values for the three drugs were derived in a wide range of 0.08-2.32 h^{-1} , and seemed to be drug dependent. Byron (1986) and Gonda (1988) reported 0.4-0.7 h^{-1} as first order rate constant of mucociliary clearance from central lung (k_{mcc}) and 0.17 h^{-1} as first order rate constant of mucociliary clearance from peripheral lung (k_{mcp}) in humans. (Sakagami 2004) The k_{nal} values for calcitonin were greater than that of k_{mcc} and k_{mcp} values, perhaps due to local lung metabolism by proteolysis, as similarly suggested for the k_{nal} values for inhaled insulin by Sakagami (2004). On the other hand, the k_{nal} values for tobramycin were smaller than the k_{mcc} and k_{mcp} values, which might be associated with lung tissue binding of this drug which will be polycationic in nature at physiological pH. Li and Byron (2013) suggested the lung tissue binding of polycationic tobramycin in the isolated perfused rat lung (IPRL) at 0.02-100 mg/ml. With 10-30 ml of the lung surface fluid, 27.4 mg of tobramycin in DTL would result in 0.91–2.74 mg/ml of the lung surface concentration. Thus, it is possible that tobramycin is highly bound in the lungs. However, Li and Byron (2003) describe tobramycin's binding as a biphasic process, involving sequestration/binding followed by a slow desequestration/dissociation, which implies that it may be released from the lung tissue in a time-dependent manner, and this released

fraction will then be available for absorption and non-absorptive clearance pathways including mucociliary clearance. Thus, caution must be exercised when interpreting the 0.08 h^{-1} of the derived k_{nal} values of tobramycin as caused by tissue binding alone, because the lung deposition and disposition model (Figure 3.3) does not account for such time-dependent slow desequestration/dissociation of tobramycin. In that respect, the k_{nal} value for ciprofloxacin was found comparable to the k_{mcc} value, which was consistent with its lack of local lung metabolism and lung tissue binding.

Table 3.14 Physicochemical properties and the k_a and k_{nal} values derived by curve fitting for tobramycin, calcitonin and ciprofloxacin.

Drug	MW (Da)	Log K_D	Inhaler device	P/C ratio	k_a (h^{-1}) (95% CI)	k_{nal} (h^{-1}) (95% CI)
Tobramycin	468	-10	DPI	1.6 ± 0.4	0.45 (0.35, 0.55)	0.08 (0.02, 0.17)
			NEB	1.5 ± 0.4	0.34 (0.28, 0.40)	0.08 (0.01, 0.15)
Calcitonin	3,432	-33	DPI	0.8 ± 0.3	0.06 (0.04, 0.07)	2.32 (1.24, 3.40)
			NEB	1.4 ± 0.3	0.05 (0.04, 0.06)	1.22 (0.84, 1.61)
Ciprofloxacin	331	-2	DPI	0.6	0.98 (0.71, 1.25)	0.61 (0.36, 0.86)

P/C ratio: Peripheral-to-central deposition ratio

3.4 Conclusions

Using inhaled and IV PK profiles alongside DTL from the lung deposition data in the literature, the lung disposition kinetic descriptors (k_a and k_{nal}) in humans were successfully derived for three drugs delivered by DPI and/or NEB via curve fitting. The k_a

values were found to be dependent on the drug's MW, as passive diffusion appeared to be the predominant pathway for these drugs' absorption. However, regional lung deposition influenced the k_a values in case of tobramycin, and the greater k_a value was seen with higher P/C ratio, i.e., greater deposition in the peripheral lung. While the k_{nal} values did not seem to depend on the physicochemical properties, physiological processes such as local lung tissue binding, metabolism and mucociliary clearance seem to affect the k_{nal} values. The k_{nal} value for ciprofloxacin was consistent with the k_{mcc} and the lung tissue binding may have decreased the k_{nal} value for tobramycin. In contrast, calcitonin is a peptide and thus highly susceptible to proteolytic degradation by proteases in the lung, including trypsin, chymotrypsin and aminopeptidase. This may have contributed to its high k_{nal} values.

The k_a values were shown to be well correlated with the drug's MW, while also being affected by regional deposition within the lung. The k_{nal} values were determined by the presence of binding, local metabolism and mucociliary clearance. While similar attempts should continue with different drugs, these results have suggested that this curve fitting approach seems to be useful in deriving the accurate descriptors that determine the lung disposition kinetics and predicting the lung kinetic behavior of new drug entities in humans.

CHAPTER 4

LUNG DISPOSITION KINETIC ANALYSIS VIA MOMENT-BASED APPROACH

4.1 Introduction

In Chapter 3, the inhaled PK profile data for three inhaled drugs (tobramycin, calcitonin and ciprofloxacin) were analyzed with the lung deposition and disposition compartment model by curve fitting approach. As a result, the kinetic descriptors of lung absorption (k_a) and non-absorptive loss (k_{nal}) were reasonably determined. In this chapter, the same PK data sets were used with a different approach of the moment-based analyses. The same lung disposition kinetic model was then applied to derive the k_a and k_{nal} values. The k_a and k_{nal} values derived by these two different methods were finally compared and discussed.

4.2 Methods

4.2.1 Literature data collection

The IV PK profile data and the inhaled γ -scintigraphy and PK profile data for tobramycin, calcitonin and ciprofloxacin were those taken from the literature and used in the curve fitting-based analysis of the lung disposition kinetics described in Chapter 3. Table 4.1 lists the respective literature sources for each drug. The mean plasma/serum

drug concentration vs. time profile data were extracted using GetData Graph Digitizer, as completed in Chapter 3.

Table 4.1 Literature used in the moment-based lung disposition kinetics analyses.

Drug	IV PK	Inhaled γ -scintigraphy and PK
Tobramycin	Pleasants et al., 1988	Newhouse et al., 2003
Calcitonin	Buclin et al., 2002	Clark et al., 2008
Ciprofloxacin	Brunner et al., 1999	Stass et al., 2016

4.2.2 Moment-based analyses for IV and inhaled PK profiles

Moment-based PK profile analyses were carried out, as described in Gibaldi & Perrier (1982). The total area under the plasma/serum concentration vs. time profile curve (AUC_{tot}) was first calculated by:

$$AUC_{tot} = AUC_{0-last} + AUC_{last-\infty} \quad \text{Equation 4.1}$$

where AUC_{0-last} is the AUC between time 0 and the last sampling time (t_{last}), calculated by the trapezoidal method; and $AUC_{last-\infty}$ is the extrapolated AUC after the last sampling time up to time infinity, which was calculated by:

$$AUC_{last-\infty} = C_{Clast} / \lambda \quad \text{Equation 4.2}$$

where C_{Clast} is the plasma/serum concentration at the last sampling time; and λ is the terminal-phase slope in the semi-natural logarithmic plasma/serum concentration vs. time plot. Separately, the total area under the moment plasma/serum concentration vs. time profile curve ($AUMC_{tot}$) was calculated by:

$$AUMC_{tot} = AUMC_{0-last} + AUMC_{last-\infty} \quad \text{Equation 4.3}$$

where $AUMC_{0-last}$ is the AUMC between time 0 and the last sampling time (t_{last}), calculated with the profile of $[C_c \times \text{time}]$ vs. time by the trapezoidal method; and $AUMC_{last-\infty}$ is the extrapolated AUMC after the last sampling time up to time infinity, which was calculated by:

$$AUMC_{last-\infty} = (C_{Clast} / \lambda^2) + (C_{Clast} \cdot t_{last} / \lambda) \quad \text{Equation 4.4}$$

Accordingly, the mean residence time (MRT) after administration was calculated by:

$$MRT = AUMC_{tot} / AUC_{tot} - T_{dose} / 2 \quad \text{Equation 4.5}$$

where T_{dose} is the time required for constant rate administration, i.e., time of infusion or nebulization and otherwise 0 for IV bolus and inhaled administration with DPI (or pMDI). From the IV and inhaled PK profile data, the MRT values were respectively determined by the method described above, as MRT_{iv} and MRT_{inh} .

4.2.3 Moment-based determination of lung disposition kinetic parameters

To analyze the lung disposition kinetics with these MRT values, the lung disposition kinetic model used in the curve fitting approach in Chapter 3 and now shown in Figure 4.1 was used in following the moment-based analysis described above. Given the linear PK assumption, the MRT in the lung (MLRT) was calculated by:

$$MLRT = MRT_{inh} - MRT_{iv} \quad \text{Equation 4.6}$$

Now, in the model shown in Scheme 4.1, the lung absorption and non-absorptive loss were kinetically rate-controlled with the respective rate constants, k_a and k_{nal} , as assumed in Chapter 3. Hence, by definition, the MLRT was described by:

$$MLRT = 1 / (k_a + k_{nal}) \quad \text{Equation 4.7}$$

Notably, the fractional bioavailability of inhaled administration (F_L) was also defined by:

$$F_L = k_a / (k_a + k_{nal}) \quad \text{Equation 4.8}$$

Therefore, from Equations 4.7 and 4.8, the k_a and k_{nal} values were estimated with:

$$k_a = F_L / \text{MLRT} \quad \text{Equation 4.9}$$

$$k_{nal} = 1 / \text{MLRT} - k_a \quad \text{Equation 4.10}$$

It should be noted that the F_L value was calculated with the AUC values normalized with dose for IV and inhaled administration, as described below:

$$F_L = (\text{AUC}_{\text{tot,inh}}/\text{DTL}) / (\text{AUV}_{\text{tot,iv}}/\text{Dose}_{\text{iv}}) \quad \text{Equation 4.11}$$

where Dose_{iv} is the IV dose by bolus injection or infusion; and DTL is the dose to the lung determined from γ -scintigraphy.

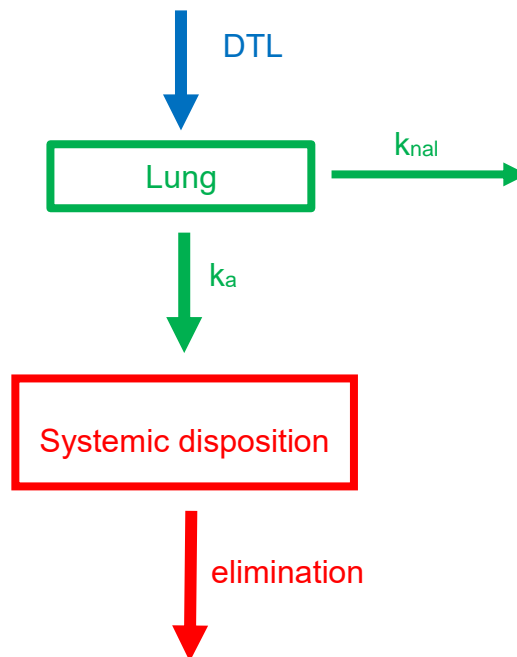


Figure 4.1 The lung deposition and disposition model that incorporates absorption and non-absorptive loss, along with the systemic elimination. The lung receives dose-to-the lung (DTL) upon inhaled administration. Lung's absorption and non-absorptive loss are kinetically described with the first-order rate constants, k_a and k_{nal} , respectively. The systemic disposition kinetics were controlled not only with elimination from the systemic circulation but also by lung absorption as the first-order input rate, k_a .

4.3 Results and Discussion

4.3.1 Tobramycin

The moment-based analyses of the IV and inhaled PK profile data for tobramycin are summarized in Table 4.2. The derived lung disposition kinetic parameters, k_a and k_{nal} , are shown in Table 4.3 and compared with those derived by the curve fitting approach in Chapter 3, as shown in Table 4.4. The k_a and k_{nal} values for tobramycin inhaled with the DPI and NEB were each bracketed by the 95% CI of the corresponding rate constant values derived by the curve fitting approach.

Table 4.2 The IV and inhaled PK parameters for tobramycin in the moment-based analyses.

PK parameter	IV	Inhalation	
		DPI	NEB
AUC_{0-last} (mg/L*h)	17.8	3.37	1.65
Terminal slope λ (h^{-1})	0.32	0.27	0.30
$AUC_{last-\infty}$ (mg/L*h)	1.40	0.85	0.40
AUC_{tot} (mg/L*h)	19.2	4.22	2.05
$AUMC_{0-last}$ (mg/L*h ²)	41.6	11.9	6.02
$AUMC_{last-\infty}$ (mg/L*h ²)	15.6	10.0	4.56
$AUMC_{tot}$ (mg/L*h ²)	57.2	21.9	10.6
MRT (h)	2.73	5.06	5.04

Table 4.3 The lung disposition kinetic parameters for tobramycin derived through the moment-based analyses.

Lung disposition kinetic parameter	DPI	NEB
MLRT (h)	2.34	2.32
1/MLRT (h^{-1})	0.43	0.43
F_L	0.94	0.84
k_a (h^{-1})	0.40	0.36
k_{nal} (h^{-1})	0.03	0.07

Table 4.4 The k_a and k_{nal} values of tobramycin derived by the curve fitting- and moment-based approaches.

Device	k_a (h^{-1}) (95% CI)		k_{nal} (h^{-1}) (95% CI)	
	Curve fitting	Moment analysis	Curve fitting	Moment analysis
DPI	0.45 (0.35, 0.55)	0.40	0.08 (0.02, 0.17)	0.03
NEB	0.34 (0.28, 0.40)	0.36	0.08 (0.01, 0.15)	0.07

4.3.2 Calcitonin

The moment-based analyses of the IV and inhaled PK profile data for calcitonin are summarized in Table 4.5. The derived lung disposition kinetic parameters k_a and k_{nal} are shown in Table 4.6 and compared with those derived by the curve fitting approach in Chapter 3, as shown in Table 4.7. The k_{nal} values for calcitonin inhaled with the DPI and NEB were each bracketed by the 95% CI of the k_{nal} values derived by the curve-fitting approach. However, the k_a values derived were outside the 95% CI of the k_a values derived by the curve fitting approach. Notably, these values were greater than the upper side of the 95% CI.

Table 4.5 The IV and inhaled PK parameters for calcitonin in the moment-based analyses.

PK parameter	IV	Inhalation	
		DPI	NEB
AUC _{0-last} (µg/L*h)	0.16	0.05	0.07
Terminal slope λ (h ⁻¹)	3.72	0.85	0.77
AUC _{last-∞} (µg/L*h)	0	0	0
AUC _{tot} (µg/L*h)	0.16	0.05	0.07
AUMC _{0-last} (µg/L*h ²)	0.12	0.05	0.09
AUMC _{last-∞} (µg/L*h ²)	0	0	0
AUMC _{tot} (µg/L*h ²)	0.12	0.05	0.09
MRT (h)	0.28	0.96	1.21

Table 4.6 The lung disposition kinetic parameters for calcitonin derived through the moment-based analyses.

Lung disposition kinetic parameter	DPI	NEB
MLRT (h)	0.68	0.93
1/MLRT (h ⁻¹)	1.47	1.08
F _L	0.07	0.08
k _a (h ⁻¹)	0.10	0.09
k _{nal} (h ⁻¹)	1.37	0.99

Table 4.7 The k_a and k_{nal} values of calcitonin derived by the curve fitting and moment-based approaches.

Device	k _a (h ⁻¹) (95% CI)		k _{nal} (h ⁻¹) (95% CI)	
	Curve fitting	Moment analysis	Curve fitting	Moment analysis
DPI	0.06 (0.04, 0.07)	0.10	2.32 (1.24, 3.40)	1.37
NEB	0.05 (0.04, 0.06)	0.09	1.22 (0.84, 1.61)	0.99

4.3.3 Ciprofloxacin

The moment-based analyses of the IV and inhaled PK profile data for ciprofloxacin are summarized in Table 4.8. The contribution of $AUC_{last-\infty}$ to AUC_{tot} was 26%, greater than the gold standard of 20%. This may be because of insufficient sampling duration and not the sampling intervals, because Brunner et al. employed sufficient number of sampling intervals over the 8 h sampling duration. The derived lung disposition kinetic parameters k_a and k_{nal} are shown in Table 4.9 and compared with those derived by the curve fitting approach in Chapter 3, as shown in Table 4.10. The k_a value for ciprofloxacin inhaled with the DPI was bracketed by the 95% CI of the corresponding rate constant value derived by the curve fitting approach. However, the k_{nal} value derived was outside the 95% CI of the k_{nal} value derived by the curve fitting approach. Notably, this value was smaller than the lower side of the 95% CI.

Table 4.8 The IV and inhaled PK parameters for ciprofloxacin in the moment-based analyses.

PK parameter	IV	Inhalation
		DPI
AUC_{0-last} (mg/L*h)	2.39	0.18
Terminal slope λ (h^{-1})	0.18	0.17
$AUC_{last-\infty}$ (mg/L*h)	0.85	0.03
AUC_{tot} (mg/L*h)	3.25	0.21
$AUMC_{0-last}$ (mg/L*h ²)	6.92	0.75
$AUMC_{last-\infty}$ (mg/L*h ²)	11.6	0.59
$AUMC_{tot}$ (mg/L*h ²)	18.5	1.35
MRT (h)	5.61	6.39

Table 4.9 The lung disposition kinetic parameters for ciprofloxacin derived by the moment-based analyses.

Lung disposition kinetic parameter	DPI
MLRT (h)	0.78
1/MLRT (h ⁻¹)	1.28
F _L	0.78
k _a (h ⁻¹)	1.00
k _{nal} (h ⁻¹)	0.28

Table 4.10 The k_a and k_{nal} values of ciprofloxacin derived by the curve fitting- and moment-based approaches.

Device	k _a (h ⁻¹) (95% CI)		k _{nal} (h ⁻¹) (95% CI)	
	Curve fitting	Moment analysis	Curve fitting	Moment analysis
DPI	0.98 (0.71, 1.25)	1.00	0.61 (0.36, 0.86)	0.28

4.4 Comparison between moment-based analysis and curve fitting-based approaches

Moment analysis-based approach was successfully used to derive the k_a and k_{nal} values for all three drugs. This approach employed the same IV and inhaled PK profile data as those used in the curve fitting-based approach in Chapter 3. The approach used integrated equations to calculate the AUC and AUMC of the plasma/serum concentration-time curves, followed by the use of the lung disposition PK model to derive the k_a and k_{nal} values. In contrast, the curve fitting approach used differential equation-based non-linear regression, in which IV PK parameters were fixed to derive the k_a and k_{nal} values. Note

that, in the curve fitting, the k_a and k_{nal} values were derived by fitting the PK profile data up to the last sampling time point (t_{last}).

The k_a and k_{nal} values for tobramycin (both DPI and NEB) and k_a value for ciprofloxacin (DPI) were each derived within the 95% CI of the corresponding rate constant values for the curve fitting approach. The k_{nal} values for calcitonin (DPI/NEB) were also within the 95% CI of the values for the curve fitting approach. However, the k_a values for calcitonin (both DPI and NEB) and k_{nal} value for ciprofloxacin were outside the 95% CI of the respective values derived by the curve fitting approach. In fact, calcitonin k_a values were greater than the upper side of the 95% CI and ciprofloxacin k_{nal} value was lower than the lower side of the 95% CI. It is speculated that this over-estimation of the k_a values and under-estimation of the k_{nal} values by the moment analysis-based approach may be due to its use of the AUC and AUMC beyond the t_{last} .

Despite the slight inconsistencies in the values derived by the curve fitting- and moment analysis-based approaches as described above, it was observed that the k_a values derived by moment analysis still found a good correlation with the $1/(MW)^{1/3}$ of the drug molecules when plotted alongside the curve fitting-based k_a values, as depicted in Figure 4.1, yielding equation $\log [k_a] = 2.3 + 3.0 \times \log [1/(MW)^{1/3}]$ ($R^2 = 0.92$).

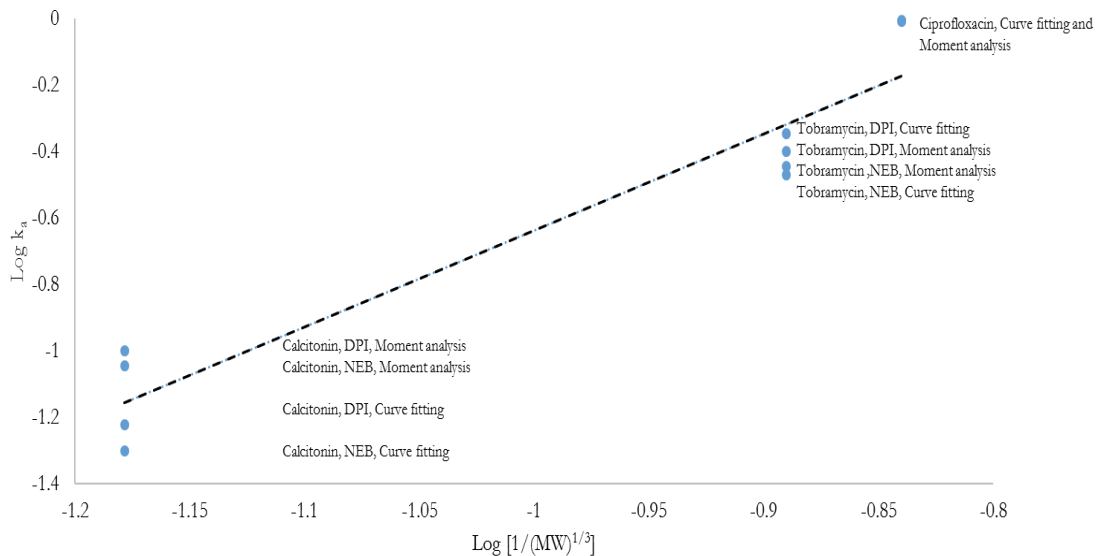


Figure 4.2 Correlation between curve fitting- and moment analysis-based k_a and $1/(MW)^{1/3}$ for tobramycin, calcitonin and ciprofloxacin.

4.5 Conclusions

Using the inhaled and IV PK profiles alongside the DTL from the γ -scintigraphic lung deposition data in the literature, the lung disposition kinetic descriptors (k_a and k_{nal}) were successfully derived for the three drugs delivered by DPI and/or NEB via the moment analysis-based approach. The values derived by these two approaches are summarized in Table 4.11. In addition, the k_a and k_{nal} values were comparable to those derived by the curve fitting-based approach in the majority of the cases. Thus, it is now possible to derive the lung disposition kinetics by this moment analysis-based approach, even though the data set are not compatible to the curve fitting approaches such as when AUC and MRT are the only available information pertinent to a drug molecule. However, the curve fitting approach can give statistical information like 95% CI, COD and MSC, and therefore, would provide greater confidence in their derived values.

Table 4.11 Physiochemical properties and the k_a and k_{nal} values derived by the curve fitting and moment analysis approaches for tobramycin, calcitonin and ciprofloxacin.

Drug	MW (Da)	Log K_D	Inhaler device	P/C ratio	k_a (h^{-1}) (95% CI)		k_{nal} (h^{-1}) (95% CI)	
					Curve fitting	Moment analysis	Curve fitting	Moment analysis
Tobramycin	468	-10	DPI	1.6±0.4	0.45 (0.35, 0.55)	0.40	0.08 (0.02, 0.17)	0.03
			NEB	1.5±0.4	0.34 (0.28, 0.40)	0.36	0.08 (0.01, 0.15)	0.07
Calcitonin	3,432	-33	DPI	0.8±0.3	0.06 (0.04, 0.07)	0.10	2.32 (1.24, 3.40)	1.37
			NEB	1.4±0.3	0.05 (0.04, 0.06)	0.09	1.22 (0.84, 1.61)	0.99
Ciprofloxacin	331	-2	DPI	0.6	0.98 (0.71, 1.25)	1.00	0.61 (0.36, 0.86)	0.28

P/C ratio: Peripheral-to-central deposition ratio

Chapter 5

EFFECTS OF LUNG DELIVERY AND DISPOSITION KINETIC CHANGES ON SYSTEMIC PK AND LUNG EXPOSURE PROFILES VIA SIMULATION

5.1 Introduction

In Chapters 3 and 4, the inhaled PK profile data for the three drugs, tobramycin, calcitonin and ciprofloxacin, have successfully derived the kinetic descriptors for lung disposition by the curve fitting and moment-based approaches, respectively. In both approaches, the identical kinetic compartment model was assumed for lung disposition, thereby resulting in plausible and comparable kinetic rate constants for lung absorption (k_a) and non-absorptive loss (k_{nal}). However, only the mean PK profile data were used, so that how variance of the PK profile data affects derivation of these kinetic descriptors is uncertain. Conversely, from the bioequivalence regulation perspective, how variance or difference of each of the kinetic descriptors affects the systemic PK and local lung exposure profile outcomes would be of interest in order to identify the key attribute(s) within the lung. Hence, this chapter used the kinetic rate constants derived through the curve fitting in Chapter 3 as the reference standard conditions and simulated the PK and lung exposure profiles upon a 20 % positive or 20 % negative change in each of the DTL,

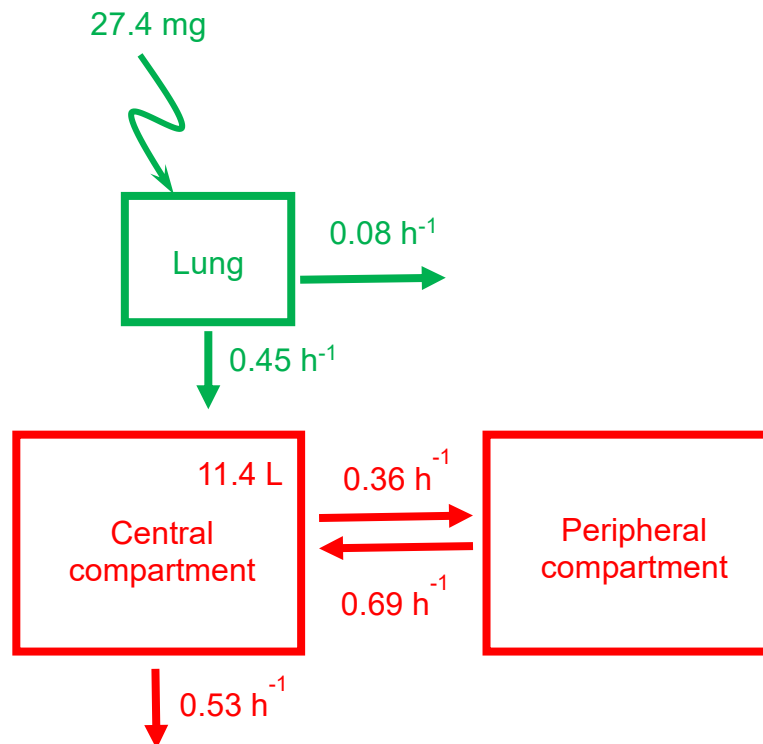
k_a and k_{nal} values. By so doing, likely changes in the model's predictions for the plasma/serum PK metrics, C_{max} , AUC and T_{max} , and for the local lung exposure metrics, AUC_{lung} (area under the drug mass in the lung vs. time curve) and $LRT_{0.5}$ (lung residence half-life), were identified and discussed for each of the three drugs.

5.2 Methods

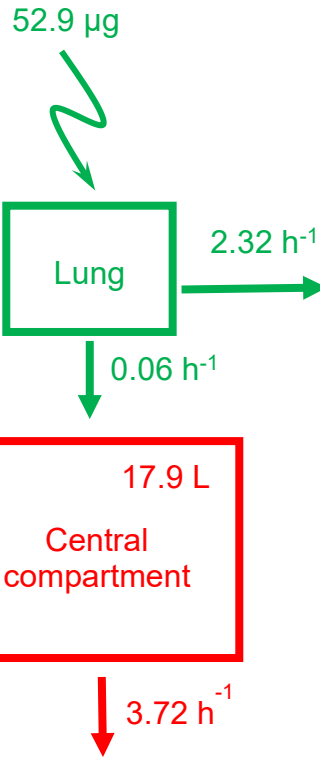
5.2.1 Models and reference standard conditions

Figure 5.1 describes the kinetic models and their model parameters and the DTL used as the reference standard conditions for A) tobramycin, B) calcitonin and C) ciprofloxacin. These were derived in Chapter 3 as the parameter estimates to best explain each of the inhaled PK profiles of the literature. Note that the model parameters for tobramycin and calcitonin were those for DPI, like ciprofloxacin.

A. Tobramycin



B. Calcitonin



C. Ciprofloxacin

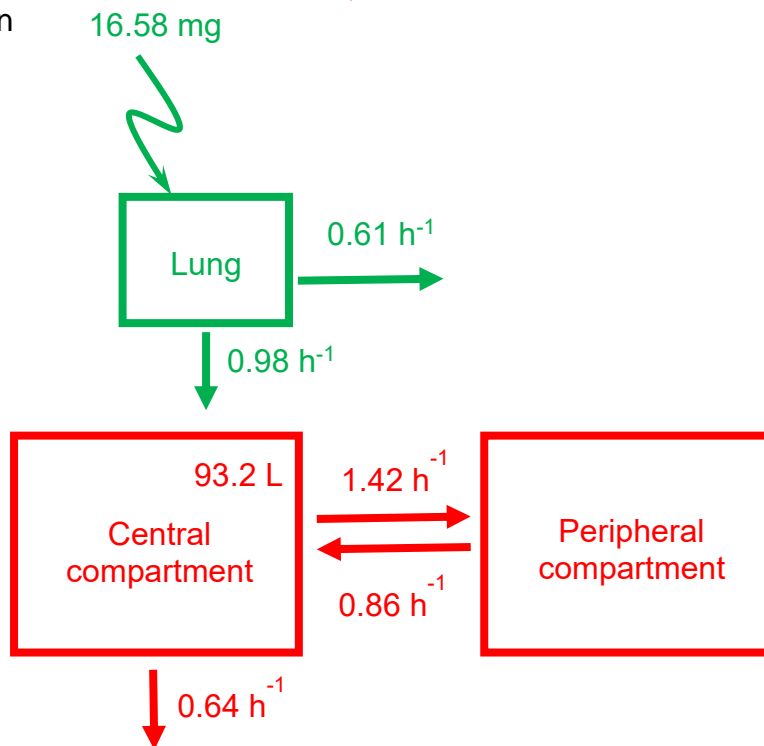


Figure 5.1 The kinetic models and their parameters and the DTL used as the reference standard conditions for A) tobramycin, B) calcitonin and C) ciprofloxacin. These parameters were derived in Chapter 3 as the parameter estimates to best explain each of the inhaled PK profiles of the literature.

5.2.2 Systemic PK profile simulation upon $\pm 20\%$ changes of the DTL, k_a and k_{nal}

With the models shown above, the DTL, k_a and k_{nal} values were each changed to a 20 % positive or a 20 % negative value, and the plasma/serum PK profiles were then predicted by simulation using Scientist. All the remaining parameters were fixed, as shown in Fig. 5.1. Simulation prediction was made every 1 min over the period of 8 h for tobramycin and ciprofloxacin and 6 h for calcitonin, as used in the literature. The C_{max} and T_{max} were identified from the predicted profile data, while the AUC was calculated by the trapezoidal method plus the residual area calculation, as described in Chapter 4.

5.2.3 Local lung exposure profile simulation upon $\pm 20\%$ changes of the DTL, k_a and k_{nal}

From the kinetic models shown in Figure 5.1, the drug mass remaining in the lung (M_L) at a given time was described by:

$$dM_L/dt = -(k_a+k_{nal}) * M_L \quad \text{Equation 5.1}$$

where M_L was DTL at time 0, i.e., immediately after inhaled administration. Hence, the local lung exposure profiles were predicted by simulation with the k_a and k_{nal} values and the DTL with or without positive and negative 20 % changes using Scientist. Like the systemic PK profile simulation, simulation prediction was made every 1 min over the period of 8 h for tobramycin and ciprofloxacin and 6 h for calcitonin, as used in the literature. With the predicted profile data, the AUC_{lung} (area under the drug mass in the lung vs. time curve) was calculated by the trapezoidal method plus the residual area calculation; and the $LRT_{0.5}$ (lung residence half-life) was by:

$$LRT_{0.5} = 0.693 / (k_a+k_{nal}) \quad \text{Equation 5.2}$$

Graphically, the slope of the semi-natural logarithmic local lung exposure profile corresponded to the (k_a+k_{nal}) value.

5.3 Results and Discussion

5.3.1 Systemic PK profile simulation upon ± 20 % changes of the DTL, k_a and k_{nal}

5.3.1.1 Tobramycin

The simulation results of ± 20 % changes of the DTL, k_a and k_{nal} to the serum concentration vs. time profile and its PK metrics for tobramycin are shown in Figure 5.2-A. When the DTL was changed by ± 20 %, the C_{max} and AUC_{∞} were identically changed by ± 20 %, respectively, while the T_{max} was unchanged. These identical changes in the C_{max} and AUC_{∞} were simply a reflection of linear lung disposition and systemic kinetics and PK. The ± 20 % changes in the k_a resulted in 11 or 13 % changes in the C_{max} , 3 or 5 % changes in the AUC_{∞} and 9 or 11 % changes in the T_{max} . This indicated that the C_{max} and T_{max} were more influenced by changes in the k_a than the AUC_{∞} . This may be attributed to the fact that the C_{max} (a measure of the rate and extent of absorption) and T_{max} (a measure of rate of absorption) were primarily determined by the sum of the k_a and k_{nal} , but for tobramycin, the k_a was a predominant contributor (by 85 %). It should be noted that the positive and negative 20 % changes did not give identical % changes in any of the parameters. The 20 % changes in k_{nal} (i.e., the minor contributor) resulted in only small 2-4 % changes in the C_{max} , AUC_{∞} and T_{max} .

5.3.1.2 Calcitonin

The simulation results of $\pm 20\%$ changes of the DTL, k_a and k_{nal} to the plasma concentration vs. time profile and its kinetic parameters for calcitonin are shown in Figure 5.2-B. As seen for tobramycin, the $\pm 20\%$ changes in DTL caused identical $\pm 20\%$ changes in the C_{max} and AUC_{∞} , but no change in the T_{max} . Similarly, the $\pm 20\%$ changes in the k_a resulted in $\pm 20\%$ changes in the C_{max} and AUC_{∞} , but again no changes in the T_{max} . This may be because, for calcitonin, the k_a is a significantly minor contributor of k_a+k_{nal} , so that the $\pm 20\%$ changes in the k_a did not cause significant changes to the rate of absorption. While the C_{max} and AUC_{∞} were suggested to be more influenced by the changes in the k_a than the T_{max} , these changes were different from the changes seen for tobramycin, presumably because of the fact that the k_a was much smaller than the k_{nal} for calcitonin and thus, the k_a changes did not cause changes in the sum of the k_a and k_{nal} . In contrast, the $\pm 20\%$ changes in the k_{nal} resulted in 8 or 9 % changes in the C_{max} , 16 or 24 % changes in the AUC_{∞} , and 10 % changes in the T_{max} . These changes in the kinetic parameters were likely because the sum of the k_a and k_{nal} changed by a greater extent with the changes in the k_{nal} .

5.3.1.3 Ciprofloxacin

The simulation results of $\pm 20\%$ changes of the DTL, k_a and k_{nal} to the plasma concentration vs. time profile and its kinetic parameters for ciprofloxacin are shown in Figure 5.2-C. When the DTL was changed by $\pm 20\%$, the C_{max} and AUC_{∞} were identically changed by $\pm 20\%$, respectively, while the T_{max} was unchanged. These identical changes

in the C_{max} and AUC_{∞} were simply a reflection of linear lung disposition kinetics and PK. The $\pm 20\%$ changes in the k_a resulted in 13 or 15 % changes in the C_{max} , 7 or 9 % changes in the AUC_{∞} and 8 or 10 % changes in the T_{max} . This indicated that the C_{max} and T_{max} were marginally more influenced by changes in the k_a than the AUC_{∞} . This may again be attributed to the fact that the C_{max} (a measure of the rate and extent of absorption) and T_{max} (a measure of rate of absorption) were primarily determined by the sum of the k_a and k_{nal} , but for ciprofloxacin, the k_a was a predominant contributor (by 62 %). Note that the positive and negative 20 % changes did not give identical % changes in any of the parameters. The 20 % changes in the k_{nal} (the minor contributor) resulted in smaller $\sim 4\%$ changes in the C_{max} and 5 % changes in the T_{max} .

5.3.1.4. Systemic PK profile simulation for three molecules

Across three molecules, when the k_a was increased, the AUC_{∞} (i.e., the extent of absorption) was increased. In general, increasing either the k_a or k_{nal} causes the sum of the k_a and k_{nal} , i.e., (k_a+k_{nal}) , to be increased, and because the (k_a+k_{nal}) determines the rate of absorption, increasing either the k_a or k_{nal} shortened the T_{max} . Because the C_{max} is determined by both the rate and extent of absorption, changes in either the k_a or k_{nal} changed the C_{max} . For calcitonin, the k_a was $\sim 3\%$ of the (k_a+k_{nal}) and hence, changes in the k_a didn't much change the (k_a+k_{nal}) . This may also be the reason for no changes in the T_{max} in response to the k_a changes. For the simplest case scenario of a bolus DPI inhalation and one-compartment model shown for calcitonin in Figure 5.1-B, the T_{max} and C_{max} are described by the following equation as derived from Gibaldi & Perrier (1982):

$$T_{\max} = \frac{2.303}{(k_a + k_{na}) - k_{10}} * \log \frac{(k_a + k_{na})}{k_{10}} \quad \text{Equation 5.1}$$

$$C_{\max} = \frac{F_L * DTL e^{-k_{10} * T_{\max}}}{V_c} \quad \text{Equation 5.2}$$

where k_{10} is the first-order elimination rate constant from the central compartment and F_L is fractional pulmonary bioavailability. Thus, for calcitonin, the k_a or k_{na} increase led to an increase in the $(k_a + k_{na})$ and subsequently to a shorter T_{\max} . Similar analogy may be applied to a bolus DPI inhalation and two-compartment model, wherein, an increase in $(k_a + k_{na})$ led to a shorter T_{\max} .

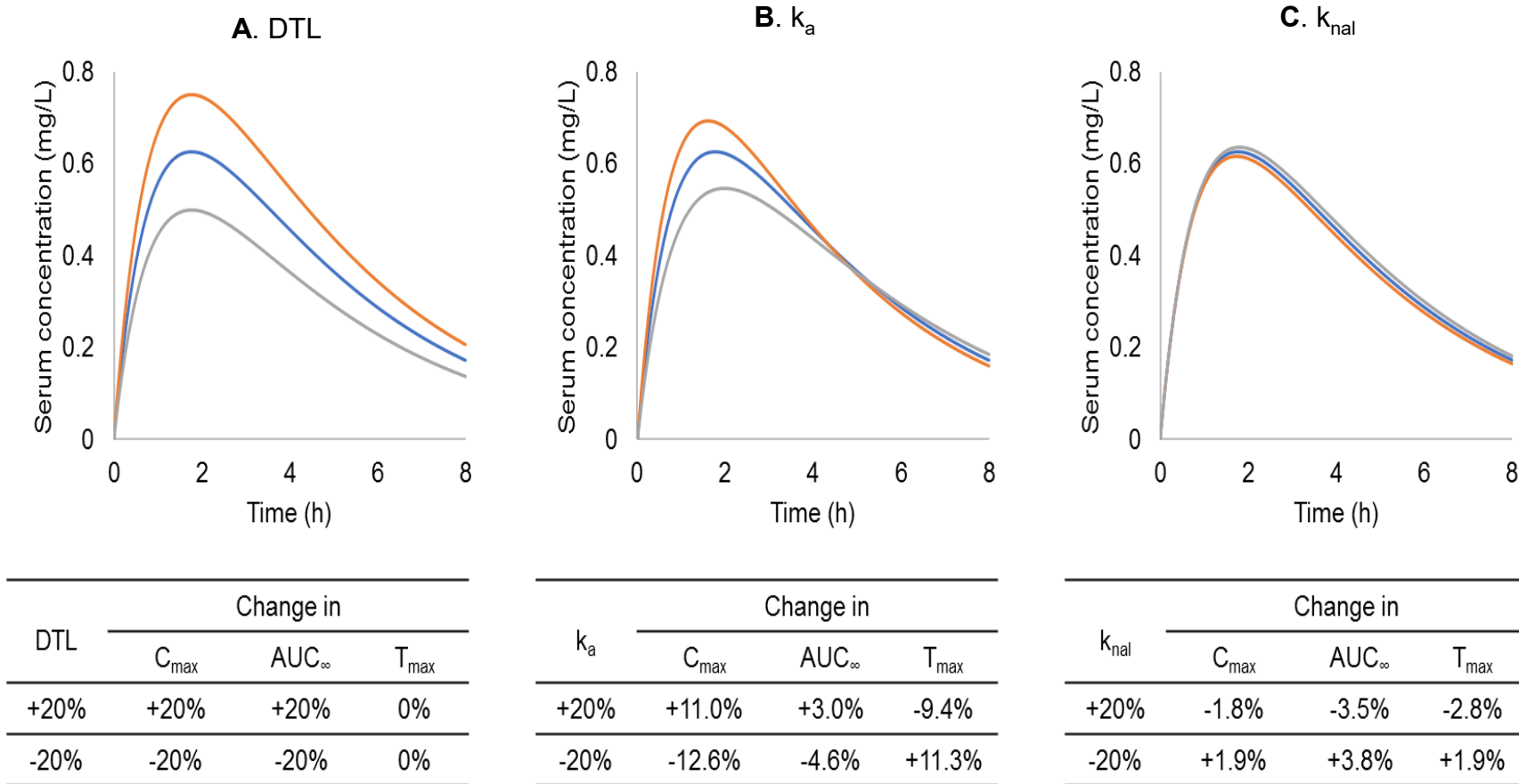
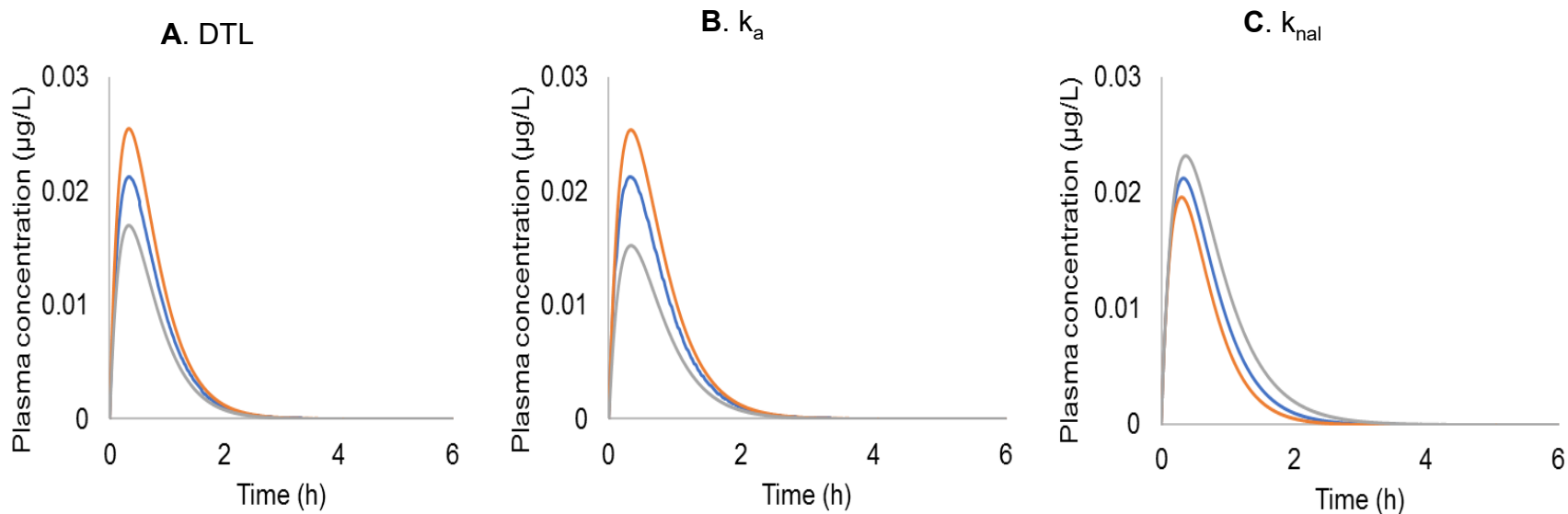


Figure 5.2-A Effects of $\pm 20\%$ changes in the A) DTL, B) k_a and C) k_{nal} values on the serum tobramycin concentration vs. time profiles following inhaled administration in healthy subjects and % changes in the C_{max} , AUC_{∞} and T_{max} values. The profiles in blue are drawn by simulation using DTL= 27.4 mg, $k_a= 0.45\text{ h}^{-1}$ and $k_{nal}= 0.08\text{ h}^{-1}$, as derived by the curve-fitting of the profile data in the literature in Chapter 3. The profiles in orange and gray are drawn by simulation upon +20 and -20 % change in the parameter of interest, while the remainders were held consistent with the values derived through the curve-fitting.

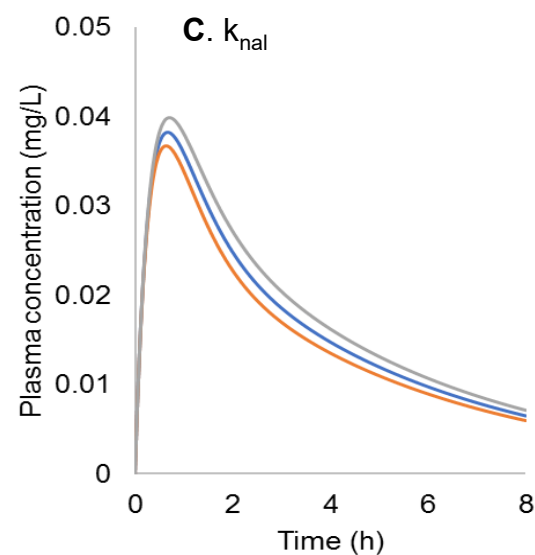
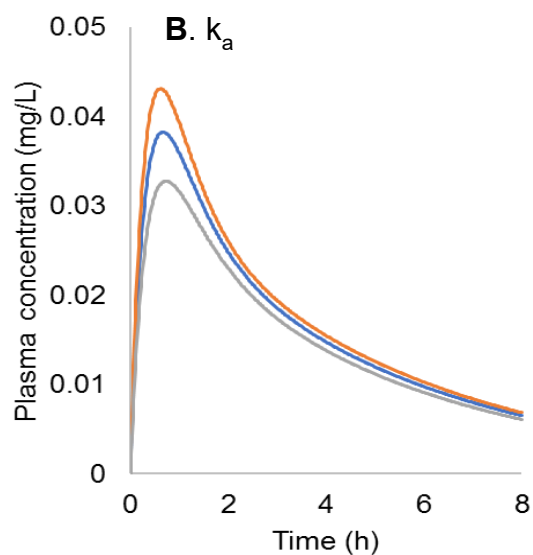
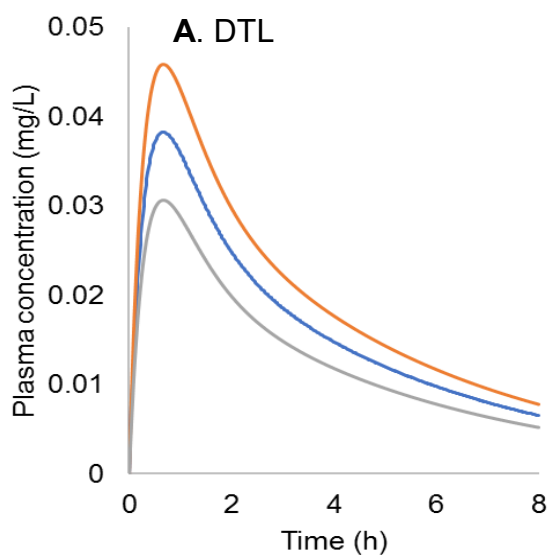


DTL	Change in		
	C_{max}	AUC_{∞}	T_{max}
+20%	+20%	+20%	0%
-20%	-20%	-20%	0%

k_a	Change in		
	C_{max}	AUC_{∞}	T_{max}
+20%	+20%	+20%	0%
-20%	-20%	-20%	0%

k_{nal}	Change in		
	C_{max}	AUC_{∞}	T_{max}
+20%	-7.6%	-16.3%	-10.0%
-20%	+9.3%	+24.0%	+10.0%

Figure 5.2-B Effects of $\pm 20\%$ changes in the A) DTL, B) k_a and C) k_{nal} values on the plasma calcitonin concentration vs. time profiles following inhaled administration in healthy subjects and % changes in the C_{max} , AUC_{∞} and T_{max} values. The profiles in blue are drawn by simulation using DTL = 52.9 μg , $k_a = 0.06 \text{ h}^{-1}$ and $k_{nal} = 2.32 \text{ h}^{-1}$, as derived by the curve-fitting of the profile data in the literature in Chapter 3. The profiles in orange and gray are drawn by simulation upon +20 and -20 % change in the parameter of interest, while the remainders were held consistent with the values derived through the curve-fitting.



DTL	Change in		
	C_{max}	AUC_{∞}	T_{max}
+20%	+20%	+20%	0%
-20%	-20%	-20%	0%

k_a	Change in		
	C_{max}	AUC_{∞}	T_{max}
+20%	+13.0%	+7%	-7.5%
-20%	-14.6%	-9%	+10.0%

k_{nal}	Change in		
	C_{max}	AUC_{∞}	T_{max}
+20%	-3.8%	-7%	-5%
-20%	+4.2%	+8%	+5%

Figure 5.2-C Effects of $\pm 20\%$ changes in the A) DTL, B) k_a and C) k_{nal} values on the plasma ciprofloxacin concentration vs. time profiles following inhaled administration in healthy subjects and % changes in the C_{max} , AUC_{∞} and T_{max} values. The profiles in blue are drawn by simulation using $DTL = 16.58$ mg, $k_a = 0.98$ h⁻¹ and $k_{nal} = 0.61$ h⁻¹, as derived by the curve-fitting of the profile data in the literature in Chapter 3. The profiles in orange and gray are drawn by simulation upon +20 and -20 % change in the parameter of interest, while the remainders were held consistent with the values derived through the curve-fitting.

5.3.2 Local lung exposure profile simulation upon ± 20 % changes of the DTL, k_a and k_{nal}

5.3.2.1 Tobramycin

Figure 5.3-A shows the simulation results of ± 20 % changes of the DTL, k_a and k_{nal} to the tobramycin mass remaining in the lung vs. time profiles and lung exposure kinetic parameters, AUC_{lung} and $LRT_{0.5}$. When the DTL was changed by ± 20 %, the AUC_{lung} was identically changed by ± 20 %, while the $LRT_{0.5}$ was unchanged, as similarly seen in the PK profile in Figure 5.2-A. In contrast, with the ± 20 % changes in the k_a , both the AUC_{lung} and $LRT_{0.5}$ changed by 14 or 19 % and 15 or 21 %, respectively. However, with the ± 20 % changes in the k_{nal} , the changes in the AUC_{lung} and $LRT_{0.5}$ were small and ~ 4 %. These may be again consistent with the fact that, for tobramycin, the k_a was kinetically a predominant contributor (by 85 %) in the lung exposure profile, given its rate-control by the sum of the k_a and k_{nal} .

5.3.2.2 Calcitonin

Figures 5.3-B shows the simulation results of ± 20 % changes of the DTL, k_a and k_{nal} to the calcitonin mass remaining in the lung vs. time profiles and lung exposure kinetic parameters, AUC_{lung} and $LRT_{0.5}$. As was the case for tobramycin, the ± 20 % changes in the DTL identically changed the AUC_{lung} by ± 20 %, while the $LRT_{0.5}$ was unchanged. With the ± 20 % changes in the k_a , both the AUC_{lung} and $LRT_{0.5}$ changed by only 0.5 %. However, with the ± 20 % changes in the k_{nal} , the changes in both AUC_{lung} and $LRT_{0.5}$ were much greater, 16 or 24 %. These were consistent with the fact that, for calcitonin,

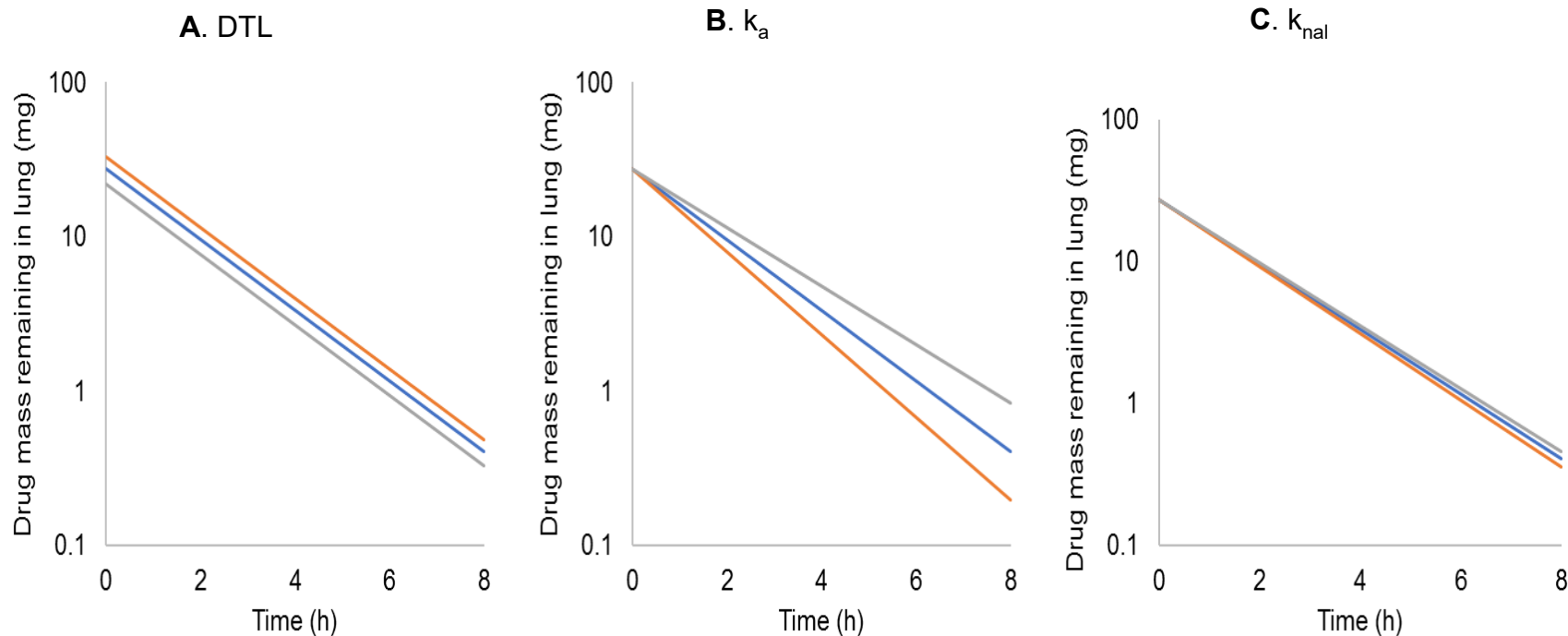
the k_{nal} was kinetically a predominant contributor (by 97.5 %) in the lung exposure profile, given its rate control by the sum of the k_a and k_{nal} .

5.3.2.3 Ciprofloxacin

Figure 5.3-C shows the simulation results of ± 20 % changes of the DTL, k_a and k_{nal} to the ciprofloxacin mass remaining in the lung vs. time profiles and lung exposure kinetic parameters, AUC_{lung} and $LRT_{0.5}$. When the DTL was changed by ± 20 %, the AUC_{lung} was identically changed by ± 20 %, while the $LRT_{0.5}$ was unchanged. In contrast, with the ± 20 % changes in the k_a , both the AUC_{lung} and $LRT_{0.5}$ changed by 11 or 14 %. However, with the ± 20 % changes in the k_{nal} , the changes in both AUC_{lung} and $LRT_{0.5}$ were smaller, 7 or 8 %. These may be again consistent with the fact that, for ciprofloxacin, the k_a was kinetically a major contributor (by 62 %) in the lung exposure profile, given its rate-control by the sum of the k_a and k_{nal} .

5.3.2.4 Local lung exposure profile simulation for three molecules

For all three molecules, ± 20 % changes in the DTL produced identical ± 20 % changes in the AUC_{lung} , while the $LRT_{0.5}$ remained unchanged as this parameter is dose-independent. For any changes in the k_a and k_{nal} , the AUC_{lung} and $LRT_{0.5}$ changed and the changes were dependent on the relative contribution of the k_a and k_{nal} , as related to the changes in the (k_a+k_{nal}) . In other words, changes made to the major contributor of k_a+k_{nal} caused greater changes in the AUC_{lung} and $LRT_{0.5}$, compared to changes made to the minor contributor.

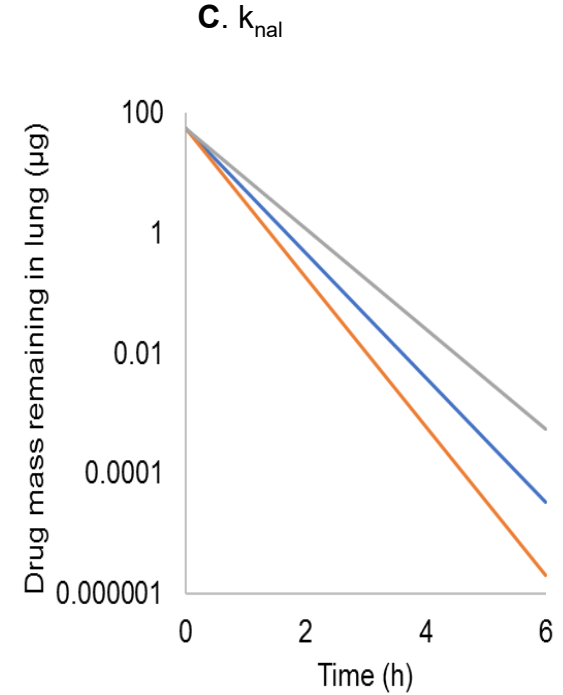
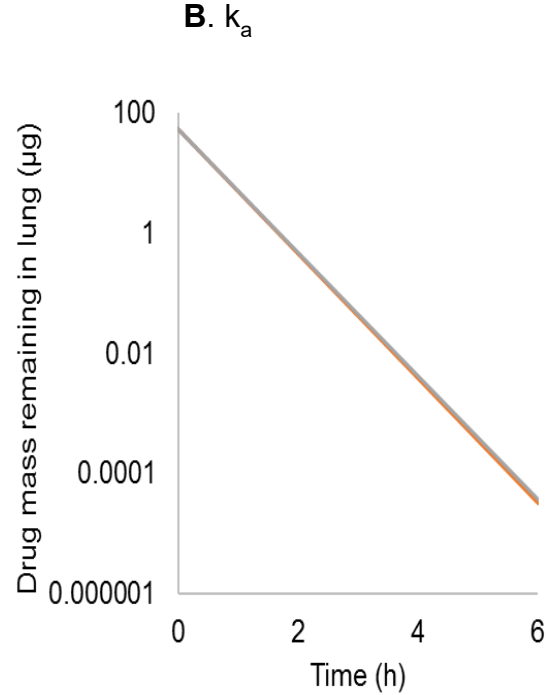
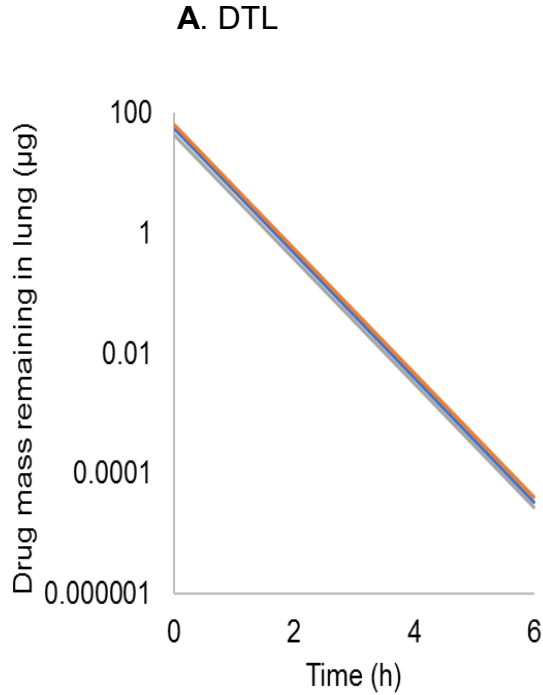


DTL	Change in	
	AUC _{lung}	LRT _{0.5}
+20%	+20%	0%
-20%	-20%	0%

k _a	Change in	
	AUC _{lung}	LRT _{0.5}
+20%	-14.0%	-14.5%
-20%	+18.6%	+20.5%

k _{nal}	Change in	
	AUC _{lung}	LRT _{0.5}
+20%	-3.4%	-3.6%
-20%	+3.7%	+3.9%

Figure 5.3-A Effects of $\pm 20\%$ changes in the A) DTL, B) k_a and C) k_{nal} values on the tobramycin drug mass remaining in the lungs vs. time profiles following inhaled administration in healthy subjects and % changes in the AUC_{lung} and LRT_{0.5} values. The profiles in blue are drawn by simulation using DTL= 27.4 mg, $k_a = 0.45 \text{ h}^{-1}$ and $k_{nal} = 0.08 \text{ h}^{-1}$, as derived by the curve-fitting of the profile data in the literature in Chapter 3. The profiles in orange and gray are drawn by simulation upon +20 and -20 % change in the parameter of interest.

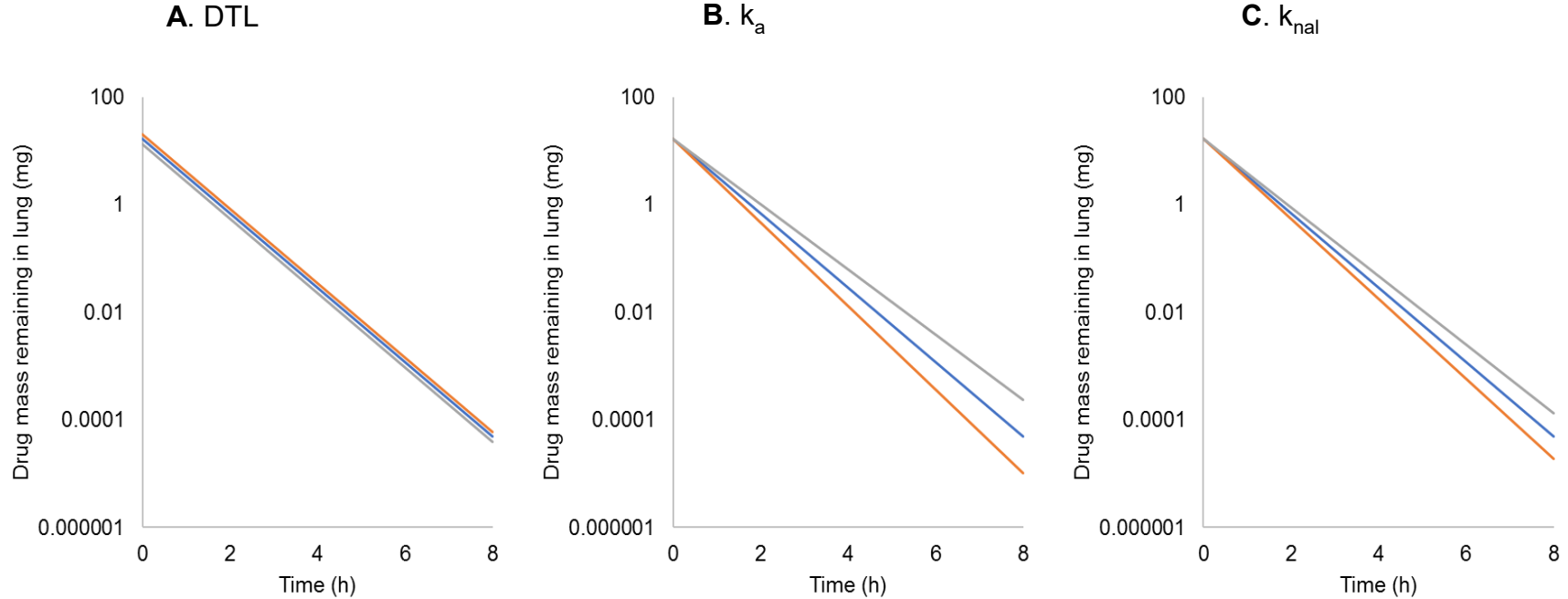


DTL	Change in	
	AUC_{lung}	$LRT_{0.5}$
+20%	+20%	0%
-20%	-20%	0%

k_a	Change in	
	AUC_{lung}	$LRT_{0.5}$
+20%	-0.5%	-0.5%
-20%	+0.5%	+0.5%

k_{nal}	Change in	
	AUC_{lung}	$LRT_{0.5}$
+20%	-16%	-16%
-20%	+24%	+24%

Figure 5.3-B Effects of $\pm 20\%$ changes in the A) DTL, B) k_a and C) k_{nal} values on the calcitonin drug mass remaining in the lungs vs. time profiles following inhaled administration in healthy subjects and % changes in the AUC_{lung} and $LRT_{0.5}$ values. The profiles in blue are drawn by simulation using $DTL = 52.9 \mu\text{g}$, $k_a = 0.06 \text{ h}^{-1}$ and $k_{nal} = 2.32 \text{ h}^{-1}$, as derived by the curve-fitting of the profile data in the literature in Chapter 3. The profiles in orange and gray are drawn by simulation upon +20 and -20 % change in the parameter of interest.



DTL	Change in	
	AUC _{lung}	LRT _{0.5}
+20%	+20%	0%
-20%	-20%	0%

k _a	Change in	
	AUC _{lung}	LRT _{0.5}
+20%	-11%	-11%
-20%	+14%	+14%

k _{nal}	Change in	
	AUC _{lung}	LRT _{0.5}
+20%	-7%	-7%
-20%	+8%	+8%

Figure 5.3-C Effects of $\pm 20\%$ changes in the A) DTL, B) k_a and C) k_{nal} values on the ciprofloxacin drug mass remaining in the lungs vs. time profiles following inhaled administration in healthy subjects and % changes in the AUC_{lung} and LRT_{0.5} values. The profiles in blue are drawn by simulation using DTL= 16.58 mg, $k_a = 0.98 \text{ h}^{-1}$ and $k_{nal} = 0.61 \text{ h}^{-1}$, as derived by the curve-fitting of the profile data in the literature in Chapter 3. The profiles in orange and gray are drawn by simulation upon +20 and -20 % change in the parameter of interest.

5.4 Conclusions

In this chapter, simulation was used to study the effects of $\pm 20\%$ changes in drug delivery (DTL) and lung disposition kinetics (k_a and k_{nal}) on the systemic PK and local lung exposure profiles following inhaled administration. It was clear that the DTL changes caused identical changes in the C_{max} and AUC_{∞} and did not affect the T_{max} across all three drugs. In contrast, the impact of the k_a and k_{nal} changes on the changes in C_{max} , AUC_{∞} and T_{max} appeared to depend on how each kinetic process (k_a or k_{nal}) contributes to the overall rate of drug disposition in the lung. Similarly, the local lung exposure was a direct correlation with the sum of the k_a and k_{nal} and thus, its impact again depended on how each kinetic process (k_a and k_{nal}) contributes to the overall rate of drug disposition in the lung.

The FDA bioequivalence criteria states that a test product is bioequivalent to a reference product, when the 95 % confidence interval (CI) of the test product exposure metrics (i.e., C_{max} and AUC_{∞}) falls within 80-125 % range of those for the reference product. This was with the understanding that the 80-125 % range of the C_{max} and AUC_{∞} represents a $\pm 20\%$ of the systemic exposure. Therefore, as a starting point, it was of interest to perform simulations to understand what % changes were observed in the C_{max} and AUC_{∞} by introducing $\pm 20\%$ changes in the DTL, k_a and k_{nal} . While further simulations with different molecules are necessary to identify a more solid trend or classification regarding changes in the kinetic metrics, these simulation strategies can be an important tool to allow us studying changes in the PK metrics in response to drug delivery (DTL) and lung disposition kinetics (k_a and k_{nal}).

CHAPTER 6

OVERALL CONCLUSIONS, LIMITATIONS AND FUTURE DIRECTIONS

This thesis project aimed to develop the lung deposition and disposition kinetic model to derive and predict the kinetic descriptors of lung disposition, namely, the rate constants for absorption (k_a) and non-absorptive loss (k_{nal}). The model incorporated the dose delivered to the lung (DTL) and the first-order k_a and k_{nal} in the lung, along with one- or two-compartment kinetic model for first-order systemic disposition. Appropriate selection of drugs and study design allowed elimination of gastrointestinal (GI) absorption from this model. An exhaustive literature search found that three drugs, tobramycin, calcitonin and ciprofloxacin, published all necessary data sets, i.e., intravenous (IV) PK profiles, inhaled PK profiles without GI absorption and corresponding lung deposition data by γ -scintigraphy.

The two approaches of curve fitting- and moment analysis-based approaches were developed and used to derive the k_a and k_{nal} values for the three drugs delivered via dry powder inhalers (DPIs) and/or nebulizers (NEB). In the curve fitting approach, each inhaled PK profile data were fitted to the model to derive the k_a and k_{nal} values, while the DTL was fixed, as reported by the γ -scintigraphy data, and the systemic PK parameters were derived and fixed with the IV PK profiles. All the curve fittings showed acceptable

“goodness-of-fit” to the profiles in the literature. The k_a values for all the three hydrophilic drug molecules were well correlated to their molecular weight. The k_{nal} values appear to be well aligned with the literature reporting tissue binding, lung metabolism and mucociliary clearance. In the moment-based analysis, the same data sets were used. The MRT_{iv} and MRT_{inh} were calculated after IV and inhaled administration, respectively, to estimate the mean lung residence time (MLRT) after inhalation. With the DTL, the bioavailability due to lung absorption (F_L) was also determined. Given $F_L = MLRT \cdot k_a = k_a / (k_a + k_{nal})$, the k_a and k_{nal} values were then derived, which were found to be comparable to those derived by the curve fitting in majority of the cases.

The curve fitting derived k_a and k_{nal} values were used to predict the systemic PK and local lung exposure profiles by simulation upon $\pm 20\%$ changes in lung delivery (DTL) and lung disposition (k_a and k_{nal}). The DTL changes caused identical changes in the C_{max} and AUC_{∞} without changing the T_{max} across all three drugs. In contrast, impacts of the k_a and k_{nal} changes to the C_{max} , AUC_{∞} and T_{max} appeared to depend on how each process (k_a or k_{nal}) contributes to the overall rate of drug disposition in the lung.

One of the significant limitations of this thesis research is a use of mean PK profile data from the literature by extraction, so that original PK data variability could not be taken into account in the k_a and k_{nal} derivation. In addition, the lung disposition model was minimalist, combining multiple non-absorptive clearances into one first-order kinetic process and disregarding possible within-lung kinetic differences. While incorporating detailed distinctions would be ideal to understand the lung region-dependent disposition kinetics, it would not derive such many parameter estimates in an accurate manner, as

has been obtained in this thesis research. The data availability is also a limitation. The inhaled PK profile data and corresponding γ -scintigraphic lung deposition data are required along with the IV PK profile data. For the moment analysis-based approach, this limitation may be eased, if the DTL, AUC and MRT values are reported in the literature despite a lack of the PK profile data points. Even so, this approach does not provide statistics for “goodness”, so that assessment and comparison of the derived k_a and k_{nal} values would still remain difficult.

This project has attempted to resolve the kinetic complexities by lung delivery, deposition and disposition to understand and identify critical factors and attributes that contribute to outcome measures of systemic PK and local lung exposure profiles. While the project has been successful with the three drug molecules of its choice, it is clear that the study should be extended to more molecules with different physicochemical properties and indications to further solidify the utility of the approaches. Particularly, fluticasone propionate would be of most interest, as to recent efforts of developing its generic inhaler products.

REFERENCES

REFERENCES

Boer, F., 2003. Drug handling by the lungs. *British Journal of Anaesthesia*, **91**(1), pp.50–60.

Borghardt, J.M. et al., 2015. Review Article Pharmacometric Models for Characterizing the Pharmacokinetics of Orally Inhaled Drugs. *The AAPS Journal*, **17**(4), pp.853–870.

Brunner, M. et al., 1999. Distribution and Antimicrobial Activity of Ciprofloxacin in Human Soft Tissues Distribution and Antimicrobial Activity of Ciprofloxacin in Human Soft Tissues. *Antimicrobial agents and Chemotherapy*, **43**(5), pp.1307–1309.

Buclin, T. et al., 2002. Bioavailability and biological efficacy of a new oral formulation of salmon calcitonin in healthy volunteers. *Journal of bone and mineral research : the official journal of the American Society for Bone and Mineral Research*, **17**(8), pp.1478–1485.

Byron, P.R., 1986. Prediction of drug residence times in regions of the human respiratory tract following aerosol inhalation. *Journal of Pharmaceutical Sciences*, **75**(5), pp.433–438.

Byron, P.R. & Patton, J.S., 1994. Drug delivery via the respiratory tract. *Journal of Aerosol Medicine*, **7**(1), pp.49–75.

Chrystyn, H., 2001. Methods to identify drug deposition in the lungs following inhalation. *British Journal of Clinical Pharmacology*, **51**(4), pp.289–299.

Clark, A. et al., 2008. A comparison of the pulmonary bioavailability of powder and liquid aerosol formulations of salmon calcitonin. *Pharmaceutical Research*, **25**(7), pp.1583–1590.

Daley-Yates, P.T. et al., 2014. Pharmacokinetics and pharmacodynamics of fluticasone propionate and salmeterol delivered as a combination dry powder from a capsule-based inhaler and a multidose inhaler in asthma and COPD patients. *J Aerosol Med Pulm Drug Deliv*, **27**(4), pp.279–289.

Gibaldi, M. & Perrier, D., 1982. *Pharmacokinetics* Second. J. Swarbrick, ed., New York: New York: Marcel Dekker.

Gonda, I., 1988. Drugs Administered Directly into the Respiratory Tract: Modeling of the Duration. *Journal of Pharmaceutical Sciences*, **77**(4), pp.340–346.

Haughey, D.B. et al., 1980. High-pressure liquid chromatography analysis and single-dose disposition of tobramycin in human volunteers. *Antimicrobial Agents and Chemotherapy*, **17**(4), pp.649–653.

Hirst, P.H. et al., 2002. In vivo lung deposition of hollow porous particles from a pressurized metered dose inhaler. *Pharmaceutical Research*, **19**(3), pp.258–264.

Hochhaus, G., 2007. Pharmacokinetic and pharmacodynamic properties important for inhaled corticosteroids. *Annals of Allergy, Asthma & Immunology*, **98**(2), pp.S7–S15.

Ibrahim, M., Verma, R. & Garcia-Contreras, L., 2015. Inhalation drug delivery devices: technology update. *Medical devices (Auckland, N.Z.)*, **8**, pp.131–9.

Labiris, N.R. & Dolovich, M.B., 2003. Pulmonary drug delivery. Part I: Physiological factors affecting therapeutic effectiveness of aerosolized medications. *British Journal of Clinical Pharmacology*, **56**(6), pp.588–599.

Li, M. & Byron, P.R., 2013. Tobramycin disposition in the rat lung following airway administration. *The Journal of pharmacology and experimental therapeutics*, **347**(2), pp.318–24.

Miller, N.A. et al., 2010. Development of a Physiologically Based Pharmacokinetic (PBPK) Model for Predicting Deposition and Disposition Following Inhaled and Intranasal Administration. *Respiratory Drug Delivery* **2010**, pp.579–584.

Newhouse, M., 1991. Advantages of pressurized canister metered dose inhalers. *Journal of Aerosol Medicine*, **4**(3), pp.139–150.

Newhouse, M.T. et al., 2003. Inhalation of a dry powder tobramycin pulmosphere formulation in healthy volunteers. *Chest*, **124**(1), pp.360–366.

Olsson, B. et al., 2011. Pulmonary Drug Metabolism , Clearance , and Absorption. In H. A. Smyth HDC, ed. *Controlled Pulmonary Drug Delivery*. Springer, pp. 21–50.

Ong, H.X. et al., 2013. Ciprofloxacin is actively transported across bronchial lung epithelial cells using a calu-3 air interface cell model. *Antimicrobial Agents and*

Chemotherapy, **57**(6), pp.2535–2540.

Patil, J.S. & Sarasija, S., 2012. Pulmonary drug delivery strategies: A concise, systematic review. *Review article, Lung India*, **29**(1), pp.44–49.

Patton, J.S. & Byron, P.R., 2007. Inhaling medicines: delivering drugs to the body through the lungs. *Nature Reviews.Drug discovery*, **6**(1), pp.67–74.

Péchére, J., Roy, B. & Dugal, R., 1976. Distribution and elimination kinetics of intravenously and intramuscularly administered tobramycin in man. *International journal of clinical pharmacology, therapy and toxicology*, **14**(4), pp.313–318.

Pilcer, G. et al., 2008. Pharmacoscintigraphic and pharmacokinetic evaluation of tobramycin DPI formulations in cystic fibrosis patients. *European Journal of Pharmaceutics and Biopharmaceutics*, **68**(2), pp.413–421.

Pleasant, R. et al., 1988. Effect of four intravenous infusion methods on tobramycin pharmacokinetics. *Clinical Pharmacy*, **7**(5), pp.374–379.

Ruge, C.C., Kirch, J. & Lehr, C.M., 2013. Pulmonary drug delivery: From generating aerosols to overcoming biological barriers-therapeutic possibilities and technological challenges. *The Lancet Respiratory Medicine*, **1**(5), pp.402–413.

Sakagami, M., 2014. Fluticasone Pharmacokinetics: Meta-Analysis and Models. In *Respiratory Drug Delivery 2014*. pp. 143–154.

Sakagami, M., 2004. Insulin disposition in the lung following oral inhalation in humans: A meta-analysis of its pharmacokinetics. *Clinical Pharmacokinetics*, **43**(8), pp.539–552.

Snell, N.J.C. & Ganderton, D., 1999. Workshop of the British Association for Lung Research, Institute of Biology, London, U.K., 17 April 1998: Assessing lung deposition of inhaled medications: Consensus statement. *Respiratory Medicine*, **93**(2), pp.123–133.

Stass, H. et al., 2016. Ciprofloxacin Dry Powder for Inhalation in Patients with Noncystic Fibrosis Bronchiectasis or Chronic Obstructive Pulmonary Disease, and in Healthy Volunteers. *Journal of Aerosol Medicine and Pulmonary Drug Delivery*, **29**(1), pp.53–63.

Tfelt-Hansen, P. et al., 2000. Ergotamine in the acute treatment of migraine: A review and European consensus. *Brain*, **123**(1), pp.9–18.

Thorsson, L., Edsbacker, S. & Conradson, T.B., 1994. Lung deposition of budesonide from Turbuhaler?? is twice that from a pressurized metered-dose inhaler P-MDI. *European Respiratory Journal*, **7**(10), pp.1839–1844.

Verma, P. et al., 2010. Routes of drug administration. *International Journal of Pharmaceutical Studies and Research*, **1**(1), pp.54–59.

Weber, B. & Hochhaus, G., 2013. A pharmacokinetic simulation tool for inhaled corticosteroids. *The AAPS journal*, **15**(1), pp.159–71.

APPENDICES

APPENDIX A

METHOD OF RESIDUALS USED FOR DERIVING INITIAL PARAMETER ESTIMATES OF IV PK PROFILE

This Appendix will briefly describe the steps involved in estimating the initial estimates of model parameters after IV administration as detailed in Gibaldi & Perrier (1982).

When the drug follows a one-compartment model after zero-order input and its elimination rate constant is first-order like in case of calcitonin, the concentration of the drug in central compartment as a function of time can be derived by:

$$C_c = \frac{k_0 * (1 - e^{-k_{10} * t})}{V_c * k_{10}} \quad \text{Equation A.1}$$

where C_c is the concentration of drug in the central compartment (plasma/serum drug concentration) at time t , k_0 is the zero-order infusion rate for IV infusion during the infusion period; k_{10} is the first-order elimination rate constant from the central compartment; V_c is the apparent volume of distribution of the central compartment. Equation A.1 was used

to calculate initial estimates of one-compartment model parameters k_{10} and V_C for calcitonin to explain the IV PK profile after IV infusion reported in Buclin et al.

When the drug follows a two-compartment model like in case of tobramycin and ciprofloxacin, the concentration in the central compartment as a function of time can be derived by the following biexponential equation after administration of drug intravenously as a bolus or at a constant rate infusion:

$$C_C = A * e^{-\alpha t} + B * e^{-\beta t} \quad \text{Equation A.2}$$

where C_C is the concentration of drug in the central compartment (plasma/serum drug concentration) at time t ; α , β are apparent first order fast (distribution and elimination) and slow (elimination) disposition rate constants, respectively; and A and B are zero-time intercepts corresponding to α and β , respectively.

The pharmacokinetic macro-rate constants A , α , B and β in equation A.2 can be derived from the biexponential central compartment drug concentration (C_C) versus time curve by using method of residuals. (Gibaldi & Perrier 1982) Method of residuals is a PK technique for resolving a curve into its various exponential components. Since α is larger than β , by definition, the term $A * e^{-\alpha t}$ will approach zero more rapidly than $B * e^{-\beta t}$ and equation A.2 will then reduce to equation A.3:

$$C_C = B * e^{-\beta t} \quad \text{Equation A.3}$$

Equation A.3 in natural-logarithmic terms will be:

$$\ln C_C = \ln B - \beta t \quad \text{Equation A.4}$$

This equation describes the terminal linear phase of the curve resulting from a plot of the natural-logarithm of plasma/serum drug concentration versus time. This terminal linear phase has a slope of $-\beta$, and when extrapolated to zero, it yields an intercept of $\ln B$.

By subtracting the concentration-time values on the extrapolated line from the corresponding true plasma concentration-time values, a series of residual concentration (C_r)-time values will be obtained, which are described as in equation A.5:

$$C_r = A \cdot e^{-\alpha t} \quad \text{Equation A.5}$$

Equation A.5 in natural-logarithmic terms will be:

$$\ln C_r = \ln A - \alpha t \quad \text{Equation A.6}$$

Thus, a plot of the natural-logarithm of the residual concentration values versus time will yield a straight line with a slope of $-\alpha$ and a zero-time intercept of $\ln A$. Resolution of the biexponential curve thereby enables the determination of all parameters in equation A.2, which will in turn permit the estimation of the two-compartment model parameters k_{21} , k_{10} , and k_{12} by using the following equations:

$$k_{21} = \frac{A\beta + B\alpha}{A+B} \quad \text{Equation A.7}$$

$$k_{10} = \frac{\alpha \cdot \beta}{k_{21}} \quad \text{Equation A.8}$$

$$k_{12} = \alpha + \beta - k_{21} - k_{10} \quad \text{Equation A.9}$$

These steps to calculate two-compartment model parameters after IV bolus/infusion were then followed to calculate initial estimates of model parameters k_{10} ,

k_{12} , k_{21} and V_C for tobramycin and ciprofloxacin to explain the IV PK profile after IV infusion reported in Pleasants et al. and Brunner et al., respectively.

APPENDIX B

ORIGINAL DATA SETS FROM CURVE FITTING APPROACH FOR TOBRAMYCIN IV AND INHALED PK PROFILES

Table B.1 Tobramycin mean serum concentration vs. time profile data reported in Pleasants et al. after IV infusion.

T (h)	Mean serum concentration (mg/L)
0.17	3.8267
0.33	6.05078
0.50	8.18939
0.67	7.18595
0.83	6.37492
1.00	6.07669
1.33	4.90413
1.50	4.18039
1.67	3.67043
2	2.94884
2.5	2.56958
3	2.10497
4	1.56
6	0.811938
8	0.448589

Table B.2 Macro-rate constants derived from tobramycin IV PK profile reported in Pleasants et al. by using method of residuals.

A (mg/L)	8.76
α (h^{-1})	1.65
B (mg/L)	5.53
β (h^{-1})	0.32

The macro-rate constants in Table B.2 were used to calculate initial estimates of k_{10} , k_{12} , k_{21} and V_c which are reported in Chapter 3.

A)

```

// Tobramycin IV Two Compartment Model File
IndVars: T
DepVars: Cc
Params: Vc, k10, k12, k21
//INPUT
Dose=118.2
TINF1=0.5
RATEON1=Dose/TINF1
TON1=0
TOFF1=TON1+TINF1
FLAGON1=UNIT(T-TON1)
FLAGOFF1=UNIT(T-TOFF1)
ARATE1=RATEON1*FLAGON1*(1-FLAGOFF1)
Mc'=ARATE1+k21*MP-(k12+k10)*Mc
Mp'=k12*Mc-k21*MP
CC=Mc/Vc
//Initial conditions
T=0
Mc=0
Mp=0
***

```

B)

Parameter Name	Value	Lower Limit	Upper Limit	Fixed?
Vc	11.4	0	Infinity	Yes
k10	0.53	0	Infinity	Yes
k12	0.36	0	Infinity	Yes
k21	0.69	0	Infinity	Yes

C)

T (h)	Predicted serum concentration (mg/L)
0.17	3.2811
0.33	5.9637
0.50	8.4579
0.67	7.3666
0.83	6.5131
1.00	5.7559
1.33	4.6225
1.50	4.1703
1.67	3.7861
2	3.1897
2.5	2.5444
3	2.0917
4	1.4911
6	0.82231
8	0.46466

Figure B.1 A) model file, B) Parameter file and C) Predicted profile of the Scientist® for curve-fitting the mean serum concentration vs. time profile of tobramycin following IV infusion.

Table B.3 Goodness-of-fit statistics and statistical output for tobramycin IV PK profile curve fitting.

Goodness-of-fit statistics	Weighted	Unweighted
Sum of squared observations:	325.55	325.55
Sum of squared deviations:	0.68872	0.68872
Standard deviation of data:	0.25022	0.25022
R-squared:	0.99788	0.99788
Coefficient of determination:	0.9912	0.9912
Correlation:	0.99585	0.99585
Model Selection Criterion:	4.1997	4.1997
Confidence Intervals		
Parameter Name:	V_c	
Estimated Value:	11.376	
Standard Deviation:	0.42058	
95% Range (Univariate):	10.45	12.302
95% Range (Support Plane):	9.8349	12.917
Parameter Name:	k_{10}	
Estimated Value:	0.53304	
Standard Deviation:	0.054272	
95% Range (Univariate):	0.41359	0.65249
95% Range (Support Plane):	0.33417	0.7319
Parameter Name:	k_{12}	
Estimated Value:	0.36143	
Standard Deviation:	0.10101	
95% Range (Univariate):	0.1391	0.58376
95% Range (Support Plane):	0.0087132	0.73157
Parameter Name:	k_{21}	
Estimated Value:	0.69437	
Standard Deviation:	0.35579	
95% Range (Univariate):	0.088723	1.4775
95% Range (Support Plane):	0.60935	1.9981
Variance-Covariance Matrix		
0.17689		
-0.012348	0.0029454	
-0.033879	0.0013208	0.010204
-0.086985	0.015858	0.020584
Correlation Matrix		
1		
-0.54099	1	
-0.79744	0.24093	1
-0.5813	0.82127	0.57272

Table B.4-A Tobramycin mean (\pm SD) serum concentration vs. time profile data reported in Newhouse et al. after inhalation from DPI.

T (h)	Mean serum concentration (mg/L)	SD (mg/L)
0	0	0
0.25	0.36923	0.134998
0.5	0.42528	0.127047
1	0.56703	0.182634
1.5	0.57363	0.164767
2	0.56044	0.15684
3	0.53571	0.125062
4	0.45659	0.113151
6	0.33626	0.087345
8	0.23077	0.06

Table B.4-B Tobramycin mean (\pm SD) serum concentration vs. time profile data reported in Newhouse et al. after inhalation from NEB.

T (h)	Mean serum concentration (mg/L)	SD (mg/L)
0	0	0
0.25	0.15041	0.091
0.5	0.17851	0.08
1	0.25893	0.103
1.5	0.26116	0.091
2	0.26446	0.089
3	0.26116	0.077
4	0.23141	0.07
6	0.17686	0.052
8	0.12066	0.052

A)

//Tobramycin lung deposition and disposition PK model

IndVars: T

DepVars: C_cParams: Dose, V_c, k₁₀, k₁₂, k₂₁, k_a, k_{nal}

$$M_L' = -(k_a + k_{nal}) * M_L$$

$$M_C' = k_{21} * M_P - (k_{12} + k_{10}) * M_C + k_a * M_L$$

$$M_P' = k_{12} * M_C - k_{21} * M_P$$

$$C_C = M_C / V_C$$

//Initial conditions

$$T = 0$$

$$M_L = \text{Dose}$$

$$M_C = 0$$

$$M_P = 0$$

B)

Parameter Name	Parameter Value	Lower Limit	Upper Limit	Fixed?
Dose (DPI)	27.4	0	Infinity	Yes
Dose (NEB)	15	0	Infinity	Yes
V _c	11.4	0	Infinity	Yes
k ₁₀	0.53	0	Infinity	Yes
k ₁₂	0.36	0	Infinity	Yes
k ₂₁	0.69	0	Infinity	Yes
k _a (DPI)	0.45	0	Infinity	Yes
k _{nal} (DPI)	0.08	0	Infinity	Yes
k _a (NEB)	0.34	0	Infinity	Yes
k _{nal} (NEB)	0.08	0	Infinity	Yes

C)

DPI		NEB	
T (h)	Predicted serum concentration (mg/L)	T (h)	Predicted serum concentration (mg/L)
0	0	0	0
0.25	0.22763	0.25	0.095597
0.5	0.38466	0.5	0.16382
1	0.55816	1	0.2446
1.5	0.6196	1.5	0.27948
2	0.62223	2	0.28876
3	0.55315	3	0.27092
4	0.4572	4	0.23507
6	0.28769	6	0.16033
8	0.17271	8	0.10243

Figure B.2 A) model file, B) Parameter file and C) Predicted profile of the Scientist[®] for curve-fitting the mean serum concentration vs. time profiles of tobramycin following inhalation from DPI and NEB.

Table B.5-A Goodness-of-fit statistics and statistical output for tobramycin DPI PK profile curve fitting.

Goodness-of-fit statistics	Weighted	Unweighted
Sum of squared observations:	1.9437	1.9437
Sum of squared deviations:	0.033747	0.033747
Standard deviation of data:	0.064949	0.064949
R-squared:	0.98264	0.98264
Coefficient of determination:	0.88728	0.88728
Correlation:	0.96655	0.96655
Model Selection Criterion:	1.7829	1.7829
Confidence Intervals		
Parameter Name:	k_a	
Estimated Value:	0.45025	
Standard Deviation:	0.041451	
95% Range (Univariate):	0.35467	0.54584
95% Range (Support Plane):	0.32647	0.57404
Parameter Name:	k_{nal}	
Estimated Value:	0.076506	
Standard Deviation:	0.042511	
95% Range (Univariate):	0.021525	0.17454
95% Range (Support Plane):	0.050444	0.20346
Variance-Covariance Matrix		
0.0017182		
0.00086527	0.0018072	
Correlation Matrix		
1		
0.49104	1	

Table B.5-B Goodness-of-fit statistics and statistical output for tobramycin NEB PK profile curve fitting.

Goodness-of-fit statistics	Weighted	Unweighted
Sum of squared observations:	0.42727	0.42727
Sum of squared deviations:	0.0050663	0.0050663
Standard deviation of data:	0.025165	0.025165
R-squared:	0.98814	0.98814
Coefficient of determination:	0.92196	0.92196
Correlation:	0.97592	0.97592
Model Selection Criterion:	2.1505	2.1505
Confidence Intervals		
Parameter Name:	k_a	
Estimated Value:	0.34124	
Standard Deviation:	0.024899	
95% Range (Univariate):	0.28382	0.39866
95% Range (Support Plane):	0.26688	0.41559
Parameter Name:	k_{nal}	
Estimated Value:	0.078354	
Standard Deviation:	0.030372	
95% Range (Univariate):	0.0083153	0.14839
95% Range (Support Plane):	0.012347	0.16905
Variance-Covariance Matrix		
0.00061996		
0.00040206	0.00092247	
Correlation Matrix		
1		
0.53166	1	

APPENDIX C

ORIGINAL DATA SETS FROM CURVE FITTING APPROACH FOR CALCITONIN IV AND INHALED PK PROFILES

Table C.1 Calcitonin mean (\pm SD) plasma concentration vs. time profile data reported in Buclin et al. after IV infusion.

Time (h)	Mean plasma concentration ($\mu\text{g/L}$)	SD ($\mu\text{g/L}$)
0	0	0
0.25	0.096952	0.0199
0.5	0.11276	0.025
0.76	0.12175	0.02924
1.01	0.17277	0.038
1.51	0.0141	0.0037
2	0.00399	0.0009

A)

```

// Calcitonin IV One Compartment Model File
IndVars: T
DepVars: Cc
Params: Vc, k10
//INPUT
Dose=10
TINF1=1
RATEON1=Dose/TINF1
TON1=0
TOFF1=TON1+TINF1
FLAGON1=UNIT(T-TON1)
FLAGOFF1=UNIT(T-TOFF1)
ARATE1=RATEON1*FLAGON1*(1-FLAGOFF1)
Mc'=ARATE1-k10*Mc
Cc=Mc/Vc
//Initial conditions
T=0
Mc=0
***

```

B)

Parameter Name	Parameter Value	Lower Limit	Upper Limit	Fixed?
Vc	3.72	0	Infinity	Yes
k10	17.9	0	Infinity	Yes

C)

Time (h)	Predicted plasma concentration (µg/L)
0	0
0.25	0.090789
0.5	0.12658
0.76	0.14069
1.01	0.14626
1.51	0.022731
2	0.003533

Figure C.1 A) model file, B) Parameter file and C) Predicted profile of the Scientist® for curve-fitting the mean plasma concentration vs. time profile of calcitonin following IV infusion.

Table C.2 Goodness-of-fit statistics and statistical output for calcitonin IV PK profile curve fitting.

Goodness-of-fit statistics	Weighted	Unweighted
Sum of squared observations:	6.72E-08	6.72E-08
Sum of squared deviations:	1.36E-09	1.36E-09
Standard deviation of data:	1.65E-05	1.65E-05
R-squared:	0.97973	0.97973
Coefficient of determination:	0.95156	0.95156
Correlation:	0.9758	0.9758
Model Selection Criterion:	2.456	2.456
Confidence Intervals		
Parameter Name:	V _c	
Estimated Value:	17.921	
Standard Deviation:	3.7647	
95% Range (Univariate):	8.2433	27.598
95% Range (Support Plane):	5.114	30.728
Parameter Name:	k ₁₀	
Estimated Value:	3.7232	
Standard Deviation:	0.96678	
95% Range (Univariate):	1.238	6.2083
95% Range (Support Plane):	0.43438	7.012
Variance-Covariance Matrix		
1.42E+01		
-3.4649	0.93466	
Correlation Matrix		
1		
-0.95198	1	

Table C.3-A Calcitonin mean (\pm SD) plasma concentration vs. time profile data reported in Clark et al. after inhalation from DPI.

Time (h)	Mean plasma concentration ($\mu\text{g/L}$)	SD ($\mu\text{g/L}$)
0	0	0
0.08	0.02128	0.009
0.17	0.04217	0.0086
0.33	0.038	0.0131
0.5	0.03611	0.0128
1	0.02	0.0067
2	0.00961	0.0067
4	0	0
6	0	0

Table C.3-B Calcitonin mean (\pm SD) plasma concentration vs. time profile data reported in Clark et al. after inhalation from NEB.

Time (h)	Mean plasma concentration ($\mu\text{g/L}$)	SD ($\mu\text{g/L}$)
0	0	0
0.08	0.02166	0.009
0.17	0.03534	0.0086
0.33	0.039	0.0131
0.5	0.04143	0.0128
1	0.03083	0.0067
2	0.0106	0.0067
4	0.0029	0.002
6	0	0

A)

//Calcitonin lung deposition and disposition PK model

IndVars: T

DepVars: C_cParams: Dose, V_c, k₁₀, k_a, k_{nal}

$$M_L' = -(k_a + k_{nal}) * M_L$$

$$M_C' = k_a * M_L - k_{10} * M_C$$

$$C_c = M_C / V_c$$

//Initial conditions

$$T = 0$$

$$M_L = \text{Dose}$$

$$M_C = 0$$

B)

Parameter Name	Parameter Value	Lower Limit	Upper Limit	Fixed?
Dose (DPI)	52.9	0	Infinity	Yes
Dose (NEB)	56.9	0	Infinity	Yes
V _c	11.4	0	Infinity	Yes
k ₁₀	0.53	0	Infinity	Yes
k ₁₂	0.36	0	Infinity	Yes
k ₂₁	0.69	0	Infinity	Yes
k _a (DPI)	0.06	0	Infinity	Yes
k _{nal} (DPI)	2.32	0	Infinity	Yes
k _a (NEB)	0.05	0	Infinity	Yes
k _{nal} (NEB)	1.22	0	Infinity	Yes

C)

DPI		NEB	
Time (h)	Predicted plasma concentration (µg/L)	Time (h)	Predicted plasma concentration (µg/L)
0	0	0	0
0.08	0.021041	0.08	0.016758
0.17	0.035067	0.17	0.030866
0.33	0.042564	0.33	0.042273
0.5	0.038973	0.5	0.043841
1	0.017993	1	0.030332
2	0.0021036	2	0.0092892
4	0.000019237	4	0.0007408
6	1.6529E-07	6	0.000058635

Figure C.2 A) model file, B) Parameter file and C) Predicted profile of the Scientist[®] for curve-fitting the mean plasma concentration vs. time profiles of calcitonin following inhalation from DPI and NEB.

Table C.4-A Goodness-of-fit statistics and statistical output for calcitonin DPI PK profile curve fitting.

Goodness-of-fit statistics	Weighted	Unweighted
Sum of squared observations:	5.47E-09	5.47E-09
Sum of squared deviations:	1.42E-10	1.42E-10
Standard deviation of data:	4.50E-06	4.50E-06
R-squared:	0.97411	0.97411
Coefficient of determination:	0.93887	0.93887
Correlation:	0.97487	0.97487
Model Selection Criterion:	2.3503	2.3503
Confidence Intervals		
Parameter Name:	k_a	
Estimated Value:	0.059249	
Standard Deviation:	0.0064283	
95% Range (Univariate):	0.044049	0.07445
95% Range (Support Plane):	0.039462	0.079036
Parameter Name:	k_{nal}	
Estimated Value:	2.3214	
Standard Deviation:	0.45545	
95% Range (Univariate):	1.2444	3.3984
95% Range (Support Plane):	0.91947	3.7233
Variance-Covariance Matrix		
4.13E-05		
0.0024008	0.20743	
Correlation Matrix		
1		
0.82003	1	

Table C.4-B Goodness-of-fit statistics and statistical output for calcitonin NEB PK profile curve fitting.

Goodness-of-fit statistics	Weighted	Unweighted
Sum of squared observations:	6.03E-09	6.03E-09
Sum of squared deviations:	7.25E-11	7.25E-11
Standard deviation of data:	3.22E-06	3.22E-06
R-squared:	0.98799	0.98799
Coefficient of determination:	0.96806	0.96806
Correlation:	0.98934	0.98934
Model Selection Criterion:	2.9994	2.9994
Confidence Intervals		
Parameter Name:	k_a	
Estimated Value:	0.045027	
Standard Deviation:	0.0029126	
95% Range (Univariate):	0.03814	0.061915
95% Range (Support Plane):	0.036062	0.053993
Parameter Name:	k_{nal}	
Estimated Value:	1.2232	
Standard Deviation:	0.1642	
95% Range (Univariate):	0.83892	1.6114
95% Range (Support Plane):	0.71777	1.7286
Variance-Covariance Matrix		
8.48E-06		
0.00036168	0.02696	
Correlation Matrix		
1		
0.75628	1	

APPENDIX D

ORIGINAL DATA SETS FROM CURVE FITTING APPROACH FOR CIPROFLOXACIN IV AND INHALED PK PROFILES

Table D.1 Ciprofloxacin mean (\pm SE) serum concentration vs. time profile data reported in Brunner et al. after IV infusion.

T (h)	Mean serum concentration (mg/L)	SE (mg/L)
0.33	1.3631	0.08793
0.67	0.7819	0.070346
1.00	0.6240	0.035182
1.33	0.5312	0.030769
1.67	0.4244	0.069972
2.00	0.3967	0.026373
2.33	0.3643	0.021978
2.67	0.3366	0.0206374
3.00	0.2996	0.021978
3.33	0.2858	0.030752
3.67	0.2441	0.021978
4.00	0.2257	0.026373
4.33	0.2306	0.026356
4.67	0.2122	0.030752
5.00	0.1891	0.026376
5.33	0.1800	0.021978
5.67	0.1662	0.022356
6.00	0.1757	0.013187
6.33	0.1713	0.021961
6.67	0.1622	0.017582
7.00	0.1391	0.010769
7.33	0.1439	0.012989
7.67	0.1395	0.017582
8.00	0.1536	0.026373

Table D.2 Macro-rate constants derived from ciprofloxacin IV PK profile reported in Brunner et al. by using method of residuals.

A (mg/L)	1.58
α (h^{-1})	2.06
B (mg/L)	0.51
β (h^{-1})	0.18

The macro-rate constants in Table D.2 were used to calculate initial estimates of k_{10} , k_{12} , k_{21} and V_c which are reported in Chapter 3.

A)

```
// Ciprofloxacin IV Two Compartment Model File
IndVars: T
DepVars: Cc
Params: Vc, k10, k12, k21
//INPUT
Dose=200
TINF1=0.17
RATEON1=Dose/TINF1
TON1=0
TOFF1=TON1+TINF1
FLAGON1=UNIT(T-TON1)
FLAGOFF1=UNIT(T-TOFF1)
ARATE1=RATEON1*FLAGON1*(1-
FLAGOFF1)
MC'=ARATE1+k21*MP-(k12+k10)*MC
MP'=k12*MC-k21*MP
CC=MC/VC
//Initial conditions
T=0
MC=0
MP=0
***
```

B)

Parameter Name	Value	Lower Limit	Upper Limit	Fixed?
V _C	93.2	0	Infinity	Yes
k ₁₀	0.64	0	Infinity	Yes
k ₁₂	1.42	0	Infinity	Yes
k ₂₁	0.86	0	Infinity	Yes

C)

T (h)	Predicted serum concentration (mg/L)
0.33	1.3536
0.67	0.8231
1.00	0.59845
1.33	0.48998
1.67	0.42847
2.00	0.38949
2.33	0.35969
2.67	0.33381
3.00	0.31144
3.33	0.29096
3.67	0.27143
4.00	0.25379
4.33	0.23733
4.67	0.22149
5.00	0.20713
5.33	0.19371
5.67	0.18079
6.00	0.16907
6.33	0.15812
6.67	0.14757
7.00	0.13801
7.33	0.12906
7.67	0.12045
8.00	0.11265

Figure D.1 A) model file, B) Parameter file and C) Predicted profile of the Scientist[®] for curve-fitting the mean serum concentration vs. time profile of ciprofloxacin following IV infusion.

Table D.3 Goodness-of-fit statistics and statistical output for ciprofloxacin IV PK profile curve fitting.

Goodness-of-fit statistics	Weighted	Unweighted
Sum of squared observations:	4.37	4.37
Sum of squared deviations:	0.0094903	0.0094903
Standard deviation of data:	0.021783	0.021783
R-squared:	0.99783	0.99783
Coefficient of determination:	0.99455	0.99455
Correlation:	0.99729	0.99729
Model Selection Criterion:	4.8796	4.8796
Confidence Intervals		
Parameter Name:	V_c	
Estimated Value:	93.249	
Standard Deviation:	4.2449	
95% Range (Univariate):	84.395	102.1
95% Range (Support Plane):	78.876	107.62
Parameter Name:	k_{10}	
Estimated Value:	0.64064	
Standard Deviation:	0.036048	
95% Range (Univariate):	0.56544	0.71583
95% Range (Support Plane):	0.51858	0.76269
Parameter Name:	k_{12}	
Estimated Value:	1.4245	
Standard Deviation:	0.14872	
95% Range (Univariate):	1.1142	1.7347
95% Range (Support Plane):	0.92091	1.928
Parameter Name:	k_{21}	
Estimated Value:	0.8639	
Standard Deviation:	0.077395	
95% Range (Univariate):	0.70246	1.0253
95% Range (Support Plane):	0.60185	1.126
Variance-Covariance Matrix		
18.02		
-0.13651	0.0012995	
-0.58014	0.0044918	0.022119
-0.19787	0.0021057	0.0086923
Correlation Matrix		
1		
-0.89207	1	
-0.91893	0.83782	1
-0.60226	0.75473	0.75517

Table D.4 Ciprofloxacin mean (\pm SD) plasma concentration vs. time profile data reported in Stass et al. after inhalation from DPI.

T (h)	Mean plasma concentration (mg/L)	SD (mg/L)
0	0	0
0.5	0.04	0.0101695
1	0.0311	0.0101695
1.5	0.02655	0.0067796
2	0.024859	8.47E-03
2.5	0.022599	0.0080508
3	0.02033	0.0076271
4	0.017514	0.0063559
6	0.012429	0.0029661
8	0.00904	0.004661

A)

//Ciprofloxacin lung deposition and disposition PK model

IndVars: T

DepVars: C_C

Params: Dose, V_C, k₁₀, k₁₂, k₂₁, k_a, k_{nal}

$$M_L' = -(k_a + k_{nal}) * M_L$$

$$M_C' = k_{21} * M_P - (k_{12} + k_{10}) * M_C + k_a * M_L$$

$$M_P' = k_{12} * M_C - k_{21} * M_P$$

$$C_C = M_C / V_C$$

//Initial conditions

$$T = 0$$

$$M_L = \text{Dose}$$

$$M_C = 0$$

$$M_P = 0$$

B)

Parameter Name	Parameter Value	Lower Limit	Upper Limit	Fixed?
Dose (DPI)	16.58	0	Infinity	Yes
V _C	93.2	0	Infinity	Yes
k ₁₀	0.64	0	Infinity	Yes
k ₁₂	1.42	0	Infinity	Yes
k ₂₁	0.86	0	Infinity	Yes
k _a	0.98	0	Infinity	Yes
k _{nal}	0.61	0	Infinity	Yes

C)

T (h)	Predicted plasma concentration (mg/L)
0	0
0.5	0.039072
1	0.035802
1.5	0.029719
2	0.024721
2.5	0.021133
3	0.018492
4	0.014705
6	0.0097214
8	0.0064798

Figure D.2 A) model file, B) Parameter file and C) Predicted profile of the Scientist[®] for curve-fitting the mean plasma concentration-time profiles of ciprofloxacin following inhalation from DPI.

Table D.5 Goodness-of-fit statistics and statistical output for ciprofloxacin DPI PK profile curve fitting.

Goodness-of-fit statistics	Weighted	Unweighted
Sum of squared observations:	0.005357	0.005357
Sum of squared deviations:	6.83E-05	6.83E-05
Standard deviation of data:	0.0029216	0.0029216
R-squared:	0.98725	0.98725
Coefficient of determination:	0.94204	0.94204
Correlation:	0.97792	0.97792
Model Selection Criterion:	2.4481	2.4481
Confidence Intervals		
Parameter Name:	k_a	
Estimated Value:	0.98005	
Standard Deviation:	0.11634	
95% Range (Univariate):	0.71178	1.2483
95% Range (Support Plane):	0.63264	1.3275
Parameter Name:	k_{nal}	
Estimated Value:	0.61366	
Standard Deviation:	0.10884	
95% Range (Univariate):	0.36267	0.86464
95% Range (Support Plane):	0.28863	0.93869
Variance-Covariance Matrix		
0.013534		
0.0095603	0.011846	
Correlation Matrix		
1		
0.75503	1	

APPENDIX E

MODEL FILE FOR LOCAL LUNG EXPOSURE PROFILE SIMULATION

//Local lung exposure profile/Drug mass remaining in lung vs. time profile simulation
model file

IndVars: T

DepVars: ML

Params: k_a , k_{nal}

//INPUT

Dose=INPUT DOSE

$M_L' = -(k_a + k_{nal}) * M_L$

//Initial condition

T=0

$M_L = \text{Dose}$

VITA

Anuja Raut was born on January 18, 1990 in India. She graduated with a Bachelor of Pharmacy degree from MAEER's Maharashtra Institute of Pharmacy, University of Pune, India in 2011 and her undergraduate research lead to two first author research publications in peer-reviewed journals as well as a poster presentation at Indian Pharmaceutical Congress 2010. She joined the Master of Science program in Pharmaceutical Sciences at University of Southern California, Los Angeles in 2012, wherein her research involved studying the preclinical effects of a long-term, nanoparticle-bound, *in vivo* drug administration module on lacrimal gland extra-cellular matrix (ECM) protein expression in Sjögren's syndrome using a well characterized mouse model, leading to presentation of a scientific poster at Moving Targets 2013 Symposium. Following graduation from this program at USC in 2014, Anuja was admitted to the Master of Science program in Pharmaceutics at the School of Pharmacy, Virginia Commonwealth University (VCU), Richmond, VA under the guidance of Dr. Masahiro Sakagami. With this thesis project, she has made several intramural presentations and will be working on publishing the results in a peer-reviewed journal.

At VCU, Anuja has been elected Pharmaceutics Graduate Student Association (PCEU-GSA) Scholarship Chair 2015-2016, Vice-President 2016-2017 as well as Graduate Women in Science (GWIS)-Richmond Chapter Founding member 2014-2015, Historian 2015-2016 and Secretary 2016-2017. She is also on the Vice Provost for Student Affairs Advisory Council 2016-2017. She has been actively involved in the Richmond community by volunteering at Habitat for Humanity, the Science Museum of Virginia and a Richmond based homeless shelter. She is currently the member of three professional associations: AAPS, ASCPT and International Society of Pharmacometrics (ISoP).